Mitofusins Mfn1 and Mfn2 are required to preserve glucose- but not incretin-stimulated beta cell connectivity and insulin secretion

Journal:	*Diabetes*
Manuscript ID	DB21-0800.R2
Manuscript Type:	Original Article: Islet Studies
Date Submitted by the Author:	n/a
Complete List of Authors:	Georgiadou, Eleni; Imperial College London Muralidharan, Charanya; Indiana University School of Medicine Martinez, Michelle; Indiana University School of Medicine Chabosseau, Pauline; Imperial College London Tomas, Alejandra; Imperial College London, Medicine Yong Su Wern, Fiona; Imperial College London Akalestou, Elina; Imperial College London Stylianides, Theonides; Loughborough University Wretlind, Asger; Steno Diabetes Center Copenhagen, Legido-quigley, Cristina; Steno Diabetes Center Copenhagen Jones, Ben; Imperial College London Lopex-Noriega, Livia; Imperial College London Xu, Yanwen; Vanderbilt University Gu, Guoqiang; Vanderbilt University Medical Center, Cell and Developmental Biology; Vanderbilt University Alsabeeh, Nour; Kuwait University Cruciani-Guglielmacci, Celine; Sorbonne Universite Magnan, Christophe; Universite Paris Diderot-CNRS, physiology; Ibberson, Mark ; Swiss Institute of Bioinformatics Leclerc, Isabelle; Imperial College, London, Endocrinology & Metabolic Medicine; Ali, Yusuf; Nanyang Technological University Soleimanpour, Scott; University of Michigan, Endocrinology & Metabolism Linnemann, Amelia; Indiana University School of Medicine, Pediatrics Rodriguez, Tristan; Imperial College London Rutter, Guy; Imperial College London, Cell Biology, Division of Medicine;

DB21-0800.R1R2

Mitofusins *Mfn1* and *Mfn2* are required to preserve glucose- but not incretin-stimulated beta cell connectivity and insulin secretion

Eleni Georgiadou[1], Charanya Muralidharan[2], Michelle Martinez[2], Pauline Chabosseau[1], Elina Akalestou[1], Alejandra Tomas[1], Fiona Yong Su Wern[3], Theodoros Stylianides[4], Asger Wretlind[5], Cristina Legido-Quigley[5,6], Ben Jones[7], Livia Lopez Noriega[1], Yanwen Xu[8], Guoqiang Gu[8], Nour Alsabeeh[9], Céline Cruciani-Guglielmacci[10], Christophe Magnan[10], Mark Ibberson[11], Isabelle Leclerc[1], Yusuf Ali[3], Scott A. Soleimanpour[12,13] Amelia K. Linnemann[2], Tristan A. Rodriguez[14] and Guy A. Rutter[1,3,15*].

[1]Section of Cell Biology and Functional Genomics, Division of Diabetes, Endocrinology and Metabolism, Department of Medicine, Imperial College London, London, W12 0NN, UK
[2]Center for Diabetes and Metabolic Diseases, Indiana University School of Medicine, Indianapolis, IN, 46202, USA
[3]Lee Kong Chian School of Medicine, Nanyang Technological University, 637553, Singapore
[4]Loughborough University, Centre of Innovative and Collaborative Construction Engineering, Leicestershire, LE11 3TU, UK
[5]Systems Medicin, Steno Diabetes Center Copenhagen, 2820, Denmark
[6] Institute of Pharmaceutical Science, Kings College London, London, SE1 9NH, UK
[7] Section of Endocrinology and Investigative Medicine, Imperial College London, W12 0NN,UK
[8]Department of Cell and Developmental Biology, Program of Developmental Biology, and Vanderbilt Center for Stem Cell Biology. Vanderbilt University, School of Medicine, Nashville, TN, 37232, USA.
[9]Kuwait University, Department of Physiology, Health Sciences Center, 13110, Kuwait
[10]Université de Paris, BFA, UMR 8251, CNRS, Regulation of Glycemia by Central Nervous System, Paris, 75205, France
[11]Vital-IT Group, SIB Swiss Institute of Bioinformatics, Lausanne, CH-1015, Switzerland
[12]Division of Metabolism, Endocrinology & Diabetes and Department of Internal Medicine, University of Michigan Medical School, Ann Arbor, MI 48105, USA
[13]VA Ann Arbor Healthcare System, Ann Arbor, MI 48105, USA
[14]National Heart and Lung Institute, Imperial Centre for Translational and Experimental Medicine, Imperial College London, London, W12 0NN, UK
[15] Centre of research of CHUM, University of Montreal, Quebec, H2X 0A9, Canada

*Address correspondence to Professor Guy A. Rutter, g.rutter@imperial.ac.uk, +44 20 759 43340

Word count: 41014445

Tweet: Deletion of Mitofusins 1 and 2 in beta cells of adult mice causes dramatic mitochondrial fragmentation and disrupts Ca^{2+} dynamics, insulin release and glucose homeostasis in vivo. Strikingly, these deficiencies are corrected by incretin hormones through an EPAC-dependent mechanism. Study led by @guy_rutter and @EleniGe0. **Figure**: (Suppl. Fig. 11).

Abstract

Mitochondrial glucose metabolism is essential for stimulated insulin release from pancreatic beta cells. Whether mitofusin gene expression, and hence mitochondrial network integrity, is important for glucose or incretin signalling has not previously been explored. Here, we generated mice with beta cell-selective, adult-restricted deletion of the mitofusin genes *Mfn1* and *Mfn2* (β*Mfn1/2* dKO). β*Mfn1/2* dKO mice displayed elevated fed and fasted glycaemia and a >five-fold decrease in plasma insulin. Mitochondrial length, glucose-induced polarisation, ATP synthesis, cytosolic and mitochondrial Ca^{2+} increases were all reduced in dKO islets. In contrast, oral glucose tolerance was more modestly affected in β*Mfn1/2* dKO mice and GLP-1 or GIP receptor agonists largely corrected defective GSIS through enhanced EPAC-dependent signalling. Correspondingly, cAMP increases in the cytosol, as measured with an Epac-camps based sensor, were exaggerated in dKO mice. Mitochondrial fusion and fission cycles are thus essential in the beta cell to maintain normal glucose, but not incretin, sensing. These findings broaden our understanding of the roles of mitofusins in beta cells, the potential contributions of altered mitochondrial dynamics to diabetes development and the impact of incretins on this process.

Keywords: Ca^{2+} dynamics; exendin-4; glucose-stimulated insulin secretion; incretins; intercellular connectivity; mitochondrial dysfunction; mitofusins; pancreatic beta cell; Type 2 diabetes.

List of abbreviations

$[Ca^{2+}]_{cyt}$: Cytoplasmic Ca^{2+} concentration

$[Ca^{2+}]_{mito}$: Mitochondrial free Ca^{2+} concentration

AA: Antimycin A

Ach: Acetylcholine

cAMP: adenosine 3',5'-cyclic monophosphate

Clec16a$^{\Delta panc}$: Pancreatic islet specific Clec16a knock-out

Diaz: Diazoxide

dKO: double knock-out

Ex4: Exendin-4

FCCP: Carbonyl cyanide-4-phenylhydrazone

GIP: Glucose-dependent insulinotropic peptide

GLP-1: Glucagon-like peptide-1

GSIS: Glucose-stimulated insulin secretion

IMM: Inner mitochondria membrane

IPGTT: Intraperitoneal glucose tolerance test

OGTT: Oral gavage and glucose tolerance test

Oligo: Oligomycin

OMM: Outer mitochondrial membrane

r: Pearson correlation coefficient

Rot: Rotenone

TMRE: Tetramethylrhodamine ethyl ester

T2D: Type 2 diabetes

β*Mfn1/2* dKO: beta cell specific Mitofusin 1 and 2 double knock-out

$\Delta\psi_m$: Mitochondrial membrane potential

Introduction

Mitochondria are often referred to as the powerhouses or “chief executive organelles” of the cell, using fuels to provide most of the energy required to sustain normal function [1]. Mitochondrial oxidative metabolism plays a pivotal role in the response of pancreatic beta cells to stimulation by glucose and other nutrients [2]. Thus, as blood glucose increases, enhanced glycolytic flux and oxidative metabolism lead to an increase in ATP synthesis, initiating a cascade of events which involve the closure of ATP-sensitive K^+ (K_{ATP}) channels [3], plasma membrane depolarisation and the influx of Ca^{2+} via voltage-dependent Ca^{2+} channels (VDCC). The latter, along with other, less well defined “amplifying” signals [4], drive the biphasic release of insulin [2]. Gut-derived incretin hormones including glucagon-like peptide-1 (GLP-1) and glucose-dependent insulinotropic peptide (GIP) [5] further potentiate secretion by binding to class-B G-protein coupled receptors (GPCRs) to generate adenosine 3',5'-cyclic monophosphate (cAMP) and other intracellular signals [5].

Under normal physiological conditions, mitochondria undergo fusion and fission cycles which are essential for quality control and adaptation to energetic demands [6]. Thus, highly inter-connected mitochondrial networks allow communication and interchange of contents between mitochondrial compartments, as well as with other organelles such as the endoplasmic reticulum (ER) [7]. These networks exist interchangeably with more fragmented structures, displaying more “classical” mitochondrial morphology [8]. Mitochondrial fission is also necessary for “quality control” and the elimination of damaged mitochondria by mitophagy [9].

Whilst the mitofusins MFN1 and MFN2, homologues of the *D. melanogaster* fuzzy onions (*fzo*) and mitofusin (*dmfn*) gene products [10], are GTPases that mediate fusion

of the outer mitochondrial membrane (OMM), optic atrophy protein 1 (OPA1) controls that of the inner mitochondrial membrane (IMM). Dynamin related protein 1 (DRP1) is responsible for mitochondrial fission [11]. Other regulators include FIS1, mitochondrial fission factor (MFF) and MiD49/51 [12].

Earlier studies [13-18] have shown that perturbations in mitochondrial structure in beta cells have marked effects on GSIS. Surprisingly, whether the canonical and evolutionarily-conserved machinery involved in mitochondrial fusion, i.e the mitofusins, control mitochondrial structure in beta cells has not been explored yet. Furthermore, none of the earlier studies have investigated the actions of mitochondrial structure destruction in adult mice. Finally, whether and to what extent they impact secretion stimulated by other agents including incretins is less clear. This question is important given that changes in mitochondrial oxidative metabolism [19] and structure contribute to type 2 diabetes (T2D).

Here, we first explored the potential contribution of mitofusins to the effects of diabetic conditions. We next determined whether deletion of *Mfn1* and *Mfn2* in beta cells in adult mice may impact insulin secretion. Lastly, we aimed to determine whether incretins may rescue or bypass any observed perturbations. We show that mitofusin ablation exerts profound effects on insulin release, glucose homeostasis and Ca^{2+} dynamics. Remarkably, the deficiencies in insulin secretion are largely corrected by incretin hormones. This suggests a possible approach to ameliorating the consequences of mitochondrial fragmentation with these agonists in some forms of diabetes.

Research Design and Methods

Study approval C57BL/6J mice were housed in individually ventilated cages in a pathogen-free facility at 22ºC with a 10-14 h light-dark cycle and were fed *ad libitum* with a standard mouse chow diet (Research Diets, New Brunswick, NJ, USA). All *in vivo* procedures were approved by the UK Home Office, according to the Animals (Scientific Procedures) Act 1986 with local ethical committee approval under personal project license (PPL) number PA03F7F07 to I.L.

Generation of beta cell selective *Mfn1/Mfn2* knockout (β*Mfn1/2* dKO), *Clec16a* null and Pdx1CreER mice C57BL/6J male mice bearing *Mfn1* (Mfn1^{tm2Dcc}; JAX stock #026401) and *Mfn2* (B6.129(Cg)-Mfn2^{tm3Dcc}/J; JAX stock #026525; The Jackson Laboratory, Bar Harbor, ME,USA) alleles [20] with *lox*P sites flanking exons 4 and 6 were purchased from the Jackson laboratory and crossed to C57BL/6J transgenic animals carrying an inducible *Cre* recombinase under *Pdx1* promoter control (Pdx1-Cre^{ERT2}) [21]. Mice bearing floxed *Mfn* alleles but lacking *Cre* recombinase were used as littermate controls in this study. Mice were genotyped following protocols described by the Jackson laboratory for each of these strains (See ESM Table 1). Recombination was achieved by daily tamoxifen (10mg/~~body weight~~mouse [diluted in corn oil; Sigma-Aldrich, Dorset, UK]) i.p. injections for five days at 7-8 weeks of age in both control and β*Mfn1/2* dKO (dKO) groups.

Animals with floxed *Clec16a* alleles were bred to mice carrying the Pdx1-Cre transgene (*Clec16a*$^{\Delta panc}$) as previously described [22]. Pdx1-Cre alone mice were used as littermate controls. Pdx1CreER mice were generated as previously described [21].

RNA extraction and quantitative reverse transcription PCR For measurements of mRNA levels, pancreatic islets from control and β*Mfn1/2* dKO mice were isolated by collagenase digestion [23]. Total RNA from islets (50-100) was extracted and reverse transcribed as previously described [24] (see ESM Table 2 for primer details).

Tissue DNA extraction and measurement of mtDNA copy number Total islet DNA was isolated using Puregene Cell and Tissue Kit (Qiagen, Manchester, UK) and was amplified (100ng) using NADH dehydrogenase I primers [25], also known as complex I (*mt9/mt11)* for mtDNA and *Ndufv1* for nuclear DNA.

SDS-PAGE and western blotting Islets were collected and lysed (20 µg) as previously described [24]. The antibodies used are summarised in ESM Table 3.

Intraperitoneal (i.p.) or oral gavage (OG) of glucose followed by insulin, proinsulin or ketone levels measurement and insulin tolerance test (TT) *in vivo* IPGTTs, IPIITTs, OGTTs and plasma insulin measurements were performed as previously described [24]. Plasma proinsulin levels were measured in fasted (16h) animals using a rat/mouse proinsulin ELISA kit (Mercodia). Plasma β-ketones were measured from fed or fasted (16h) mice using an Area 2K device (GlucoMen, Berkshire, UK).

***In vitro* insulin secretion** Islets were isolated from mice and incubated for 1 h in Krebs-Ringer bicarbonate buffer containing 3 mmol/l glucose as previously described [24].

Single-cell fluorescence imaging Dissociated islets were incubated with 100nM Mitotracker green (Thermo Fisher Scientific) in Krebs-Ringer bicarbonate buffer containing 11 mmol/l glucose for 30 min. Mitotracker green was then washed with Krebs buffer with 11 mmol/l glucose before fluorescence imaging. Experiments with tetramethylrhodamine ethyl ester (TMRE) were performed as previously described [24]. Clusters of dissociated islets were transduced for 48h with an adenovirus encoding the low-Ca^{2+}-affinity sensor D4 addressed to the ER, Ad-RIP-D4ER (MOI: 100), as described in [26]. Bleaching was corrected as described in [27].Clusters of dissociated islets were transduced for 24h with an adenovirus encoding Epac1-camps, as described in [28].

Mitochondrial shape analysis For each stack, one image at the top, middle and bottom of the islet was analysed. After background subtraction, the following parameters were measured for each cell: number of particles, perimeter, circularity, elongation (1/circularity), density and surface area of each particle [29].

Whole-islet fluorescence imaging Cytosolic, mitochondrial Ca^{2+} imaging, and ATP:ADP changes in whole islets were performed as previously described [24].

TIRF fluorescence imaging Experiments using the membrane-located zinc sensor ZIMIR (50 μmol/l) [30] or the fluorescent genetically-encoded and vesicle-located green marker NPY-Venus were performed as previously described [31].

Pancreas immunohistochemistry Isolated pancreata were fixed and imaged as described in [24]. The antibodies used are summarised in ESM Table 3. For

examination of apoptosis, TUNEL assay was performed using a DeadEnd Fluorometric TUNEL system kit and DNase I treatment (Promega, Madison, Wisconsin, USA) according to the manufacturer's instructions.

Metabolomics/lipidomics Metabolites were quantified using targeted ultra-high-performance liquid-chromatography coupled triple quadrupole mass spectrometry (UHPLC-QqQ-MS/MS) as described earlier [32]. Lipidomic sample preparation followed the Folch procedure with minor adjustments. Significance was tested by Student's two-tailed t-test using GraphPad Prism 8 software.

Measurement of oxygen consumption rate XF96 assays (Seahorse Bioscience, Agilent, Santa Clara, CA, USA) using mouse islets (~10 per well) were performed as described in [33]. Parameters were analysed as in [34].

Electron microscopy (EM) For conventional EM, islets were fixed and imaged as described in [35].

Connectivity analysis

Pearson (*r*)-based connectivity and correlation analyses Correlation analyses in an imaged islet were performed as previously described [36].

RNA-Seq data analysis Processing and differential expression analysis of RNA-Seq data from islets isolated from high fat high sugar (HFHS, D12331, Research Diets) and regular chow (RC) fed mice (C57Bl/6J, DBA/2J, BALB/cJ, A/J, AKR/J, 129S2/SvPas) was performed as previously described [37] using the *Limma* package

in R and p-values were adjusted for multiple comparisons using the Benjamini Hochberg procedure [38].

Statistics Data are expressed as mean ± SDEM unless otherwise stated. Significance was tested by Student's two-tailed t-test and Mann–Whitney correction or two-way ANOVA with Sidak's multiple comparison test for comparison of more than two groups, using GraphPad Prism 9 software (San Diego, CA, USA). $p < 0.05$ was considered significant. Experiments were not randomised or blinded.

Data and Resource Availability The datasets generated and/or analysed during the current study are available from the corresponding author upon reasonable request. No applicable resources were generated or analysed during the current study.

Results

Changes in *Mfn1* and *Mfn2* expression in mouse strains maintained on regular chow (RC) or high fat high sugar (HFHS) diet. To determine whether the expression of *Mfn1* or *Mfn2* might be affected under conditions of hyperglycaemia mimicking T2D in humans, we interrogated data from a previous report [37] in which RNA sequencing was performed on six mouse strains. BALB/cJ mice showed “antiparallel” changes in *Mfn1* and *Mfn2* expression in response to maintenance on high fat high sugar (HFHS) diet for 10 days, and similar changes were obtained in DBA/2J mice at 30 and 90 days (Suppl.Fig.**1A-B**).

Generation of a conditional β*Mfn1/2* dKO mouse line. Efficient deletion of *Mfn1* and *Mfn2* in the beta cell was achieved in adult mice using the Pdx1-Cre^{ERT2} transgene and tamoxifen injection at 7-8 weeks. Possession of this transgene (which does not contain the human growth hormone (hGH) cDNA [21]) alone had no effect on glycaemic phenotype or cellular composition of pancreatic islets (Suppl. Fig.**2A-C**). Deletion of mitofusin genes was confirmed by qRT-PCR (Fig.**1A**) and Western (immuno-) blotting (Fig.**1B**) analysis, ~7 weeks post-tamoxifen injection. Relative to *β-actin*, expression of the *Mfn1* and *Mfn2* transcripts in isolated islets from dKO mice decreased by ~83 and 86% accordingly vs control islets (Fig.**1A**), consistent with selective deletion in the beta cell compartment [39]. No differences were detected in the expression of other mitochondrial fission and fusion mediator genes such as *Opa1*, *Drp1* and *Fis1* in islets (Fig.**1A**) or in *Mfn1* and *Mfn2* in other relevant tissues (Suppl.Fig.**3A**). dKO mice were significantly lighter than control animals after 20-21 weeks (Suppl.Fig.**3B**).

β*Mfn1/2* dKO mice are glucose intolerant with impaired GSIS *in vivo.* Glucose tolerance was impaired in dKO mice compared to control littermates at 14 weeks (Fig.**1C-D**) and this difference was further exaggerated at 20 weeks (Suppl. Fig.**3C**). At 14 weeks, β*Mfn1/2* dKO mice (with a 27 mmol/l glycaemia at 15 min.; Fig.**1E-F**) showed a dramatically lower insulin excursion upon glucose challenge vs control animals (Fig.**1G-H**). Following an oral gavage, glucose tolerance was more modestly affected in dKO mice (Fig.**1I-J**) while plasma insulin levels in these animals (with a glycaemia of 27 mmol/l at 15min.) were indistinguishable from control animals (Fig.**1K-L**; 0 vs 15min. in dKO). Insulin tolerance was unaltered in β*Mfn1/2* dKO vs control mice (Suppl.Fig.**3D**) while proinsulin conversion was impaired (Suppl.Fig.**3E-F**). dKO mice displayed significantly elevated plasma glucose (Suppl.Fig.**3G**) under both fed and fasted conditions and β-ketones (ketone bodies) were also elevated in fasted vs control animals (Suppl.Fig.**3H**), whereas plasma insulin levels were lower (Suppl.Fig.**3I**). Apparent insulin secretion was also impaired after IP injection with a lower glucose in 14- and 20-week-old dKO vs control mice (Suppl. Fig.**4A-D**). In contrast, plasma insulin levels were not statistically different between control and dKO animals following an OGTT at either age (Suppl. Fig.**4E-H**), though a trend towards lower insulin excursion was evident in dKO mice.

Deletion of *Mfn1/2* alters mitochondrial morphology in beta cells. While the mitochondrial network was highly fragmented in dKO cells (Fig.**2A;** and inset), the number of mitochondria per cell or density were not altered (Fig.**2B**). Mitochondrial elongation, perimeter and surface area were also significantly decreased in β*Mfn1/2* dKO cells, while circularity was increased (Fig.**2B**). Transmission electron microscopy (TEM) confirmed these changes (Fig.**2C**). Cristae structure and organisation were also

altered in β*Mfn1/2* dKO cells with a single crista often running the length of a mitochondrial section. Finally, dKO islets displayed a ~75% reduction in mtDNA (Fig.**2D**).

***Mitofusin* deletion leads to modest changes in beta cell mass.** Pancreatic beta cell mass decreased by 33% whereas alpha-cell mass was not affected in dKO mice (Fig.**3A-C**). Beta cell-alpha cell ratio was decreased by 53% (Fig.**3D**) in line with an increase in TUNEL-positive beta cells in dKO vs control animals (Fig.**3E-F**)

Mitochondrial fragmentation, beta cell mass deterioration and hyperglycaemia emerge in dKO mice two weeks post tamoxifen administration. We next sought to exclude the possibility that mitochondrial fragmentation may simply be the consequence of the observed hyperglycaemia. Two distinct groups of organelles (both elongated and circular) were apparent in β*Mfn1/2* dKO cells (Suppl. Fig. **5A-B**) two weeks post tamoxifen treatment. Neither fed nor fasted glycaemia or plasma insulin levels following glucose challenge were different between groups (Suppl. Fig. **5C-E**). A trend towards lower beta cell mass and mtDNA was detected in dKO animals (Suppl. Fig. **5F-I**).

Beta cell identity is modestly altered in β*Mfn1/2* dKO islets. Whilst *Ins2*, *Ucn3* and *Glut2* (*Slc2a2*) were significantly downregulated, *Trpm5* was upregulated in dKO islets (Suppl.Fig.**6**). No changes in alpha- or beta cell disallowed genes [40] were detected. In contrast, genes involved in mitochondrial function such as *Smdt1* and *Vdac3* were upregulated in dKO beta cells (Suppl.Fig.**6**). Lastly, genes involved in ER stress and

322 mito/autophagy were also affected, with *Chop (Ddit3)* and *p62* being upregulated and
323 *Lc3* and *Cathepsin L* downregulated.
324
325 **Mitofusins are essential to maintain normal glucose-stimulated Ca^{2+} dynamics,**
326 **mitochondrial membrane potential and ATP levels.** Increased cytosolic Ca^{2+} is a
327 key trigger of insulin exocytosis in response to high glucose [2]. dKO mouse islets
328 exhibited a significantly smaller glucose-induced $[Ca^{2+}]_{cyt}$ rise *vs* control islets (Fig.**4A-**
329 **C**). When the K_{ATP} channel opener diazoxide and a depolarising K^+ concentration
330 were then deployed together to bypass the regulation of these channels by glucose,
331 cytosolic Ca^{2+} increases were not significantly impaired in dKO compared to control
332 animals (Fig.**4B-C**). A substantial reduction in mitochondrial free Ca^{2+} concentration
333 ($[Ca^{2+}]_{mito}$) in response to 17 mmol/l glucose [24] was also observed in dKO islets
334 (Fig.**4D-F**). Of note, subsequent hyperpolarisation of the plasma membrane with
335 diazoxide caused the expected lowering of mitochondrial $[Ca^{2+}]_{mito}$ in control islets
336 (reflecting the decrease in $[Ca^{2+}]_{cyt}$;**Fig.4E-F**), but was almost without effect on dKO
337 islets.
338
339 Glucose-induced increases in $\Delta\psi_m$ were also sharply reduced in dKO vs control
340 mouse islets (Fig.**4G-H**). Addition of 2-[2-[4-(trifluoromethoxy)phenyl]hydrazinylidene]-
341 propanedinitrile (FCCP) resulted in a similar collapse in apparent $\Delta\psi_m$ in islets from
342 both genotypes (Fig.**4G**). Cytosolic Ca^{2+} oscillations and synchronous $\Delta\psi_m$
343 depolarisation were also largely abolished in response to glucose in dKO cells when
344 measured by intravital imaging *in vivo* [41]. Finally, to assess whether deletion of *Mfn1*
345 and *Mfn2* may impact glucose-induced increases in mitochondrial ATP synthesis we
346 performed real-time fluorescence imaging using Perceval (Fig.**4I-J**). While control

islets responded with a time-dependent rise in the ATP:ADP ratio in response to a step increase in glucose from 3 mmol/l to 17 mmol/l, β*Mfn1/2* dKO beta cells failed to mount any response (Fig.**4J**).

Beta cell-beta cell connectivity is impaired by *Mfn1/2* ablation. Intercellular connectivity is required in the islet for a full insulin secretory response to glucose [42]. To assess this, individual Ca^{2+} traces recorded from Cal-520-loaded beta-cells in mouse islets (Fig.**4A-B**) were subjected to correlation (Pearson *r*) analysis to map cell-cell connectivity (Suppl.Fig.**7A**). Following perfusion at 17 mmol/l glucose, β*Mfn1/2* dKO beta cells tended to display an inferior, though not significantly different, coordinated activity than control cells, as assessed by counting the number of coordinated cell pairs (Suppl.Fig.**7C**; 0.94 vs 0.90 for control vs dKO, respectively). By contrast, beta cells displayed highly coordinated Ca^{2+} responses upon addition of 20 mmol/l KCl in dKO islets. Similarly, analysis of correlation strength in the same islets revealed significant differences in response to 17 mmol/l glucose between genotypes. In fact, dKO islets had weaker mean beta-beta cell coordinated activity (Suppl. Fig.**7B, D**; $p<0.05$; 0.88 vs 0.77 for control vs dKO, respectively), indicating that mitofusins affect the strength of connection rather than the number of coordinated beta cell pairs. A tending towards lower expression of the gap junction gene *Cx36/Gjd2* was observed in dKO islets (Suppl.Fig.**7E**). Beta cell "hub" and "leader" distributions [43] were also impaired in the dKO group (not shown, see [41]).

Unaltered ER Ca^{2+} mobilisation but decreased mitochondrial O_2 consumption and mtDNA depletion in β*Mfn1/2* dKO islets. No differences in cytosolic Ca^{2+} responses between genotypes were observed after agonism at the Gq-coupled

372 metabotropic acetylcholine (Ach) receptor [44, 45] (Fig.**5A-C**). In contrast,
373 measurements of O_2 consumption revealed that basal, proton leak and maximal
374 respiratory capacities were significantly impaired in dKO islets (Fig.**5D-E**).
375
376 **Impaired GSIS *in vitro* and beta cell connectivity can be rescued by incretins in**
377 **β*Mfn1/2* dKO mouse islets**. While GSIS was markedly impaired in dKO islets
378 (Fig.**6A**; Suppl. Table 4), incretins (GLP-1 or GIP), or the GLP1R agonist exendin-4,
379 at a submaximal concentration of 10 mmol/l glucose, led to a significant potentiation
380 in GSIS in both groups. Consequently, insulin secretion in response to 10 mmol/l
381 glucose was no longer different between control and β*Mfn1/2* dKO islets after incretin
382 addition (Fig.**6A-B**). Moreover, under these conditions, forced increases in intracellular
383 cAMP imposed by the addition of forskolin (FSK) or 3-isobutyl-1-methylxanthine
384 (IBMX), which activate adenylate cyclase (AC) and inhibit phosphodiesterase (PDE)
385 respectively, eliminated differences in GSIS between the genotypes (Fig.**6B**). No
386 differences in insulin secretion were observed between control and dKO islets after
387 depolarisation with KCl.
388
389 We next explored whether the incretin-mediated improvements in insulin secretion in
390 response to incretins were the result of altered $[Ca^{2+}]_{cyt}$ dynamics. Islets from isolated
391 dKO mice displayed a delayed increase in $[Ca^{2+}]_{cyt}$ in response to 10 mmol/l glucose
392 compared to control islets (Fig.**6C-D**). Addition of exendin-4 led to the emergence of
393 oscillatory activity in both groups and under these conditions, differences between
394 genotypes, as seen in Fig.**4B**, were no longer evident (Fig.**6C**). Measured at 10mmol/l
395 glucose, control and dKO islets displayed increases in ER Ca^{2+} in response to
396 exendin-4 (Fig.**6E-F**) while the response exaggerated in the latter group. Neither group

displayed significant changes in ATP:ADP ratio in response to exendin-4 (Fig.**6G-H**). Analysis of OCR revealed no significant differences between genotypes at 10mmol/l glucose in the presence or absence of exendin-4 or FSK (Fig.**6I**).

Moreover, mitofusin deletion may lead to a partial activation of "amplification" pathways of GSIS [46] at 3 mmol/l glucose since insulin secretion was enhanced in dKO islets after depolarisation of the plasma membrane with KCl in the presence of diazoxide (Fig. **6J**). Conversely, no differences between islet genotypes were observed at 17 mmol/l glucose (Fig.**6J**).

Whilst glucose-induced beta cell-beta cell connectivity, as assessed by monitoring Ca^{2+} dynamics (Fig.**6C**), was markedly impaired in dKO islets (Fig. **7A** and Suppl. Fig.**7**), these differences were largely abolished in the presence of exendin-4 (Fig. **8B-D**).

Insulin secretion is rescued by incretins through an EPAC-dependent activation. To explore the actions of mitochondrial disruption on incretin signalling, we next used a pharmacological approach. Glucose-stimulated insulin secretion was more strongly enhanced in dKO vs control islets by IBMX, FSK or the protein kinase A (PKA) inhibitor H89 alone (Fig.**8A**; Suppl. Table 4). Selective activation of EPAC also tended to lead to a larger increase in insulin secretion in dKO than control islets, and this difference became significant when PKA was inhibited with H89 (Fig.**8B**).

Glucose-dependent increases in cytosolic cAMP, assessed using the Epac-camps sensor, were also markedly amplified in dKO vs control cells (Fig.**8C-D**). This

difference persisted in the presence of IBMX and FSK, added separately or alone (Fig.**8C,E**). No changes in the expression of *Epac*, *Adcy* or *Prkar* (PKA) subunits were apparent between control and dKO islets (Fig.**8F**).

Defective glucose-stimulated insulin secretion is rescued by GLP-1R agonism in *Clec16a* null mice. To determine whether incretins may reverse defective insulin secretion in an alternative model of mitochondrial dysfunction, we examined mice lacking the mitophagy regulator *Clec16a* selectively in the pancreatic islet (*Clec16a*$^{\Delta panc}$) [22]. Glucose-stimulated insulin secretion was sharply inhibited in null vs Pdx1-Cre control mice, and these differences between genotype were largely corrected in by the addition of exendin-4 (Suppl. Fig.**8A**). Correspondingly, whereas the difference between *Clec16a*$^{\Delta panc}$ and control mice was significant for IPGTTs there was no such (significant) difference for the OGTTs at 15mins, in line with the findings above for β*Mfn1/2* dKO mice (Suppl. Fig.**8B-C**).

Defective secretion of a preserved pool of morphologically-docked granules in β*Mfn1/2* dKO mouse beta cells. To determine whether the markedly weaker stimulation of insulin secretion in dKO islets may reflect failed recruitment of secretory granules into a readily releasable or morphologically-docked pool beneath the plasma membrane, we next deployed total internal reflection fluorescence (TIRF) microscopy in dissociated beta cells. By over-expressing NPY-Venus, the number of insulin granules was significantly higher in close proximity with the plasma membrane in dKO cells after treatment with 20 mmol/l KCl (Suppl.Fig.**9A-B).** However, when we then used ZIMIR [30] in response to depolarisation as a surrogate for insulin secretion, release events were fewer in number and smaller in dKO (Suppl.Fig.**9C-E**).

Altered plasma metabolomic and lipidomic profiles in β*Mfn1/2* dKO mice. We applied an -omics approach to study metabolite and lipid changes in peripheral plasma samples from control and dKO mice (Suppl.Fig.**10**). Of 29 metabolites, the levels of five metabolic species (shown in red) were significantly altered in β*Mfn1/2* dKO animals (Suppl.Fig.**10A**). In the lipidomics analysis, the majority of lipid classes displayed a remarkably homogeneous downward trend in dKO samples (Suppl.Fig.**10B**).

Discussion

The key goal of the present study was to determine the role of mitofusins in controlling mitochondrial dynamics and hence glucose- and incretin-stimulated insulin secretion in the beta cell. Our strategy involved deleting both mitofusin isoforms since the expression of *Mfn1* and *Mfn2* is similar in the beta cell [47], suggestive of partial functional redundancy [48]. Our measurements of *Mfn1* and *Mfn2* expression in mouse models of T2D nonetheless revealed changes in the expression of these genes which may contribute to the disease.

Importantly, we show that *Mfn1* and *Mfn2* are critical regulators of the mitochondrial network in beta cells and consequently of insulin secretion *in vitro* and *in vivo* (Suppl.Fig.**11A-B**); see also [41]). These findings are in line with earlier studies, albeit involving the deletion of genes other than the mitofusins [13-18]. Additionally, we show that changes in *Mfn1* and *Mfn2* expression occur in models of diabetes and hence, their forced changes, as achieved in our study, may have relevance for the patho-etiology of beta cell failure in T2D and~~loss of *Mfn1* and *Mfn2* leads to~~ metabolic changes consistent with insulin deficiency. These include higher levels of bile acids as previously described in rodent models of T1D and T2D and in humans [49, 50], elevated leucine and isoleucine, as observed in human T1D [51], and an altered triglyceride profile [52]. Finally, these metabolomic/lipidomic data provide further support for ~~(~~the expected~~)~~ actions of mitofusin deletion via altered beta cell function, with changes that are somewhat more in line with metabolomic changes in human T1D (and models thereof) than T2D [53]. Indeed, dKO mice ~~are~~ gain~~ing~~ less weight than controls as they show the classic symptoms of diabetes mellitus [54, 55]. This is likely to be the result of metabolic dyshomeostasis in the face of lowered circulating

insulin levels, leading to impaired fat storage, loss of liver and muscle glycogen and eventually loss of muscle mass i.e. the cardinal symptoms of T1D and of advanced insulin-requiring T2D in humans.

Of note, none of the earlier reports investigating the effects of mitochondrial disruption in the beta cell explored the effects on incretin-stimulated secretion. Suggesting a differential effect on glucose- *vs* incretin-stimulated secretion we show here, firstly, that insulin secretion and glucose excursion were less markedly affected by mitofusin knockout during OGTTs, where an incretin effect is preserved [56], than during IPGTTs. Correspondingly, insulin secretion stimulated by incretins was largely preserved in dKO cells, in contrast to the ablation of glucose-stimulated secretion (Suppl. Fig. **11**C-DA-B). Strikingly, mitofusin deletion also enhanced incretin-stimulated cytosolic cAMP increases. That this effect was preserved in the face of PDE inhibition (IBMX) and AC activation was surprising, but may reflect an increase in total AC activity or distribution in dKO cells.

While PKA suppression is considered to be either neutral or inhibitory towards GSIS in WT beta cells models [57-59], our data show a rather striking increase in insulin secretion byin the presence of H89 in both islets from mice of either genotype groups. Whilst unexpected, and in contrast with those of others that support a role for PKA downstream of cAMP in the beta cell, Bryan and colleagues provide some evidence for the stimulation of GSIS by H89 under certain conditions [57]. Nevertheless, sSeveral studies have stressed the importance of both PKA-dependent and -independent effects of increased [cAMP]$_i$ on GSIS from islets [60]. More preciselThusy, PKA-independent exocytosis occurs through interactions between

Commented [RGA1]: Not really getting at the referee's specific comment about the data in the Bryan paper and ours.

Epac-2/cAMP- guanine-nucleotide-exchange factor II [61, 62], Rab3A and Rim2 (proteins involved in vesicle trafficking [57, 63, 64] and fusion) [65]. On the other hand, GLUT2, Kir6.2, and SUR1 and α-SNAP (a vesicle-associated protein), have been reported to be phosphorylated by PKA [58]. Here, we show that the effect of mitofusin deletion on GSIS is preserved when PKA is inhibited by H89, and even potentiated by EPAC-activation (Suppl. Fig. **11C-D)**. These changes appear to be exerted at the post transcriptional level, since we observed no changes in levels of mRNAs encoding the relevant beta cell isoforms of *Epac*. Whether there are changes in the level or the corresponding proteins including EPAC, their subcellular localisation or interaction with upstream regulators or downstream effectors, remains to be explored. Finally, the latter findings could indicate that an intact mitochondrial reticulum restricts signalling by EPAC through a mechanism that is inhibited by PKA. Future studies, using additional or alternative PKA inhibitors [66], will be needed to explore these possibilities.

Possibly contributing to these differences in the effects on responses to glucose vs incretin, exendin-4 treatment led to greater Ca^{2+} accumulation in the ER in dKO cells. By enhancing Ca^{2+} cycling across the ER membrane this could conceivably drive larger local increases in cytosolic Ca^{2+} which, in turn, may influence plasma membrane potential, trigger Ca^{2+} influx via VDCCs and hence, stimulate insulin release [67].

We also demonstrate that preserved mitochondrial ultra-structure is critical for normal beta cell-beta cell connectivity, itself required for normal insulin secretion [41, 68]. The mechanisms underlying impaired connectivity in the absence of mitofusins are unclear

but may involve altered *Cx36/Gjd2* expression, phosphorylation or activity, impacting gap junctions [42].

In summary, we show that acute treatment with incretins, commonly used as treatments for T2D and obesity [56], largely reverses the deficiencies in insulin secretion which follow mitochondrial disruption. Future studies will be needed to address the relevance of these findings to human beta cells and to the action of incretins in clinical settings.

Acknowledgements

We thank Stephen M. Rothery from the Facility for Imaging by Light Microscopy (FILM) at Imperial College London for support with confocal and widefield microscopy image recording and analysis. We thank Professor Julia Gorelik and Sasha Judina (Imperial College) for providing the Epac1-camps sensor. We also thank Aida Di Gregorio from the National Heart and Lung Institute (Imperial College) for genotyping the mice.

Author contributions

EG performed experiments and analysed data. EG supported the completion of confocal and widefield microscopy and analysis. ATC performed the EM sample processing and data analysis. CM, MM and AKL were responsible for the *in vivo* intravital Ca^{2+} imaging in mice presented in the bioRxiv paper. PC contributed to the analysis and manipulation of the *in vivo* intravital Ca^{2+} measurements as well as the preparation and imaging of TIRF samples. TS contributed to the generation of the MATLAB script used for connectivity analysis. FYSW and YA generated and performed Monte Carlo-based signal binarization. BJ assisted with the cAMP assays. EA and LLN performed the oral gavage in live animals. YX and GG performed studies with Pdx1CreER mice. NA assisted with Seahorse experiment protocols. CLQ and AW contributed to the metabolomics analysis. CCG, CM and MI were responsible for the RNAseq data analysis. SAS performed studies with Clec16a mice. TAR was involved in the design of the floxed *Mfn* alleles. TAR and IL were responsible for the maintenance of mouse colonies and final approval of the version to be published. GAR (University of Montreal, Imperial College) designed the study and wrote the manuscript with EG (Imperial College) with input and final approval of the version to be published from all authors. GAR is the guarantor of this work and, as such, had full access to all

562 the data in the study and takes responsibility for the integrity of the data and the
563 accuracy of the data analysis.
564
565 **Funding**
566 GAR was supported by a Wellcome Trust Senior Investigator Award (098424AIA) and
567 Investigator Award (212625/Z/18/Z), MRC Programme grants (MR/R022259/1,
568 MR/J0003042/1, MR/L020149/1), an Experimental Challenge Grant (DIVA,
569 MR/L02036X/1), an MRC grant (MR/N00275X/1), and a Diabetes UK grant
570 (BDA/11/0004210, BDA/15/0005275, BDA16/0005485). IL was supported by a
571 Diabetes UK project grant (16/0005485). This project has received funding from the
572 Innovative Medicines Initiative 2 Joint Undertaking, under grant agreement no. 115881
573 (RHAPSODY). This Joint Undertaking receives support from the European Union's
574 Horizon 2020 research and innovation programme and EFPIA. This work is supported
575 by the Swiss State Secretariat for Education, Research and Innovation (SERI), under
576 contract no. 16.0097. AT was supported by MRC project grant MR/R010676/1.
577 Intravital imaging was performed using resources and/or funding provided by National
578 Institutes of Health grants R03 DK115990 (to AKL), Human Islet Research Network
579 UC4 DK104162 (to AKL; RRID:SCR_014393). BJ acknowledges support from the
580 Academy of Medical Sciences, Society for Endocrinology, The British Society for
581 Neuroendocrinology, the European Federation for the Study of Diabetes, an EPSRC
582 capital award and the MRC (MR/R010676/1). SAS was supported by the JDRF (CDA-
583 2016-189, SRA-2018-539, COE-2019-861), the NIH (R01 DK108921, U01
584 DK127747), and the US Department of Veterans Affairs (I01 BX004444).
585
586

Conflict of interest

Authors' relationships and activities GAR has received grant funding and consultancy fees from Les Laboratoires Servier and Sun Pharmaceuticals. The remaining authors declare that there are no relationships or activities that might bias, or be perceived to bias, their work.

Guarantor Statement

GAR is the guarantor of this work and, as such, had full access to all the data in the study and takes responsibility for the integrity of the data and the accuracy of the data analysis.

Prior Presentation Information

This study has been previously presented as an oral or poster presentation at ADA 2021, Australasian Diabetes Congress 2021, ADA 2020, Diabetes UK 2019, Gordon Research conferences 2019, Rhapsody Consortium, EASD 2018.

References

1. Anderson, A.J., et al., Mitochondria-hubs for regulating cellular biochemistry: emerging concepts and networks. Open biology, 2019. 9(8): p. 190126-190126.
2. Rutter, G.A., et al., Pancreatic β-cell identity, glucose sensing and the control of insulin secretion. Biochem J, 2015. 466(2): p. 203-18.
3. Rorsman, P. and F.M. Ashcroft, Pancreatic β-Cell Electrical Activity and Insulin Secretion: Of Mice and Men. Physiol Rev, 2018. 98(1): p. 117-214.
4. Henquin, J.C., Triggering and amplifying pathways of regulation of insulin secretion by glucose. Diabetes, 2000. 49(11): p. 1751-60.
5. Jones, B., et al., Control of insulin secretion by GLP-1. Peptides, 2018. 100: p. 75-84.
6. Yang, D., et al., Mitochondrial Dynamics: A Key Role in Neurodegeneration and a Potential Target for Neurodegenerative Disease. Frontiers in Neuroscience, 2021. 15(359).
7. Rutter, G.A. and R. Rizzuto, Regulation of mitochondrial metabolism by ER Ca2+ release: an intimate connection. Trends in Biochemical Sciences, 2000. 25(5): p. 215-221.
8. Westermann, B., Bioenergetic role of mitochondrial fusion and fission. Biochim Biophys Acta, 2012. 1817(10): p. 1833-8.
9. Ma, K., et al., Mitophagy, Mitochondrial Homeostasis, and Cell Fate. Front Cell Dev Biol, 2020. 8: p. 467.
10. Filadi, R., et al., On the role of Mitofusin 2 in endoplasmic reticulum-mitochondria tethering. Proc Natl Acad Sci U S A, 2017. 114(12): p. E2266-e2267.
11. Rovira-Llopis, S., et al., Mitochondrial dynamics in type 2 diabetes: Pathophysiological implications. Redox Biol, 2017. 11: p. 637-645.
12. Serasinghe, M.N. and J.E. Chipuk, Mitochondrial Fission in Human Diseases. Handb Exp Pharmacol, 2017. 240: p. 159-188.
13. Reinhardt, F., et al., Drp1 guarding of the mitochondrial network is important for glucose-stimulated insulin secretion in pancreatic beta cells. Biochem Biophys Res Commun, 2016. 474(4): p. 646-651.
14. Hennings, T.G., et al., In Vivo Deletion of beta-Cell Drp1 Impairs Insulin Secretion Without Affecting Islet Oxygen Consumption. Endocrinology, 2018. 159(9): p. 3245-3256.
15. Supale, S., et al., Loss of prohibitin induces mitochondrial damages altering β-cell function and survival and is responsible for gradual diabetes development. Diabetes, 2013. 62(10): p. 3488-3499.
16. Stiles, L. and O.S. Shirihai, Mitochondrial dynamics and morphology in beta-cells. Best Pract Res Clin Endocrinol Metab, 2012. 26(6): p. 725-38.
17. Zhang, Z., et al., The dynamin-related GTPase Opa1 is required for glucose-stimulated ATP production in pancreatic beta cells. Mol Biol Cell, 2011. 22(13): p. 2235-45.
18. Men, X., et al., Dynamin-related protein 1 mediates high glucose induced pancreatic beta cell apoptosis. The International Journal of Biochemistry & Cell Biology, 2009. 41(4): p. 879-890.
19. Del Guerra, S., et al., Functional and Molecular Defects of Pancreatic Islets in Human Type 2 Diabetes. Diabetes, 2005. 54(3): p. 727-735.
20. Chen, H., J.M. McCaffery, and D.C. Chan, Mitochondrial fusion protects against neurodegeneration in the cerebellum. Cell, 2007. 130(3): p. 548-62.

21. Gu, G., J. Dubauskaite, and D.A. Melton, Direct evidence for the pancreatic lineage: NGN3+ cells are islet progenitors and are distinct from duct progenitors. Development, 2002. 129(10): p. 2447-57.
22. Soleimanpour, S.A., et al., The diabetes susceptibility gene Clec16a regulates mitophagy. Cell, 2014. 157(7): p. 1577-1590.
23. Ravier, M.A. and G.A. Rutter, Isolation and culture of mouse pancreatic islets for ex vivo imaging studies with trappable or recombinant fluorescent probes. Methods Mol Biol, 2010. 633: p. 171-84.
24. Georgiadou, E., et al., The pore-forming subunit MCU of the mitochondrial Ca2+ uniporter is required for normal glucose-stimulated insulin secretion in vitro and in vivo in mice. Diabetologia, 2020. 63(7): p. 1368-1381.
25. Kolesar, J.E., et al., Two-dimensional intact mitochondrial DNA agarose electrophoresis reveals the structural complexity of the mammalian mitochondrial genome. Nucleic Acids Res, 2013. 41(4): p. e58.
26. Ravier, M.A., et al., Mechanisms of control of the free Ca2+ concentration in the endoplasmic reticulum of mouse pancreatic β-cells: interplay with cell metabolism and [Ca2+]c and role of SERCA2b and SERCA3. Diabetes, 2011. 60(10): p. 2533-45.
27. Varadi, A. and G.A. Rutter, Dynamic imaging of endoplasmic reticulum Ca2+ concentration in insulin-secreting MIN6 Cells using recombinant targeted cameleons: roles of sarco(endo)plasmic reticulum Ca2+-ATPase (SERCA)-2 and ryanodine receptors. Diabetes, 2002. 51 Suppl 1: p. S190-201.
28. Nikolaev, V.O., et al., Novel Single Chain cAMP Sensors for Receptor-induced Signal Propagation. Journal of Biological Chemistry, 2004. 279(36): p. 37215-37218.
29. Wiemerslage, L. and D. Lee, Quantification of mitochondrial morphology in neurites of dopaminergic neurons using multiple parameters. J Neurosci Methods, 2016. 262: p. 56-65.
30. Li, D., et al., Imaging dynamic insulin release using a fluorescent zinc indicator for monitoring induced exocytotic release (ZIMIR). Proc Natl Acad Sci U S A, 2011. 108(52): p. 21063-8.
31. Tsuboi, T. and G.A. Rutter, Multiple forms of "kiss-and-run" exocytosis revealed by evanescent wave microscopy. Curr Biol, 2003. 13(7): p. 563-7.
32. Ahonen, L., et al., Targeted Clinical Metabolite Profiling Platform for the Stratification of Diabetic Patients. Metabolites, 2019. 9(9): p. 184.
33. Taddeo, E.P., et al., Mitochondrial Proton Leak Regulated by Cyclophilin D Elevates Insulin Secretion in Islets at Nonstimulatory Glucose Levels. Diabetes, 2020. 69(2): p. 131-145.
34. Brand, M.D. and D.G. Nicholls, Assessing mitochondrial dysfunction in cells. The Biochemical journal, 2011. 435(2): p. 297-312.
35. Carrat, G.R., et al., The type 2 diabetes gene product STARD10 is a phosphoinositide-binding protein that controls insulin secretory granule biogenesis. Molecular Metabolism, 2020. 40: p. 101015.
36. Akalestou, E., et al., Intravital imaging of islet Ca2+ dynamics reveals enhanced β cell connectivity after bariatric surgery in mice. Nature Communications, 2021. 12(1): p. 5165.
37. Cruciani-Guglielmacci, C., et al., Molecular phenotyping of multiple mouse strains under metabolic challenge uncovers a role for Elovl2 in glucose-induced insulin secretion. Molecular Metabolism, 2017. 6(4): p. 340-351.

38. Benjamini, Y. and Y. Hochberg, Controlling the false discovery rate: a practical and powerful approach to multiple testing. Journal of the Royal Statistical Society Series B, 1995. 57: p. 289–300.
39. Elayat, A.A., M.M. el-Naggar, and M. Tahir, An immunocytochemical and morphometric study of the rat pancreatic islets. J Anat, 1995. 186 (Pt 3)(Pt 3): p. 629-37.
40. Pullen, T.J., M.O. Huising, and G.A. Rutter, Analysis of Purified Pancreatic Islet Beta and Alpha Cell Transcriptomes Reveals 11β-Hydroxysteroid Dehydrogenase (Hsd11b1) as a Novel Disallowed Gene. Frontiers in Genetics, 2017. 8(41).
41. Georgiadou, E., et al., Mitofusins Mfn1 and Mfn2 are required to preserve glucose-but not incretin-stimulated beta cell connectivity and insulin secretion. bioRxiv, 2021: p. 2020.04.22.055384.
42. Rutter GA, et al., Metabolic and functional specialisations of the pancreatic beta cell: gene disallowance, mitochondrial metabolism and intercellular connectivity. Diabetologia under review, 2020.
43. Johnston, N.R., et al., Beta Cell Hubs Dictate Pancreatic Islet Responses to Glucose. Cell Metab, 2016. 24(3): p. 389-401.
44. Gautam, D., et al., A critical role for beta cell M3 muscarinic acetylcholine receptors in regulating insulin release and blood glucose homeostasis in vivo. Cell Metab, 2006. 3(6): p. 449-61.
45. Gautam, D., et al., Beneficial metabolic effects caused by persistent activation of beta-cell M3 muscarinic acetylcholine receptors in transgenic mice. Endocrinology, 2010. 151(11): p. 5185-94.
46. Gembal, M., P. Gilon, and J.C. Henquin, Evidence that glucose can control insulin release independently from its action on ATP-sensitive K+ channels in mouse B cells. The Journal of Clinical Investigation, 1992. 89(4): p. 1288-1295.
47. Benner, C., et al., The transcriptional landscape of mouse beta cells compared to human beta cells reveals notable species differences in long non-coding RNA and protein-coding gene expression. BMC Genomics, 2014. 15(1): p. 620.
48. Sidarala, V., et al., Mitofusins 1 and 2 collaborate to fuel pancreatic beta cell insulin release via regulation of both mitochondrial structure and DNA content. bioRxiv, 2021: p. 2021.01.10.426151.
49. Andersén, E., G. Karlaganis, and J. Sjövall, Altered bile acid profiles in duodenal bile and urine in diabetic subjects. Eur J Clin Invest, 1988. 18(2): p. 166-72.
50. Uchida, K., S. Makino, and T. Akiyoshi, Altered Bile Acid Metabolism in Nonobese, Spontaneously Diabetic (NOD) Mice. Diabetes, 1985. 34(1): p. 79-83.
51. Sailer, M., et al., Increased plasma citrulline in mice marks diet-induced obesity and may predict the development of the metabolic syndrome. PLoS One, 2013. 8(5): p. e63950.
52. Lamichhane, S., et al., Dynamics of Plasma Lipidome in Progression to Islet Autoimmunity and Type 1 Diabetes - Type 1 Diabetes Prediction and Prevention Study (DIPP). Scientific reports, 2018. 8(1): p. 10635-10635.
53. George, A.M., A.G. Jacob, and L. Fogelfeld, Lean diabetes mellitus: An emerging entity in the era of obesity. World journal of diabetes, 2015. 6(4): p. 613-620.

54. Mitchell, R.K., et al., The transcription factor Pax6 is required for pancreatic β cell identity, glucose-regulated ATP synthesis and Ca2+ dynamics in adult mice. Journal of Biological Chemistry, 2017.
55. Martinez-Sanchez, A., M.-S. Nguyen-Tu, and G.A. Rutter, DICER Inactivation Identifies Pancreatic β-Cell "Disallowed" Genes Targeted by MicroRNAs. Molecular endocrinology (Baltimore, Md.), 2015. 29(7): p. 1067-1079.
56. Nauck, M.A., et al., GLP-1 receptor agonists in the treatment of type 2 diabetes - state-of-the-art. Mol Metab, 2020: p. 101102.
57. Nakazaki, M., et al., cAMP-Activated Protein Kinase-Independent Potentiation of Insulin Secretion by cAMP Is Impaired in SUR1 Null Islets. Diabetes, 2002. 51(12): p. 3440-3449.
58. Kashima, Y., et al., Critical Role of cAMP-GEFII·Rim2 Complex in Incretin-potentiated Insulin Secretion*. Journal of Biological Chemistry, 2001. 276(49): p. 46046-46053.
59. Chepurny, O.G., et al., PKA-dependent potentiation of glucose-stimulated insulin secretion by Epac activator 8-pCPT-2'-O-Me-cAMP-AM in human islets of Langerhans. Am J Physiol Endocrinol Metab, 2010. 298(3): p. E622-33.
60. Renström, E., L. Eliasson, and P. Rorsman, Protein kinase A-dependent and -independent stimulation of exocytosis by cAMP in mouse pancreatic B-cells. The Journal of physiology, 1997. 502 (Pt 1)(Pt 1): p. 105-118.
61. de Rooij, J., et al., Epac is a Rap1 guanine-nucleotide-exchange factor directly activated by cyclic AMP. Nature, 1998. 396(6710): p. 474-7.
62. Kawasaki, H., et al., A family of cAMP-binding proteins that directly activate Rap1. Science, 1998. 282(5397): p. 2275-9.
63. Ozaki, N., et al., cAMP-GEFII is a direct target of cAMP in regulated exocytosis. Nat Cell Biol, 2000. 2(11): p. 805-11.
64. Kashima, Y., et al., Critical role of cAMP-GEFII--Rim2 complex in incretin-potentiated insulin secretion. J Biol Chem, 2001. 276(49): p. 46046-53.
65. Wang, Y., et al., Glucagon-like peptide-1 can reverse the age-related decline in glucose tolerance in rats. J Clin Invest, 1997. 99(12): p. 2883-9.
66. Lochner, A. and J.A. Moolman, The many faces of H89: a review. Cardiovasc Drug Rev, 2006. 24(3-4): p. 261-74.
67. Gilon, P., et al., Uptake and release of Ca2+ by the endoplasmic reticulum contribute to the oscillations of the cytosolic Ca2+ concentration triggered by Ca2+ influx in the electrically excitable pancreatic B-cell. J Biol Chem, 1999. 274(29): p. 20197-205.
68. Salem, V., et al., Leader β-cells coordinate Ca2+ dynamics across pancreatic islets in vivo. Nature Metabolism, 2019. 1(6): p. 615-629.

Figure legends

Fig.1 Generation of a conditional β*Mfn1/2* dKO mouse line which displays a highly impaired glucose tolerance *in vivo*. (A) qRT-PCR quantification of *Mfn1, Mfn2, Drp1, Opa1* and *Fis1* expression in control and dKO islets relative to *β-actin* (*n*=3-5 mice per genotype in two independent experiments).(B) Western blot analysis demonstrating efficient MFN1 (84 kDa) and MFN2 (86 kDa) deletion relative to GAPDH (36 kDa) in isolated islets (*n*=3-4 mice per genotype in three independent experiments).(C) Glucose tolerance was measured in dKO mice and littermate controls by IPGTT (1 g/kg body weight).(D) Corresponding AUC from (C) (*n*=8 mice per genotype,in 2 independent experiments). (E) Glucose tolerance measured by IPGTT (using 3 g/kg body weight) and (F) the corresponding AUC were assessed in β*Mfn1/2* dKO and control mice (*n*=8 mice per genotype in two independent experiments). (G) Plasma insulin levels during IPGTT in dKO and control mice (*n*=11-12 mice per genotype in three independent experiments) and (H) the corresponding AUC. (I) Glucose tolerance post-oral gavage (3 g/kg body weight) was measured in *n*=8 animals per genotype in two independent experiments. Glucose baseline values between control and dKO mice were significantly different (*p<0.05). Increases in glucose from baseline in control animals were ****p<0.0001, ***p<0.001 and **p<0.01 and ****p<0.0001 in dKO animals from 15 to 60mins accordingly. The corresponding AUC is shown in (J). (K) Plasma insulin levels during OGTT in dKO and control mice (*n*=8 mice per genotype in two independent experiments) and (L) the corresponding AUC. (Blue, *control* mice; red, *dKO* mice. Data are presented as mean±SD in A and mean±SEM in B-L. *p<0.05; **p<0.01; ***p<0.001; ****p<0.0001 as indicated, or *control* vs *dKO* mice at the time points as indicated in (K), analysed by unpaired two-tailed Student's t-test and Mann–Whitney correction or two-way ANOVA test and Sidak's multiple comparisons test. All experiments were performed in 14-week-old male mice.

Fig.2 Mitochondrial ultrastructure is altered following *Mfn1/2* deletion. (A) Confocal images of the mitochondrial network of dissociated beta cells stained with Mitotracker green; scale bar: 5 μm. Lower right panels: magnification of selected areas. (B) Mitochondrial morphology analysis on deconvolved confocal images of dissociated beta cells. A macro was developed to quantify the number of mitochondria

per cell and measure the elongation, perimeter, circularity (0: elongated; 1: circular mitochondria), density and surface area of the organelles in control and dKO animals (*n*=40-54 cells; *n*=3 mice per genotype). (C) Electron micrographs of mitochondria indicated with black arrows in islets isolated from control and dKO mice; scale bars: 1μm. Right panel: magnification of selected areas showing the cristae structure (black arrow heads); scale bar: 0.5 μm. Schematic representation of enlarged mitochondria. (D) The relative mitochondrial DNA copy number was measured by determining the ratio of the mtDNA-encoded gene *mt-Nd1* to the nuclear gene *Ndufv1* (*n*=3 mice per genotype). Data are presented as mean±SEM in A-C and mean±SD in D. *p<0.05, ***p<0.001, ****p<0.0001 as indicated, analysed by unpaired two-tailed Student's t-test and Mann–Whitney correction. Experiments were performed in 14-week-old male mice.

Fig.3 Absence of *Mfn1/2* in beta cells leads to decreased beta cell mass and increased beta cell apoptosis.(A) Representative pancreatic sections immunostained with glucagon (red) and insulin (green); scale bars: 50μm.(B) The beta cell and alpha cell surface (C) measured within the whole pancreatic area in control and dKO mice were determined, as well as the beta/alpha cell ratio in (D), (*n*=79-86 islets, 4 mice per genotype; experiment performed in triplicate).(E) Representative confocal images of islets with TUNEL positive (green) apoptotic beta cells (ROI) and insulin (red). Magnification of selected area displaying each fluorescent channel; scale bar: 5μm. DNase I treated sections were used as a positive control in the TUNEL assay. Scale bars: 20μm.(F) Quantification of the percentage of islets containing TUNEL positive cells (*n*=114-133 islets, 4 mice per genotype; experiment performed in triplicate). Data are presented as mean±SD. *p<0.05, assessed by unpaired two-tailed Student's t-test and Mann–Whitney correction. Experiments were performed in 14-week-old male mice.

Fig.4 *Mfn1/2* deletion from pancreatic beta cells impairs cytosolic and mitochondrial Ca^{2+} uptake and changes mitochondrial potential and ATP synthesis *in vitro*. (A) Each snapshot of isolated control (i–iv) and dKO-derived (v–viii) islets was taken during the time points indicated by the respective arrows in (B). Scale bar: 50 μm. See also ESM Video 1. (B) $[Ca^{2+}]_{cyt}$ traces in response to 3G, 3

mmol/l glucose, 17 mmol/l glucose (17G; with or without 100μmol/l diazoxide [diaz]) or 20 mmol/l KCl with diaz were assessed following Cal-520 uptake in whole islets. Traces represent mean normalised fluorescence intensity over time (F/F_{min}).(C) The corresponding AUC is also presented (*n*=17-26 islets, 4 mice per genotype); 17G AUC measured between 245 s and 1045 s, 17G+diaz AUC measured between 1200 s and 1320 s, and KCl+diaz AUC measured between 1424 s and 1500 s. For each genotype different baselines (ctrl diaz/KCl: 0.95, dKO diaz/KCl: 0.8 were taken into consideration to measure AUCs.(D) Each snapshot of isolated control (i–iv) and dKO-derived (v–viii) islets was taken during the time points indicated by the respective arrows in (E). Scale bar: 50 μm. See also ESM Video 2. (E) $[Ca^{2+}]_{mito}$ changes in response to 17G (with or without diazoxide [diaz]) and 20 mmol/l KCl were assessed in islets following R-GECO infection. Traces represent mean normalised fluorescence intensity over time (F/F_{min}) where F_{min} is the mean fluorescence recorded during imaging under 3 mmol/l glucose.(F) The corresponding AUC is also shown (*n*=20-23 islets, 3 mice per genotype; 17G AUC measured between 270 s and 1100 s, 17G+diaz AUC measured between 1101 s and 1365 s and KCl AUC measured between 1366 s and1500 s).(G) Dissociated beta cells were loaded with TMRE to measure changes in $\Delta\psi_m$, and perifused with 3 mmol/l glucose (3G), 17G or FCCP as indicated. Traces represent normalised fluorescence intensity over time (F/Fmin).(H) AUC was measured between 700–730 s (under 17G exposure) from the data shown in (G) (*n*=146-254 cells,3-6 mice per genotype).(I) Changes in the cytoplasmic ATP:ADP ratio ([ATP:ADP]) in response to 17 mmol/l glucose (17G) was examined in whole islets using the ATP sensor Perceval.(J) AUC values corresponding to (I) were measured between 418–1400 s (under 17G exposure) (data points from *n*=22-23 islets, 3-6 mice per genotype). Data are presented as mean±SDEM. *p<0.05, **p<0.01, assessed by unpaired two-tailed Student's t-test and Mann–Whitney correction or two-way ANOVA test and Sidak's multiple comparisons test. Experiments were performed in 14-week-old male mice.

Fig.5 O_2 consumption and mtDNA are deleteriously affected when *Mfn1/2* are abolished in beta cells, while $[Ca^{2+}]_{ER}$ mobilisation remains unchanged. (A) Each snapshot of isolated control (i–v) and dKO-derived (vi–x) islets was taken during the time points indicated by the respective arrows in (B). Scale bar: 50 μm. See also ESM

Video 3. (B) Changes in $[Ca^{2+}]_{ER}$ were measured in whole islets incubated with Cal-520 and perifused with 17 mmol/l glucose (17G; with or without diazoxide [diaz]), 17G with 100μmol/l acetylcholine (Ach) and diaz, or 20 mmol/l KCl with diaz (C) AUC values corresponding to (B) were measured (17G AUC measured between 260 s and 740 s, 17G+diaz AUC measured between 846 s and 1020 s, 17G+diaz+Ach AUC measured between 1021 s and 1300 s and KCl AUC measured between 1301 s and 1500 s) (n=29-31 islets, 3 mice per genotype). (D) Representative oxygen consumption rate (OCR) traces of islets (~10 per well) were acutely exposed to 20 mmol/l glucose (final concentration), 5μM Oligomycin A (Oligo), 1μM FCCP, and 5μM Rotenone with Antimycin A (AA) (performed in *n*=7 mice, in two independent experiments).(E) Mitochondrial metabolic parameters were extracted from the OCR traces shown in (D). Data are presented as mean±SD in A-C and mean±SEM in D-E. *p<0.05,**p<0.01 assessed by unpaired two-tailed Student's t-test and Mann–Whitney correction or two-way ANOVA test and Sidak's multiple comparisons test. Experiments were performed in 14-week-old male mice.

Fig.6 Impaired insulin secretion can be rescued by GLP-1R agonists *in vitro* by increasing cytosolic Ca^{2+} oscillation frequency. (A) (A) Insulin secretion measured during serial incubations in batches in 3 mmol/l glucose (3G), 10 mmol/l glucose (10G), 17 mmol/l glucose (17G), 10G supplemented with 100 nmol/l exendin-4 (ex4), GLP-1, GIP, 10 μmol/l FSK, 100 μmol/l IBMX or 3G with 20 mmol/l KCl (*n*=3-7 mice per genotype in two independent experiments); (control: 3G vs ex4; p<0.05 and dKO: 3G vs ex4; p<0.0001, or 3G vs GLP-1; p<0.001, or 3G vs GIP; p<0.001). (B) Glucose tolerance measured by IP co-injection of 1g/kg glucose and 3nmol/kg ex4 were assessed in β*Mfn1/2* dKO and control mice (*n*=4-5 mice per genotype, dotted lines). (C) $[Ca^{2+}]_{cyt}$ changes in response to 3G, 3 mmol/l glucose, 10 mmol/l glucose (10G; with or without exendin-4 [ex4]) or 20 mmol/l KCl were assessed following Cal-520 uptake in whole islets. Traces represent mean normalised fluorescence intensity over time (F/F_{min}). See also ESM video 4. Dashed ROIs represent fluorescent segments of extended time scales. Both control and dKO traces reveal faster oscillatory frequencies in response to exendin-4. (D) The corresponding AUC is also presented (*n*=19-20 islets, 3 mice per genotype; 10G AUC measured between 200 s and 660 s, 10G+ex4 AUC measured between 800 s and 950 s), and KCl AUC measured between

1200 s and 1500 s); AUC 10G: control vs dKO; p=0.09; AUC control: 10G vs ex4; p<0.05; AUC dKO: 10G vs ex4; p<0.001; ex4 vs KCl; p<0.05).(E) Dissociated beta cells were transfected with D4ER to measure changes in $[Ca^{2+}]_{ER}$, and perifused with 10 mmol/l glucose (10G), 10G+ex4 or thapsigargin (10G+thapsi) as indicated. Traces represent corrected ratio values post-linear fitting over time. (F) AUC was measured between 350–900 s (under 10G+ex4) and 900-1300 s (10G+thapsi) from the data shown in (E) (*n*=44-46 cells,4-5 mice per genotype). (G) Changes in cytoplasmic ATP:ADP ratio ([ATP:ADP]) in response to 10G or 10G with 100nmol/l ex4 was examined in whole islets.(H) AUC values corresponding to (G) were measured between 185-720s (under 10G exposure) or 721-1200s (under 10G with ex4) (data points from *n*=3 mice per genotype). (I) Average OCR values of islets (~10 per well) that were exposed to 3mmol/l or 10mmol/l glucose (final concentration), 10mmol/l glucose supplemented with ex4, FSK, Oligomycin A (Oligo), FCCP, and Rotenone with Antimycin A (AA) (*n*=3 mice per genotype; experiment performed in duplicate). (J) Insulin secretion measured during serial incubations in batches in 3 or 17 mmol/l glucose supplemented with 100μmol/l diazoxide and 30mmol/l KCl, (*n*=3 mice per genotype in two independent experiments). Data are presented as mean±SDEM. *p<0.05;**p<0.01, ****p<0.0001 assessed by two-way ANOVA test and Sidak's multiple comparisons test. Experiments were performed in 14-week-old male mice.

Fig.7 The GLP1-R agonist, exendin-4, improves intercellular connectivity in βMfn1/2 dKO β-cells. (A) Representative cartesian maps of control and dKO islets with colour coded lines connecting cells according to the strength of Pearson analysis (colour coded *r* values from 0 to 1, blue to red respectively) under 10mmol/L (10G), 10mmol/L with 100nmol/l exendin-4 (10G+ex4) glucose or 20mmol/L KCl; scale bars: 40 μm.(B) Representative heatmaps depicting connectivity strength (*r*) of all cell pairs according to the colour coded *r* values from 0 to 1, blue to yellow respectively.(C) Percentage of connected cell pairs at 10G, 10G+ex4 or KCl (*n*=19-20 islets, 3 mice per genotype).(D) *r* values between β-cells in response to glucose, exendin-4 or KCl (*n*=3 mice per genotype).Data are presented as mean±SDEM. *p<0.05,**p<0.01, ***p<0.001 assessed by two-way ANOVA test and Sidak's multiple comparisons test. Experiments were performed in 14-week-old male mice.

Fig.8 Insulin secretion is rescued through an EPAC-dependent activation in dKO islets. (A) Insulin secretion measured during serial incubations in batches in 3 mmol/l glucose (3G), 10 mmol/l glucose (10G), or 10 mmol/l glucose supplemented with 10µmol/l H89, 10 µmol/l FSK with 100 µmol/l IBMX or H89 (*n*=3 mice per genotype, in two independent experiments). (B) Insulin secretion measured during serial incubations in batches in 10 mmol/l glucose (10G), or 10 mmol/l glucose supplemented with 6µmol/l EPAC-activator, or EPAC-activator with 10µmol/l H89 (*n*=3 mice per genotype, in two independent experiments). (C) Representative Epac1-camps FRET traces in response to 3 or 10 mmol/l glucose, or 10 mmol/l glucose supplemented with 100nmol/l exendin-4 (10G+ex4), or 10 µmol/l FSK with 100 µmol/l IBMX in dissociated beta cells. (D) Fluorescence ratio peak values corresponding to (C) were measured between 200-250s (under 10G), 620-720s (under 10G with ex4) or 1110-1160s (under 10G with IBMX and FSK), (*n*=3-4 mice per genotype, 15-35 cells in two independent experiments). (E) Representative Epac1-camps FRET traces in response to 10 mmol/l glucose, 10 mmol/l glucose supplemented with 100nmol/l exendin-4 (10G+ex4), 10 µmol/l FSK (dark blue or purple traces) or 100 µmol/l IBMX (light blue or pink traces) in dissociated beta cells (*n*=3 mice per genotype,15-45 cells). (F) qRT-PCR quantification of *Epac, Adcy* and *Prka* genes expression in control and dKO islets relative to *β-actin* (*n*=3 mice per genotype in two independent experiments). Data are presented as mean±SDEM. *p<0.05,**p<0.01, ***p<0.001 assessed by two-way ANOVA test and Sidak's multiple comparisons test. Experiments were performed in 14-week-old male mice.

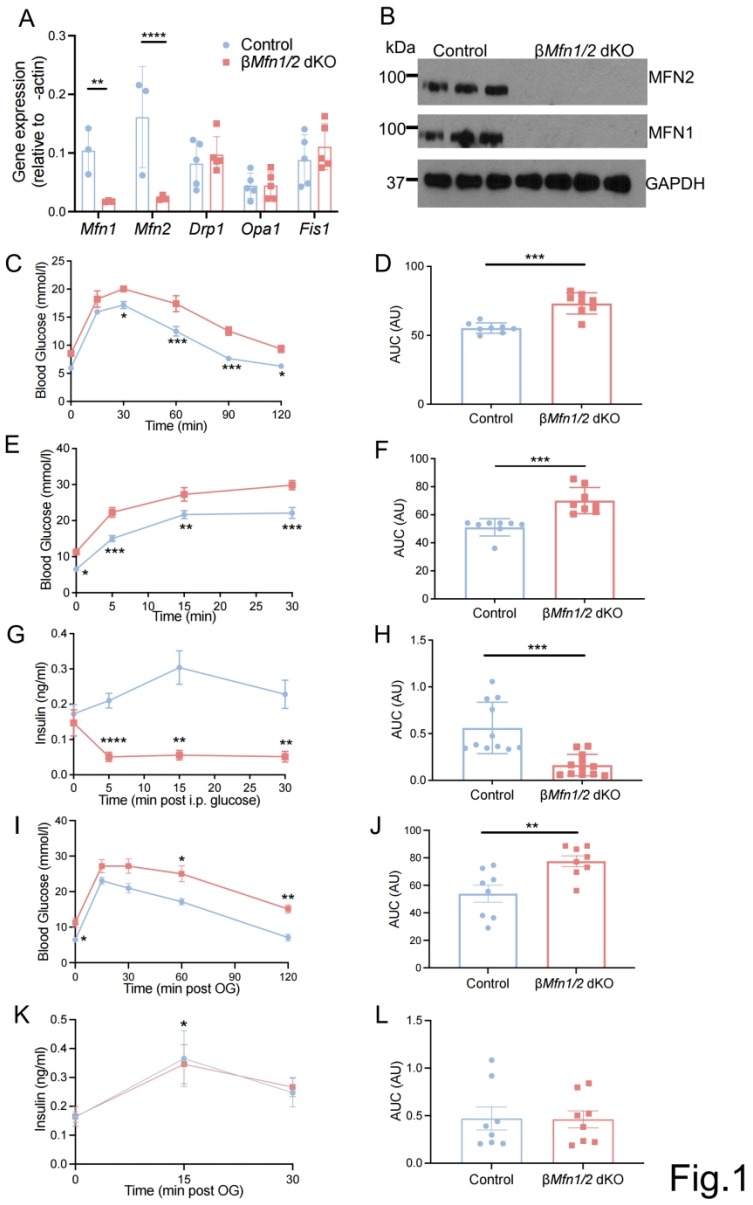

Fig.1

190x275mm (300 x 300 DPI)

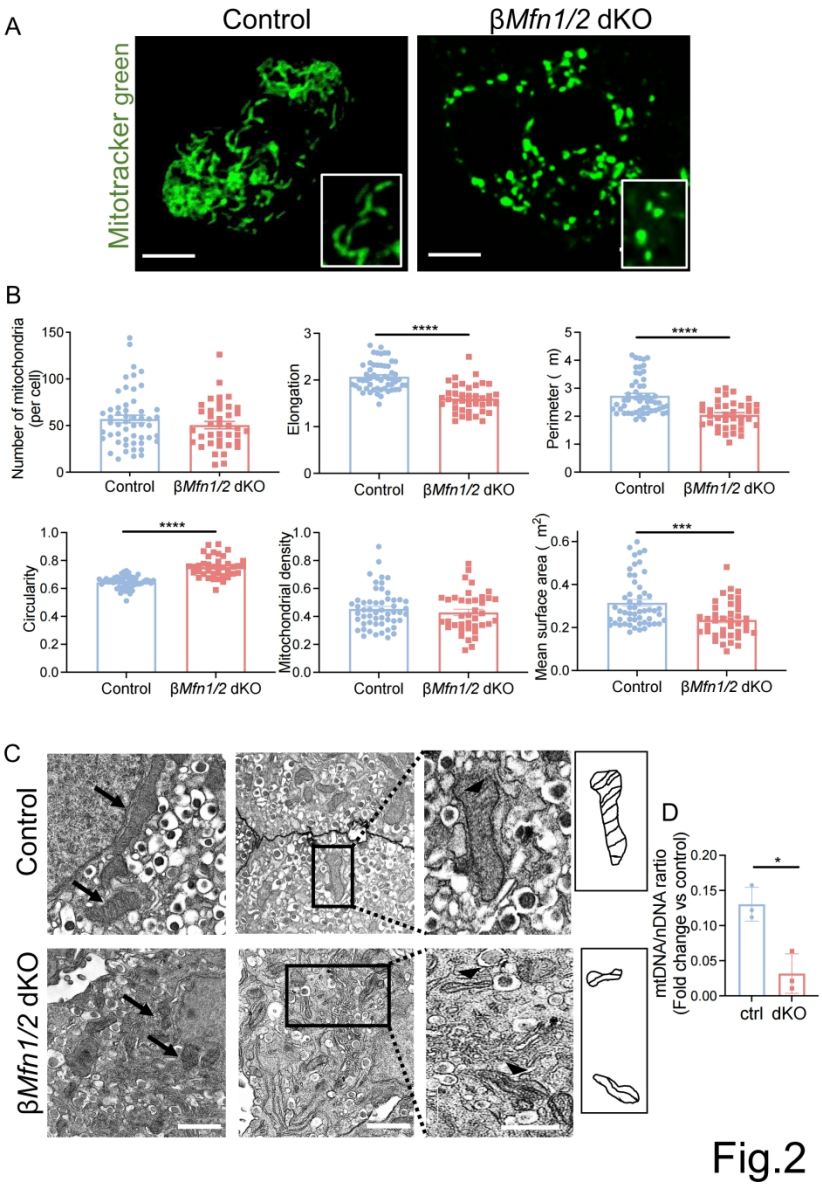

Fig.2

190x275mm (300 x 300 DPI)

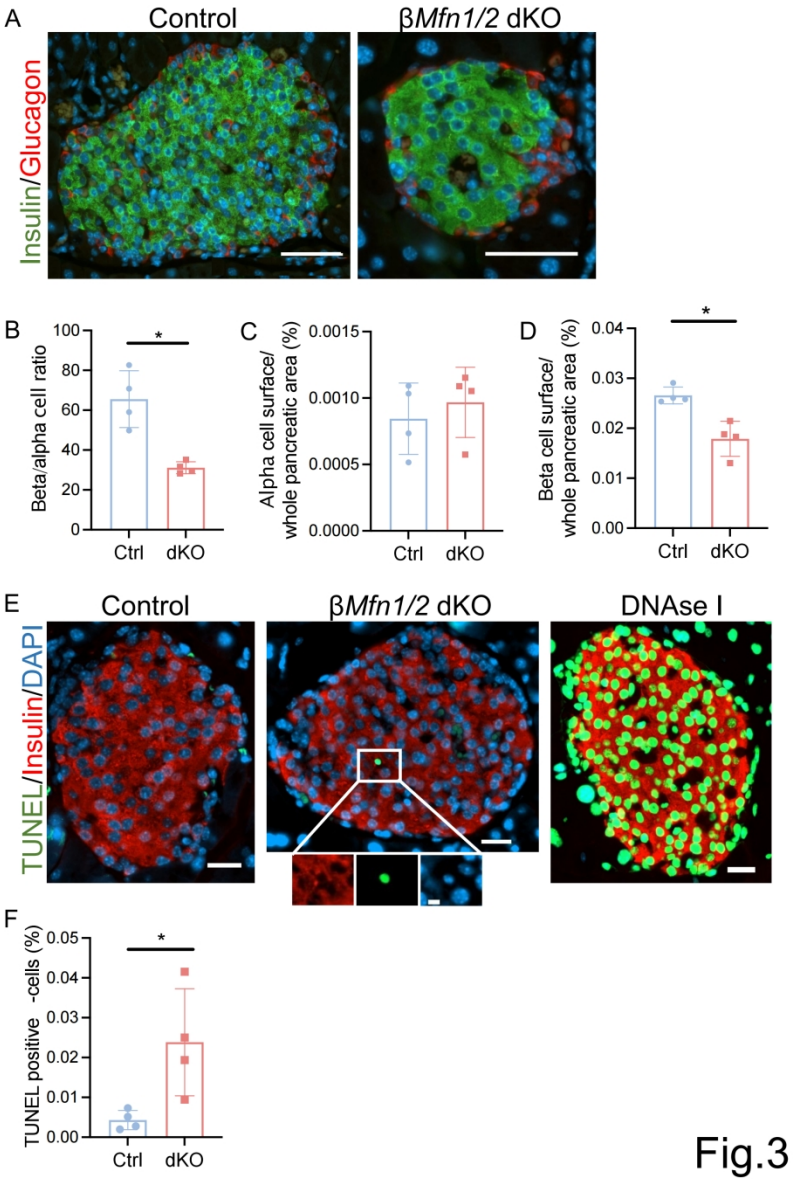

Fig.3

190x275mm (300 x 300 DPI)

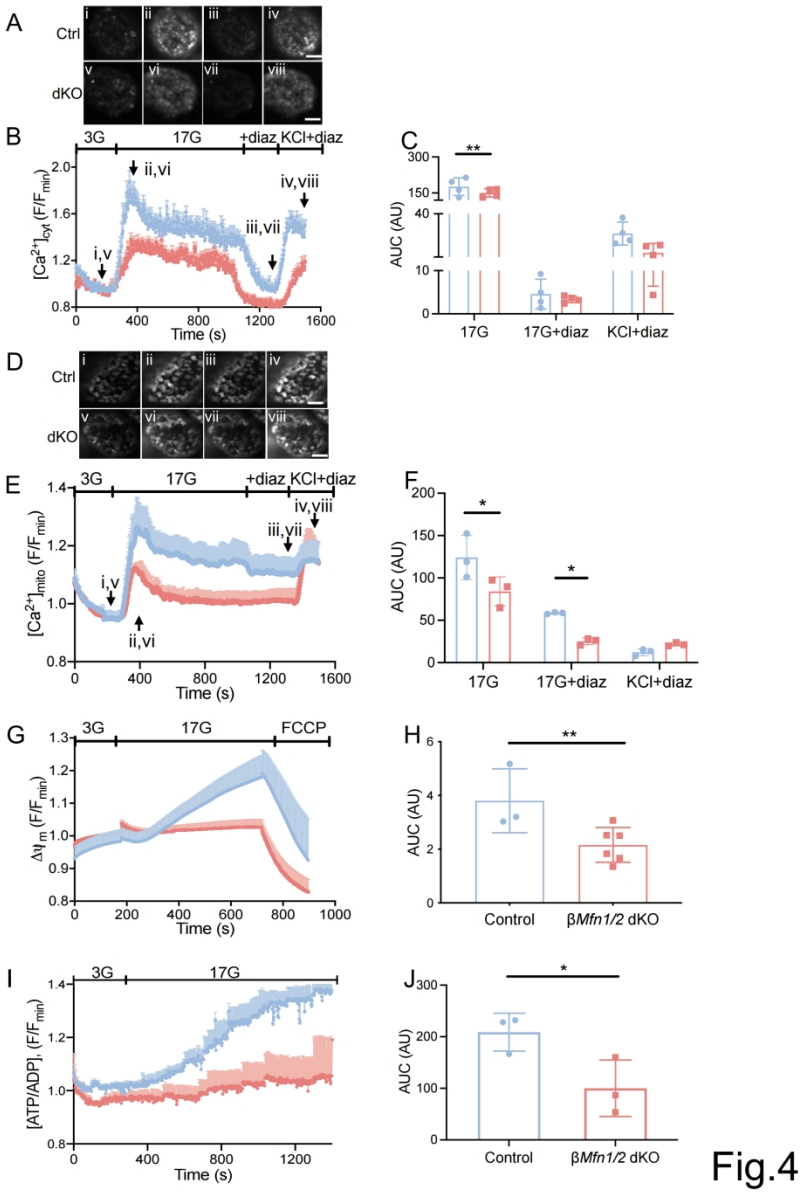

Fig.4

190x275mm (300 x 300 DPI)

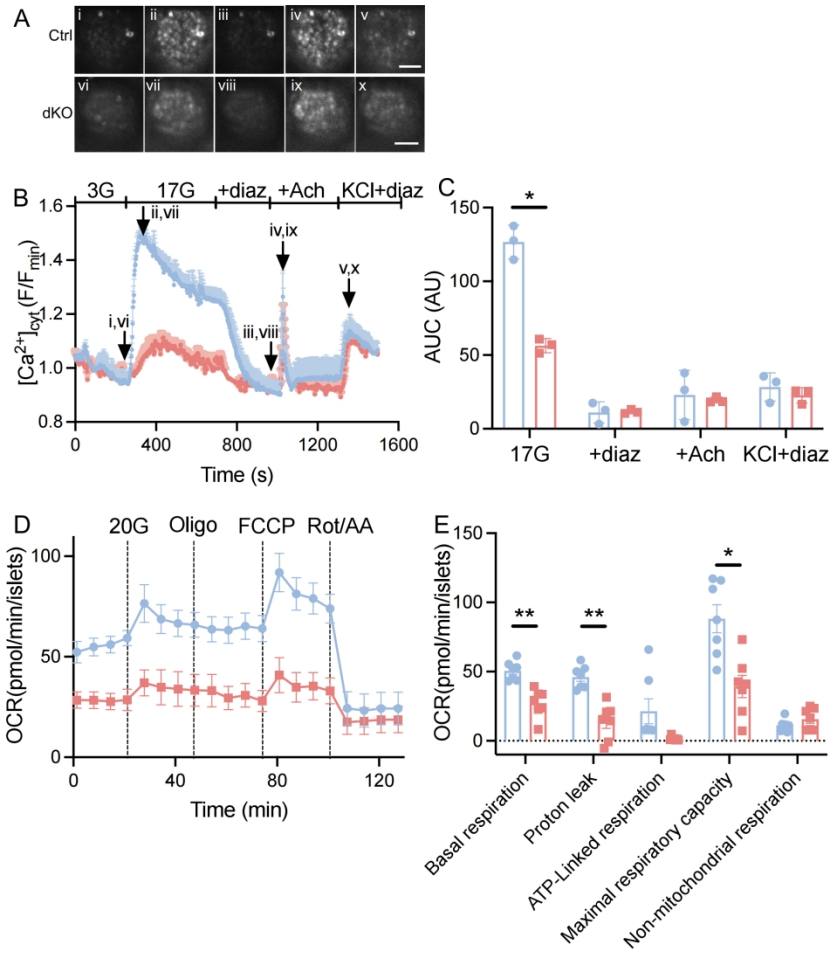

Fig.5

190x275mm (300 x 300 DPI)

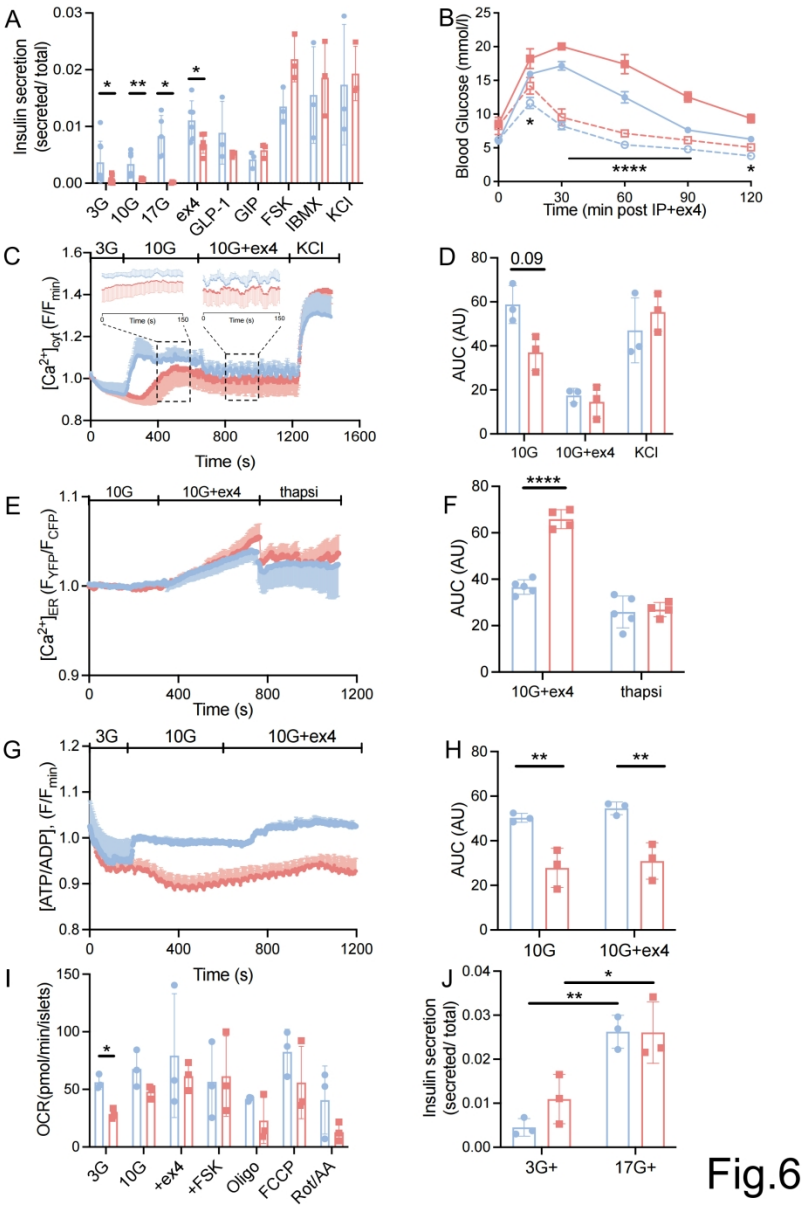

Fig.6

190x275mm (300 x 300 DPI)

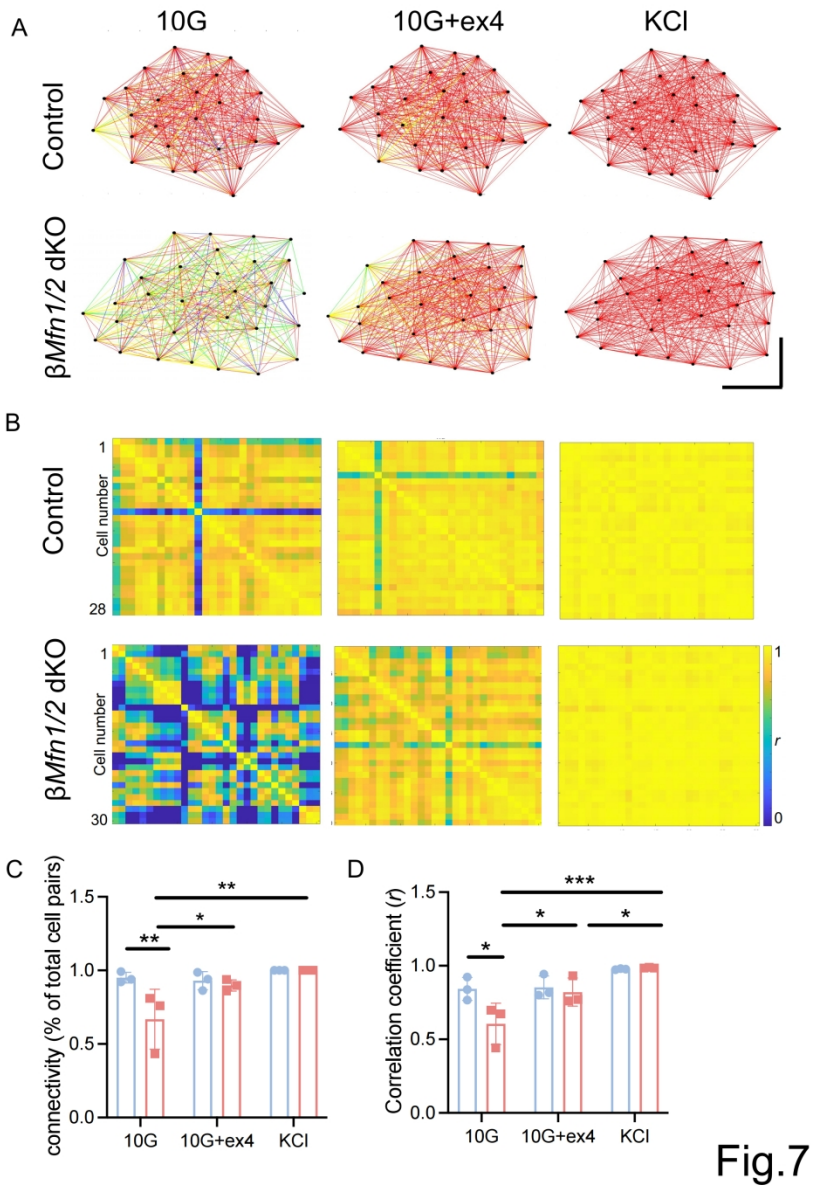

Fig.7

190x275mm (300 x 300 DPI)

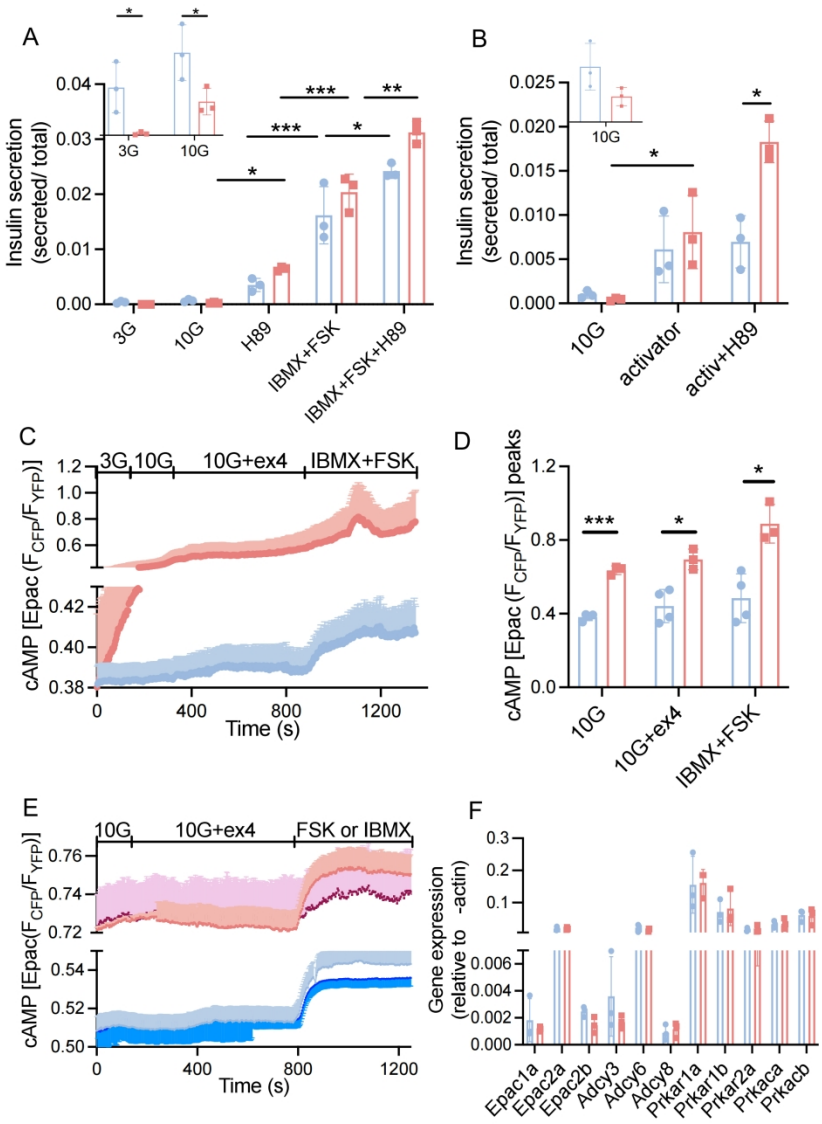

Fig.8

190x275mm (300 x 300 DPI)

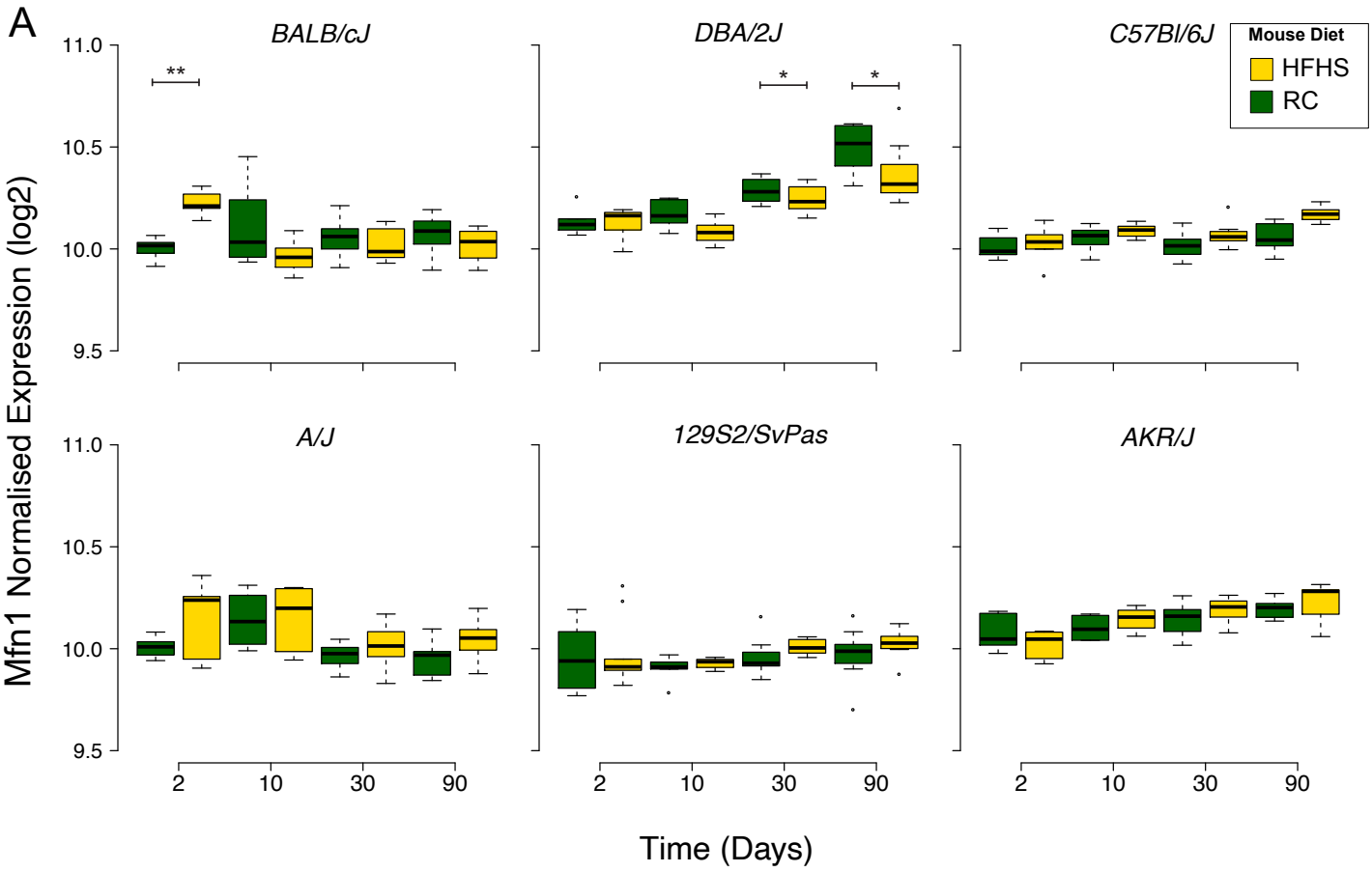

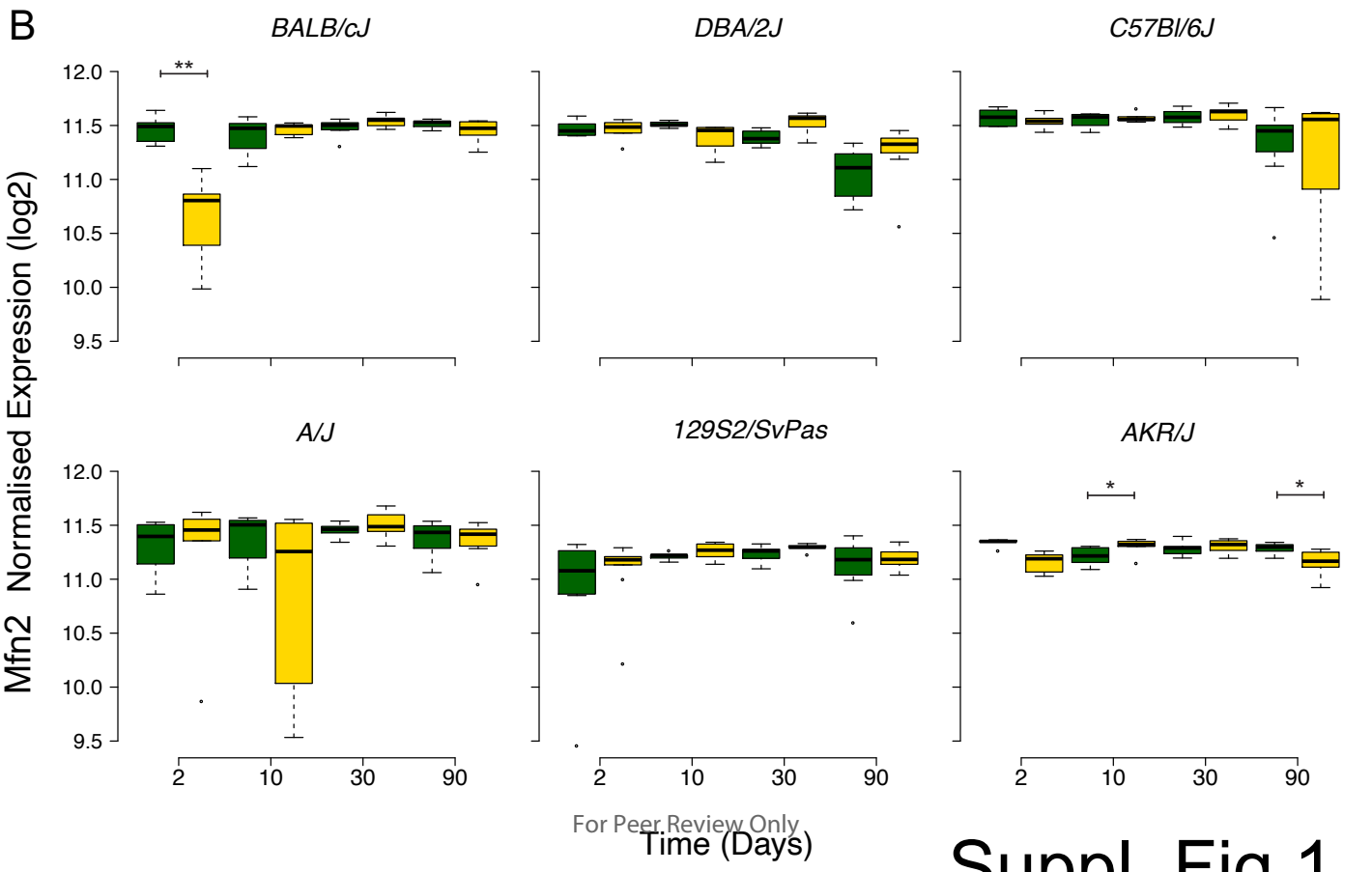

Suppl. Fig.1

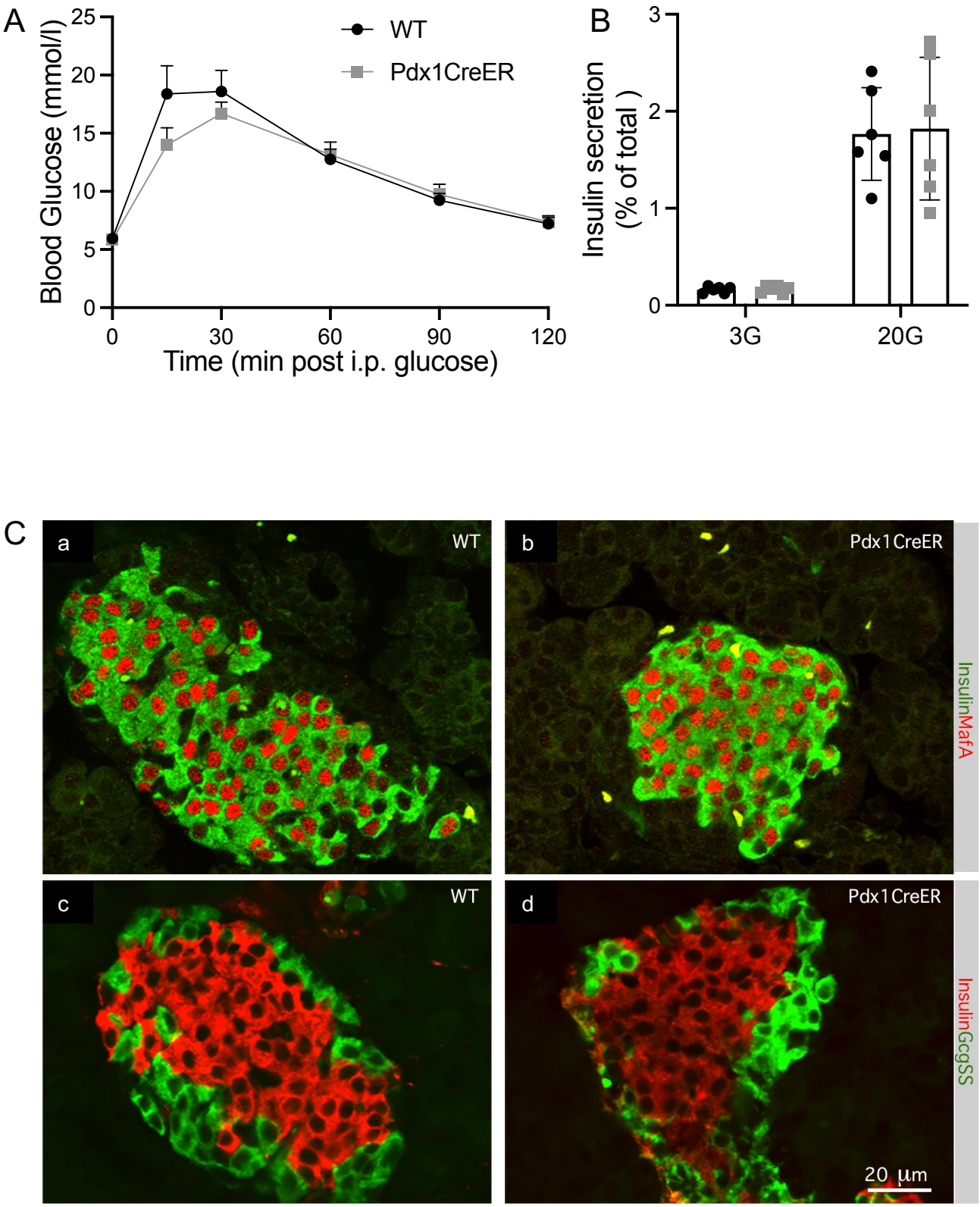
A
Blood Glucose (mmol/l)
25
20
15
10
5
0
0
30
60
90
120
Time (min post i.p. glucose)
WT
Pdx1CreER
B
Insulin secretion
(% of total)
3
2
1
0
3G
20G
C
a
WT
b
Pdx1CreER
InsulinMafA
c
WT
d
Pdx1CreER
InsulinGcgSS
20 µm

Suppl. Fig.2

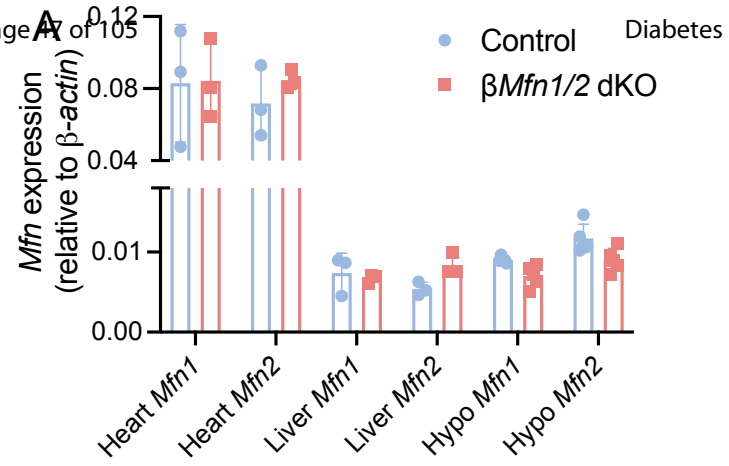

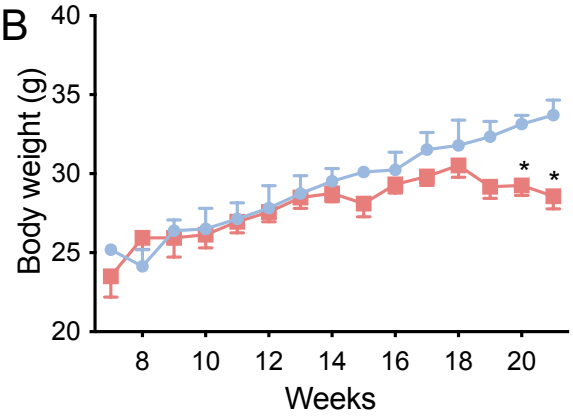

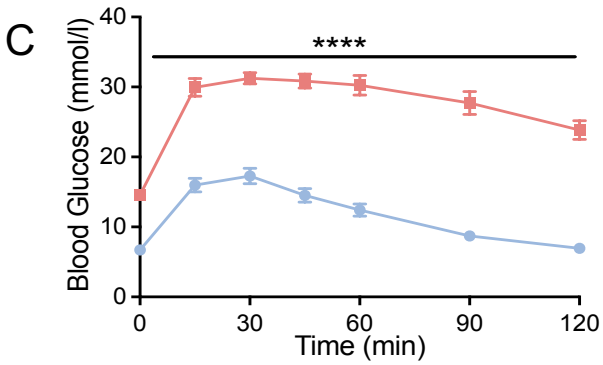

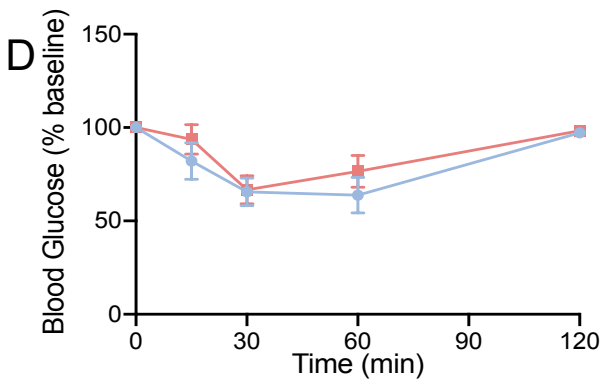

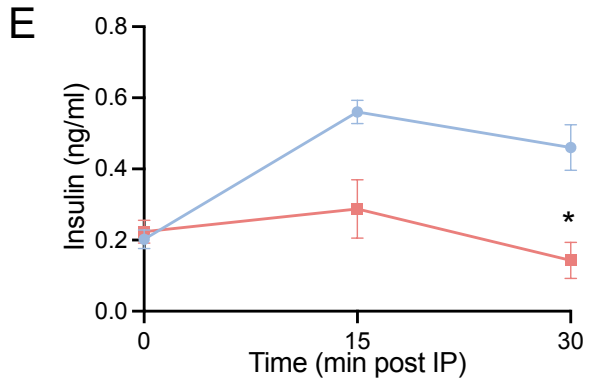

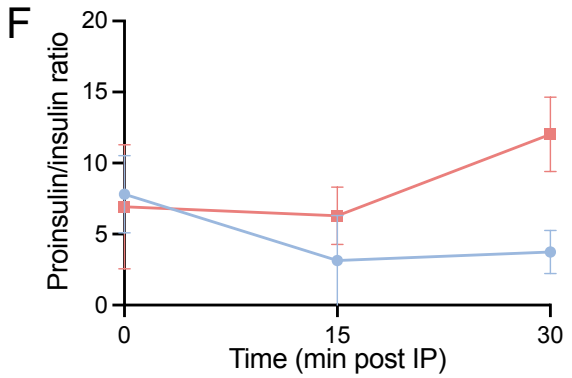

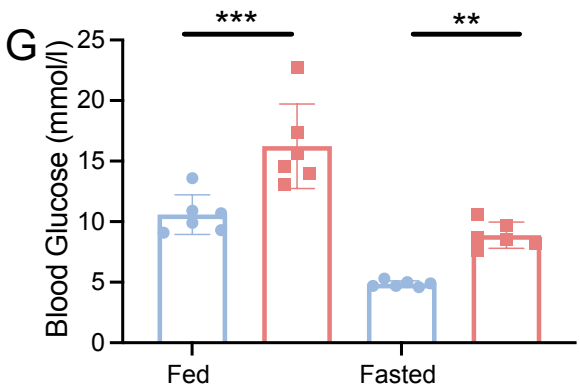

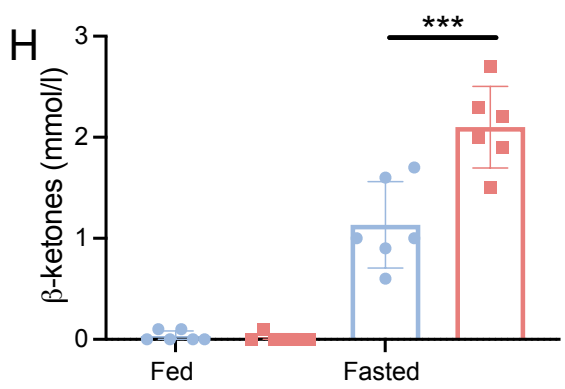

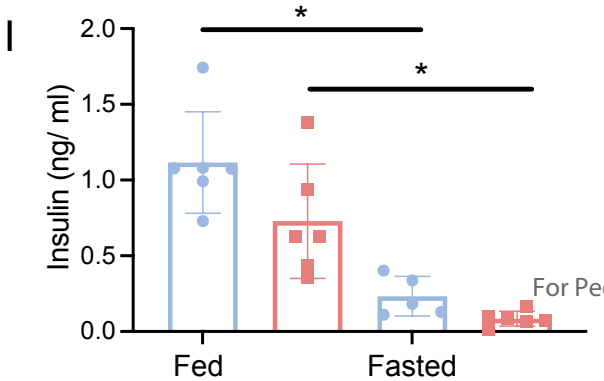

Suppl. Fig.3

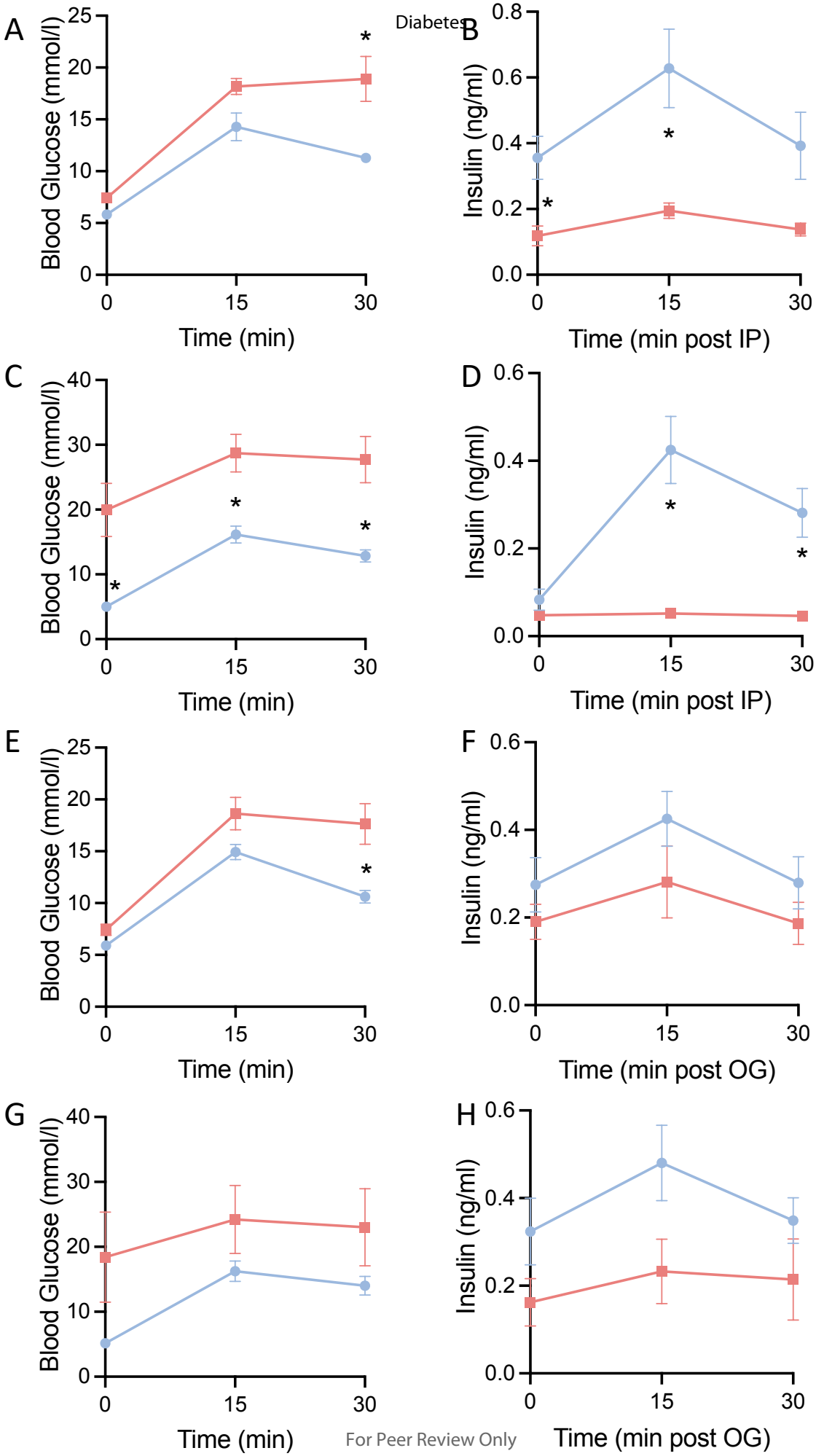

Suppl. Fig.4

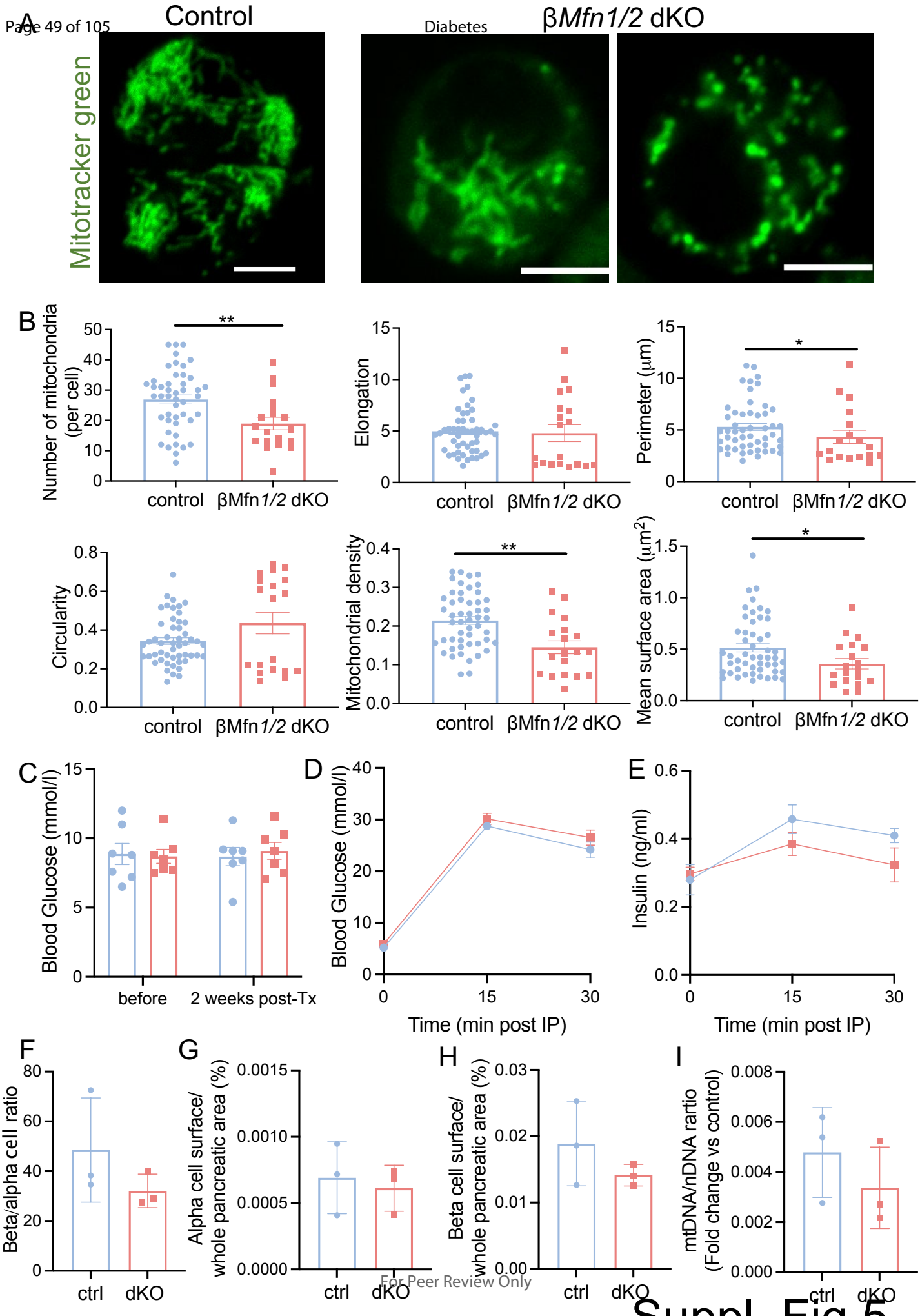

Suppl. Fig.5

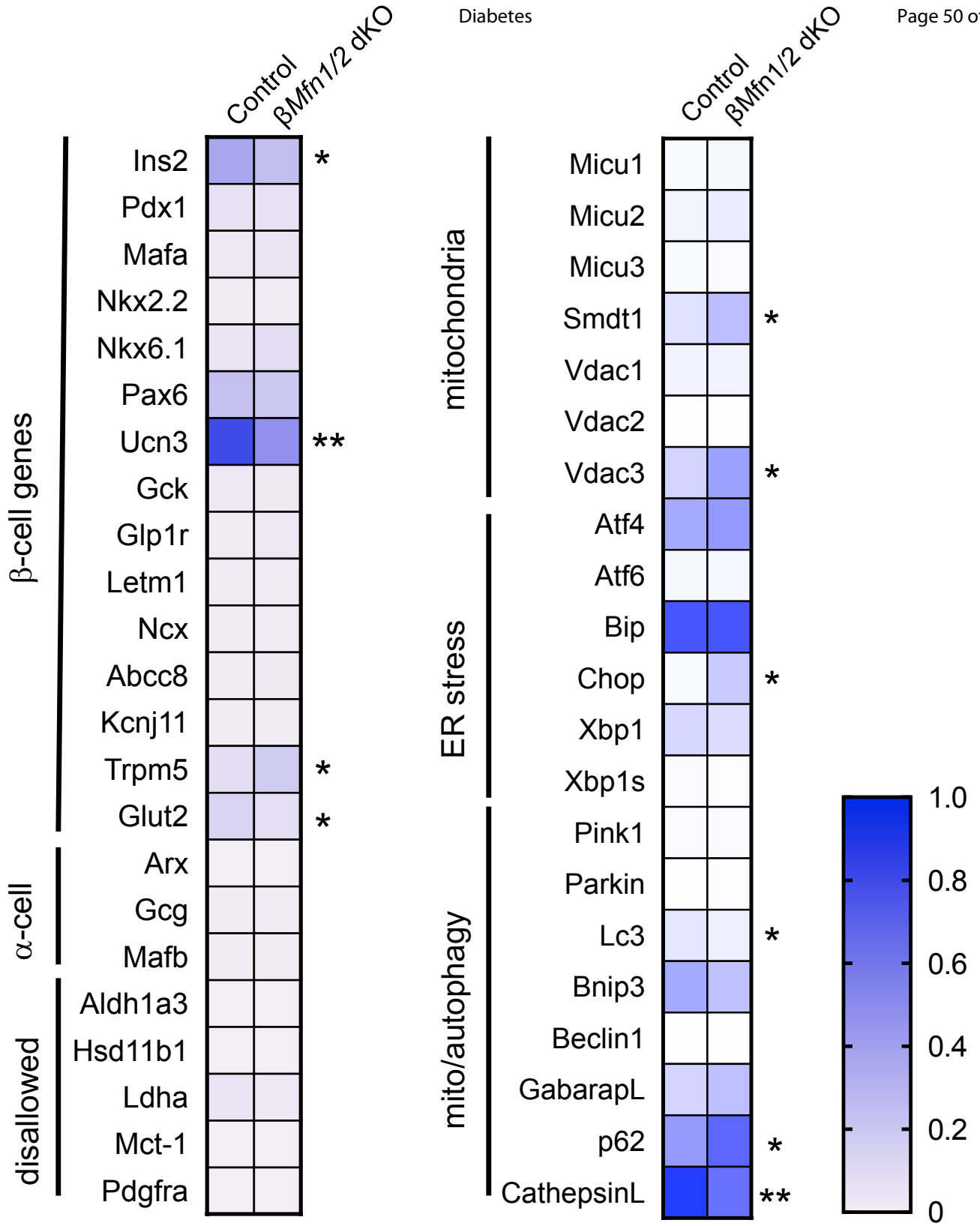
Control
βMfn1/2 dKO
β-cell genes
Ins2
Pdx1
Mafa
Nkx2.2
Nkx6.1
Pax6
Ucn3
Gck
Glp1r
Letm1
Ncx
Abcc8
Kcnj11
Trpm5
Glut2
α-cell
Arx
Gcg
Mafb
disallowed
Aldh1a3
Hsd11b1
Ldha
Mct-1
Pdgfra
*
**
*
*
mitochondria
Micu1
Micu2
Micu3
Smdt1
Vdac1
Vdac2
Vdac3
ER stress
Atf4
Atf6
Bip
Chop
Xbp1
Xbp1s
mito/autophagy
Pink1
Parkin
Lc3
Bnip3
Beclin1
GabarapL
p62
CathepsinL
*
*
*
*
**
1.0
0.8
0.6
0.4
0.2
0

Suppl. Fig.6

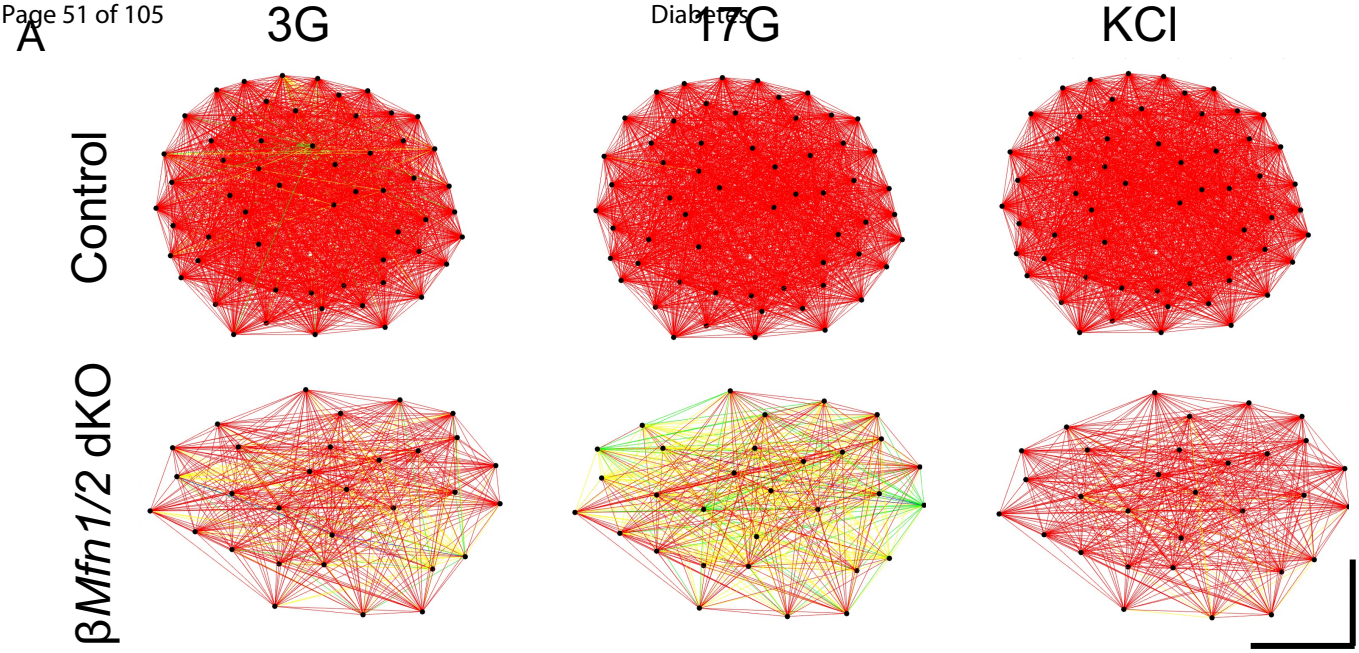

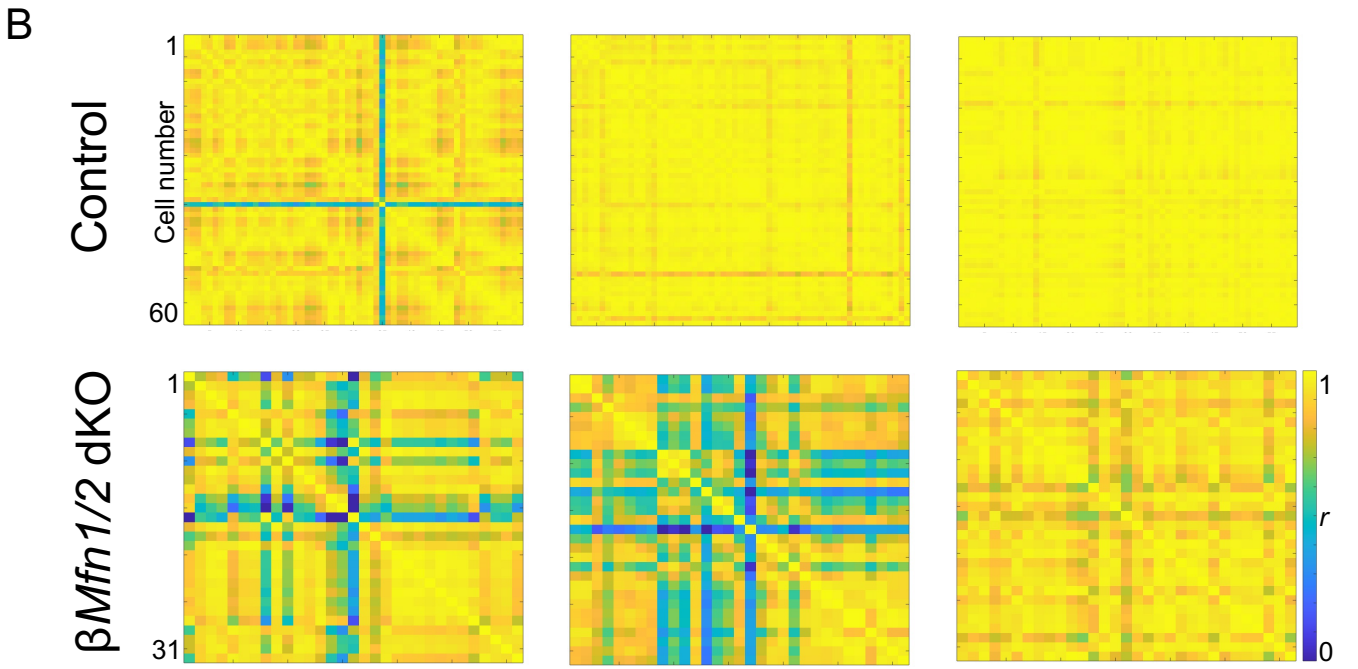

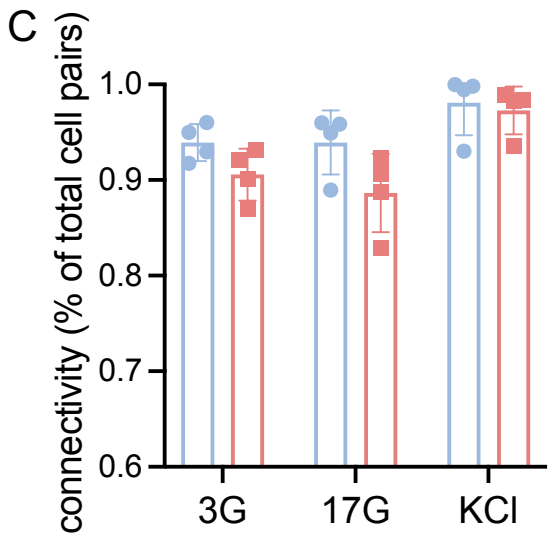

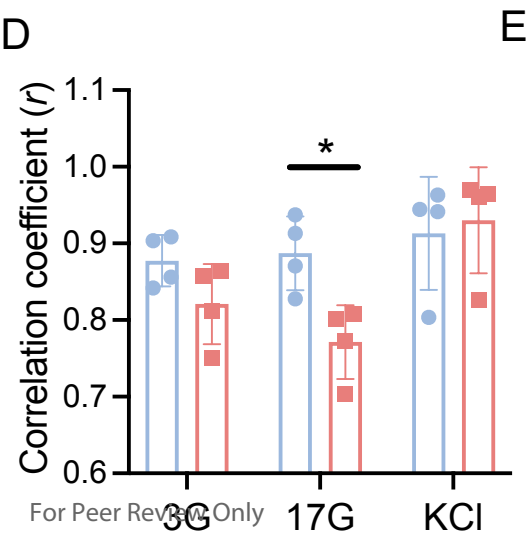

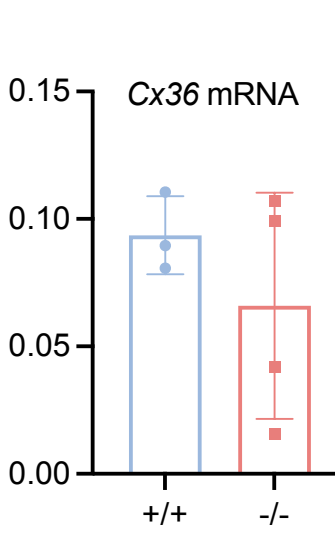

Suppl. Fig.7

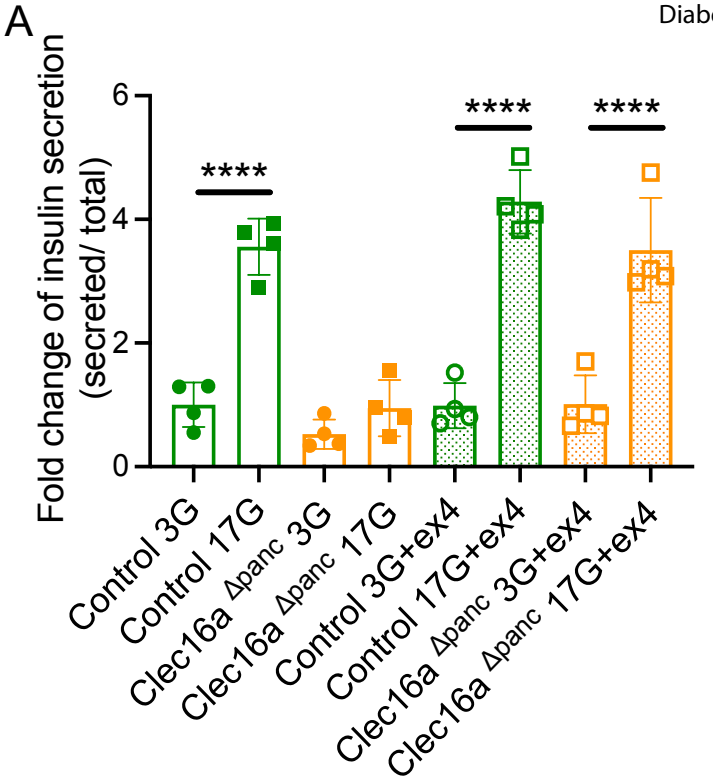
A
Fold change of insulin secretion (secreted/ total)
6
4
2
0
****
****
****
Control 3G
Control 17G
Clec16a Δpanc 3G
Clec16a Δpanc 17G
Control 3G+ex4
Control 17G+ex4
Clec16a Δpanc 3G+ex4
Clec16a Δpanc 17G+ex4

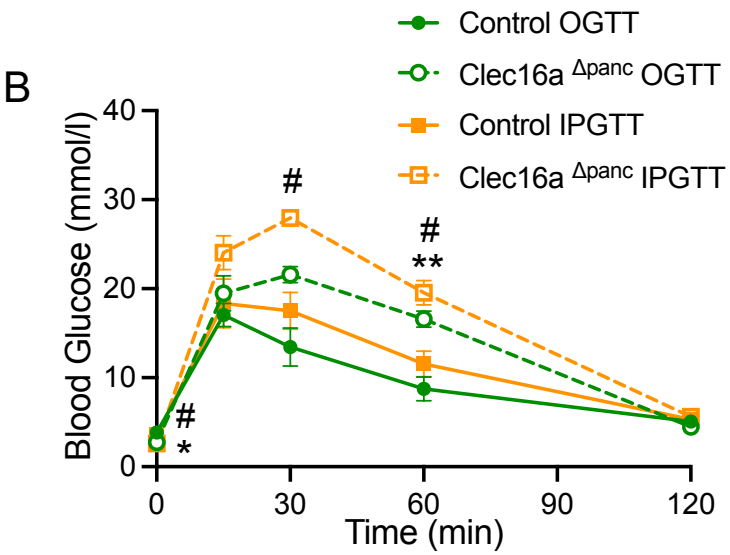
B
Control OGTT
Clec16a Δpanc OGTT
Control IPGTT
Clec16a Δpanc IPGTT
Blood Glucose (mmol/l)
40
30
20
10
0
#
#
**
#
*
0
30
60
90
120
Time (min)

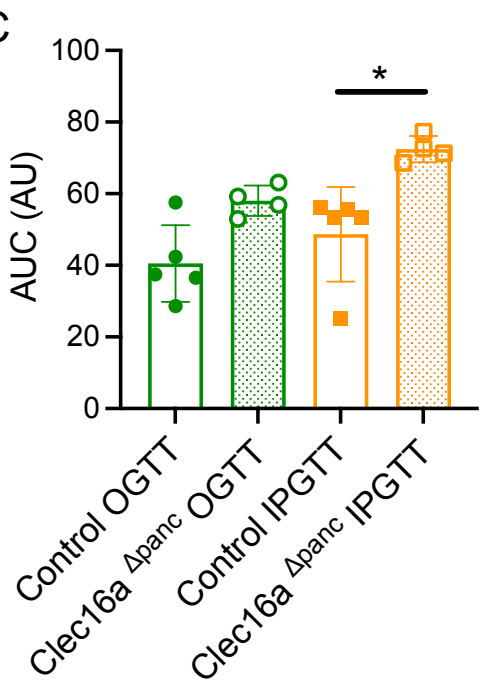
C
AUC (AU)
100
80
60
40
20
0
*
Control OGTT
Clec16a Δpanc OGTT
Control IPGTT
Clec16a Δpanc IPGTT

Suppl. Fig.8

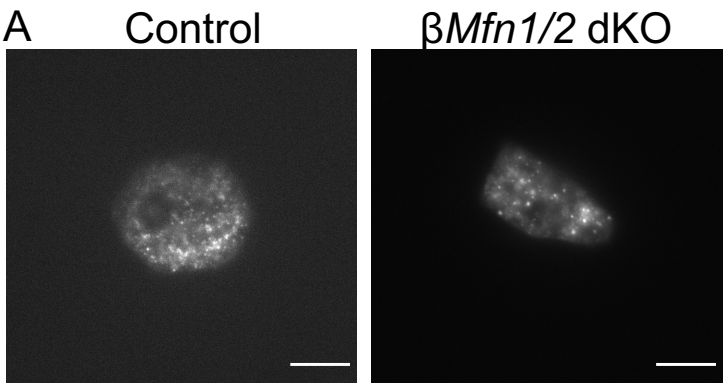
A
Control
βMfn1/2 dKO

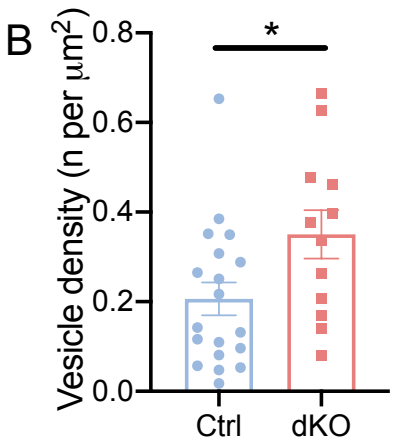
B
*
Vesicle density (n per µm²)
0.8
0.6
0.4
0.2
0.0
Ctrl
dKO

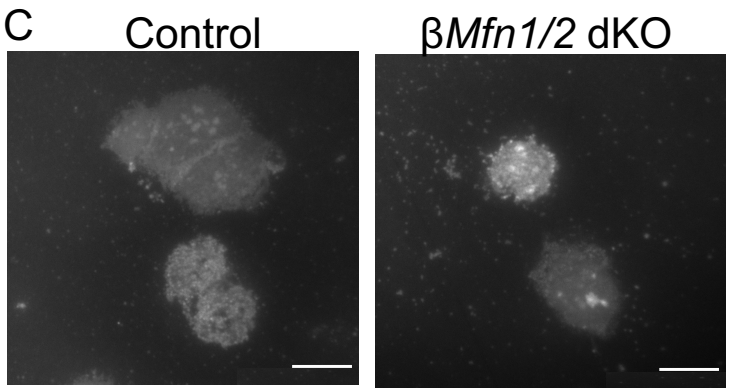
C
Control
βMfn1/2 dKO

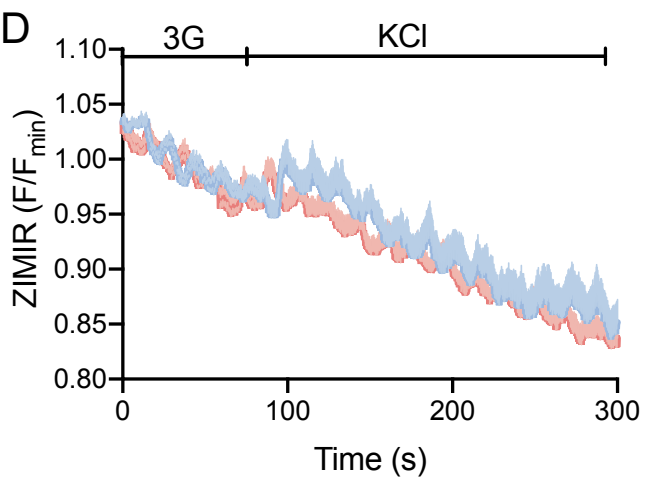
D
3G
KCl
ZIMIR (F/Fmin)
1.10
1.05
1.00
0.95
0.90
0.85
0.80
0
100
200
300
Time (s)

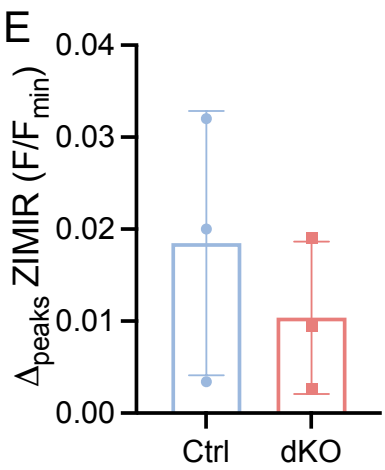
E
Δpeaks ZIMIR (F/Fmin)
0.04
0.03
0.02
0.01
0.00
Ctrl
dKO

Suppl. Fig.9

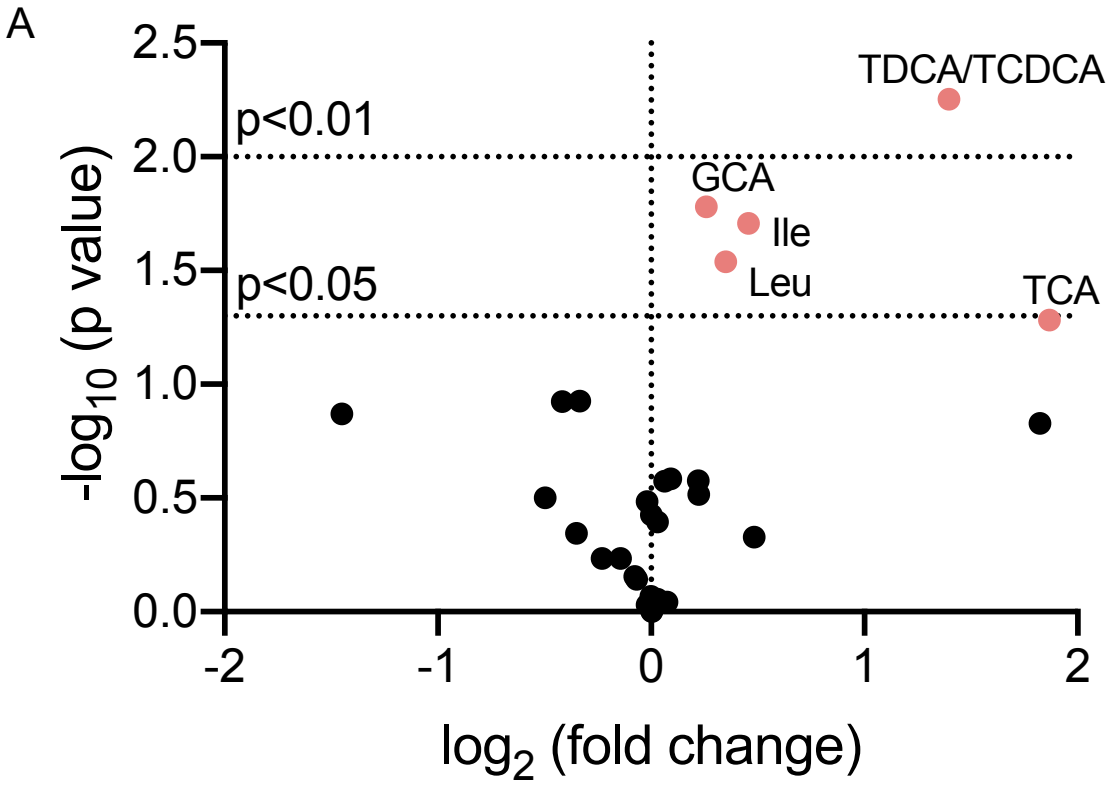

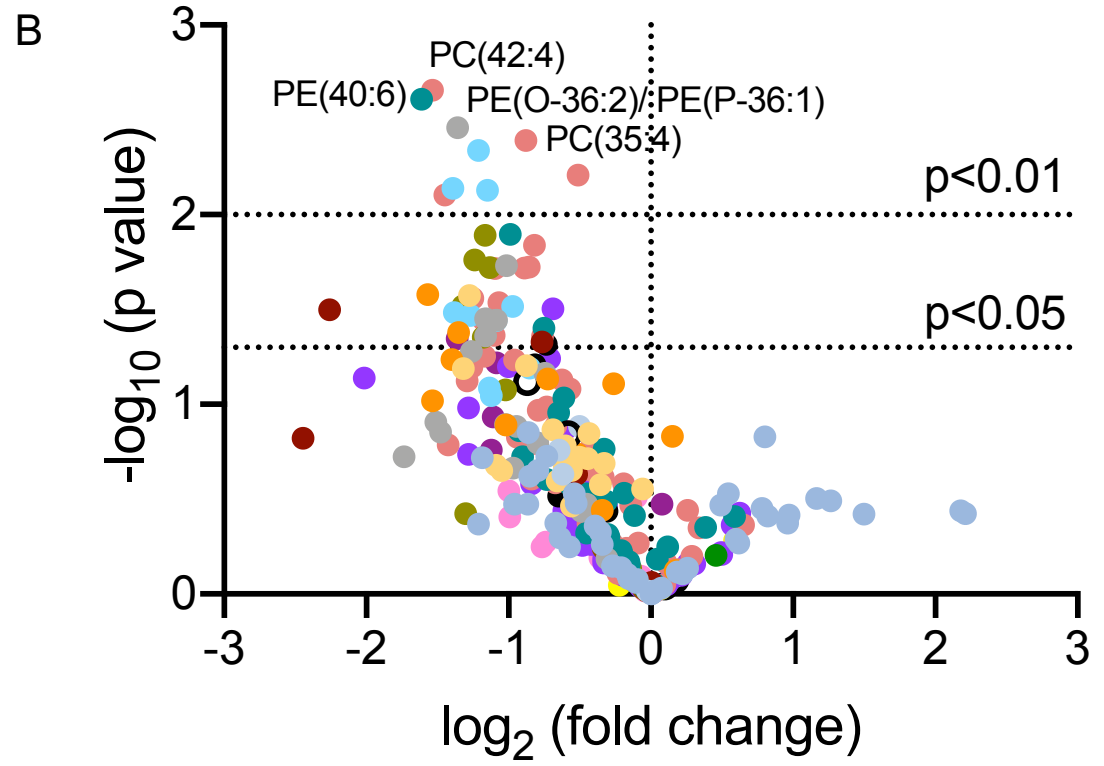

SM Cer CE DG FA TG LPC LPC-O PC
PC-O PC(P-)/PC(O-) LPE PE PE(O-) PG PI PS

Suppl. Fig.10

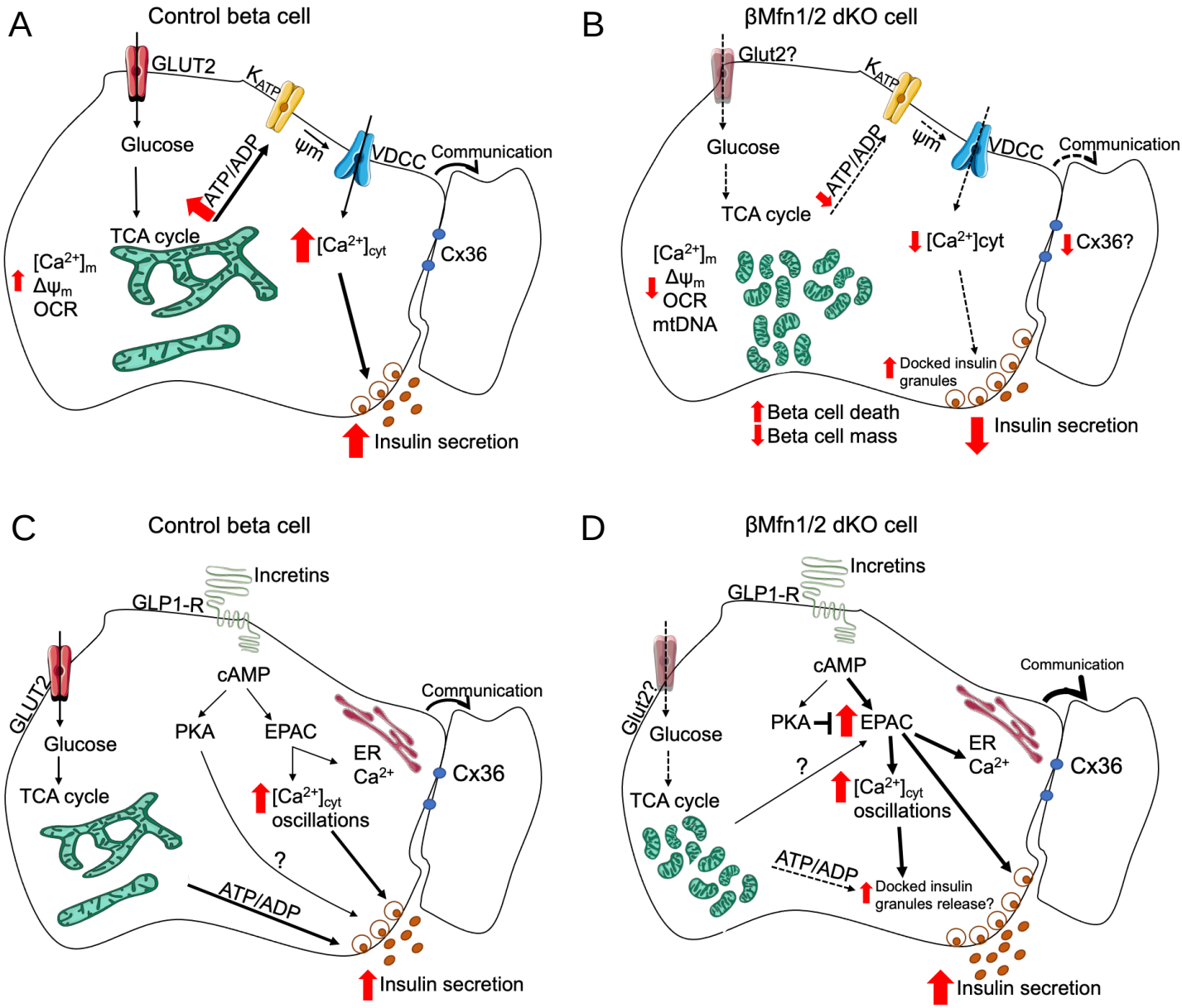
A
Control beta cell
GLUT2
K_{ATP}
Glucose
ATP/ADP
ψm
VDCC
Communication
TCA cycle
$[Ca^{2+}]_{cyt}$
Cx36
$[Ca^{2+}]_m$
$\Delta\psi_m$
OCR
Insulin secretion
B
βMfn1/2 dKO cell
Glut2?
K_{ATP}
Glucose
ATP/ADP
ψm
VDCC
Communication
TCA cycle
$[Ca^{2+}]_m$
$\Delta\psi_m$
OCR
mtDNA
$[Ca^{2+}]cyt$
Cx36?
Docked insulin granules
Beta cell death
Beta cell mass
Insulin secretion
C
Control beta cell
Incretins
GLP1-R
GLUT2
cAMP
Communication
Glucose
PKA
EPAC
ER Ca^{2+}
TCA cycle
$[Ca^{2+}]_{cyt}$ oscillations
Cx36
?
ATP/ADP
Insulin secretion
D
βMfn1/2 dKO cell
Incretins
GLP1-R
Glut2?
cAMP
Communication
Glucose
PKA
EPAC
ER Ca^{2+}
?
TCA cycle
$[Ca^{2+}]_{cyt}$ oscillations
Cx36
ATP/ADP
Docked insulin granules release?
Insulin secretion

Suppl. Fig.11

Electronic Supplemental Tables

ESM Table 1

Genes	Forward primer (5'→3')	Reverse Primer (5→3')
Mfn1	TGGTAATCTTTAGCGGTGCTC	GGAGGACTTTATCCCACAGC
Mfn2	TTTGGAAGTAGGCAGTCTCCA	CAGGCAGCACTGAAAAGAGA
Pdx1-Cre^{ERT2}	CAGGCGTTTTCTGAGCATACC	CCGGTTATTCAACTTGCACCAT

Sequence of primers used for genotyping *Mfn1* and *Mfn2* flox.

ESM Table 2

Genes	Forward primer (5'→3')	Reverse Primer (5→3')
Mfn1	GCATTTTTTGGCAGGACAAGTAG	GGAGGACTTTATCCCACAGCAT
Mfn2	AGAAGAGTGTCAAGACTGTGAACCA	GCTGCCTGCATGCAACTG
Drp1	TCAGATCGTCGTAGTGGGAA	TCTTCTGGTGAAACGTGGAC
Opa1	ATACTGGGATCTGCTGTTGG	AAGTCAGGCACAATCCACTT
Fis1	AAGTATGTGCGAGGGCTGT	TGCCTACCAGTCCATCTTTC
Ins2	TGGCTTCTTCTACACACCCATGTCCC	ACTGATCTACAATGCCACGCTTCTGCT
Slc2a2	GCAACTGGGTCTGCAATTTTG	CAAGGAAGTCCGCAATGTACTG
Gck	TGGTGGATGAGAGCTCAGTGAA	CATGTACTTTCCGCCAATGATC
Pdx1	CCAAAGCTCACGCGTGGA	TGTTTTCCTCGGGTTCCG
Nkx6.1	GCCTGTACCCCCCATCAAG	GTGGGTCTGGTGTGTTTTCTCTT
Pax6	GCACATGCAAACACACATGAAC	GGTGAAATGAGTCCTGTTGAAGTG
Ucn3	GCTGTGCCCCTCGACCT	TGGGCATCAGCATCGCT
Glp1r	CCCTGGGCCAGTAGTGTG	GCAGGCTGGAGTTGTCCTTA
Nkx2.2	CCTCCCCGAGTGGCAGAT	GAGTTCTATCCTCTCCAAAAGTTCAAA
Gcg	TCACAGGGCACATTCACCAG	CATCATGACGTTTGGCAATGTT
Arx	TCCGGATACCCCACTTAGCTT	GACGCCCCTTTCCTTTAAGTG
Mafa	CTTCAGCAAGGAGGAGGTCATC	CGTAGCCGCGGTTCTTGA
Mafb	TGAATTTGCTGGCACTGCTG	AAGCACCATGCGGTTCATACA
Vdac1	GCTAAGGATGACTCGGCTTTAAGG	AGGTTAAGTGATGGGCTAGGATGG
Vdac2	TCACTGTTGGCTGGTTCCTAGTTG	AAGACCTCGTGGATTATGCTAGGG
Vdac3	CACTTGTCCCTGGAAATGAAGAG	CATGACACTACGTTGTTGCTGAGG
Letm1	TCCTGCGTTTCCAGCTCACCAT	GTCTTCTGTGACACCGAGAGCT
Slc8a1	CCGTGACTGCCGTTGTGTT	GCCTATAGACGCATCTGCATACTG
Trpm5	CCAGCATAAGCGACAACATCT	GAGCATACAGTAGTTGGCCTG
Beclin-1	TGGAAGGGTCTAAGACGT	GGCTGTGGTAAGTAATGGA
Lc3	CACTGCTCTGTCTTGTGTAGGTTG	TCGTTGTGCCTTTATTAGTGCATC
Bnip3	TTCCACTAGCACCTTCTGATGA	GAACACCGCATTTACAGAACAA
p62	CCCAGTGTCTTGGCATTCTT	AGGGAAAGCAGAGGAAGCTC

GabarapL	CATCGTGGAGAAGGCTCCTA	ATACAGCTGGCCCATGGTAG
CathepsinL	GTGGACTGTTCTCACGCTCAAG	TCCGTCCTTCGCTTCATAGG
Pink1	TGAGGAGCAGACTCCCAGTT	AGTCCCACTCCACAAGGATG
Parkin	TGGAAAGCTCCGAGTTCAGT	CCTTGTCTGAGGTTGGGTGT
Atf4	GCAGTGTTGCTGTAACGGACA	CGCTGTTCAGGAAGCTCATCT
Atf6a	GACTCACCCATCCGAGTTGTG	CTCCCAGTCTTCATCTGGTCC
Bip	AGGACAAGAAGGAGGATGTGGG	ACCGAAGGGTCATTCCAAGTG
Chop2	CCACCACACCTGAAAGCAGAA	AGGTGAAAGGCAGGGACTCA
Xbp1	TGGCCGGGTCTGCTGAGTCCG	GTCCATGGGAAGATGTTCTGG
Xbp1s	CTGAGTCCGAA TCAGGTGCAG	GTCCATGGGAAGATGTT CTGG
Cx36	CAGCAGCACTCCACTATGATTG	GTACACCGTCTCCCCTACAA
Ldha	ATGAAGGACTTGGCGGATGA	ATCTCGCCCTTGAGTTTGTCTT
Slc16a1	GCTTGGTGACCATTGTGGAAT	CCCAGTACGTGTATTTGTAGTCTCCAT
Pdgfra	GACCCTGTTCCAGAGGAGGAA	TTCCGAAGTCTGTGAGCTGTGT
Aldh1a3	GGGCCTCAGATCGACCAAAA	CTAGCTTGGCCCCTTCCTTC
Hsd11b	GGAGCCGCACTTATCTGA	TGCCATTTCTCTTCCAATC
Mt9/mt11	GAGCATCTTATCCACGCTTCC	GGTGGTACTCCCGCTGTAAA
Ndufv1	CTTCCCCACTGGCCTCAAG	CCAAAACCCAGTGATCCAGC
Epac1a	GGACAAAGTCCCCTACGACA	CTTGGTCCAGTGGTCCTCAT
Epac2a	TGGAACCAACTGGTATGCTG	CCAATTCCCAGAGTGCAGAT
Epac2b	TCTTTGCTACCTGGGACTGG	AGCAGCCAGCCTTTATCTGA
Adcy3	GTGCTATCATCGTGGGCATC	TCCTTCAGCATCTCGTCAGC
Adcy5	GCCAATGCCATAGACTTCAG	ATCTCCTCCTTCTCTTCTGTG
Adcy6	TAAATGCCAGCACCTATGACC	TGTTCAACCCGA TCTTCA TCTG
Adcy8	TTGGGCTTCCTACACCTTGACT	CGGTAGCTGTATCCTCCATTGAG
Prkar1a	ATGGCGTCTGGCAGTATGG	GCTGCACGATGGAGTCCTTC
Prkar1b	TCTGAAAGGATGCGAGATGTACG	CTGGGAGTTTGACTTCTGCCG
Prkar2a	GAGGAGGATAACGATCCAAGGG	TGCTCGTCAGTTTTGACAATCTT
Prkaca	AGATCGTCCTGACCTTTGAGT	GGCAAAACCGAAGTCTGTCAC
Prkacb	CTCGGGACGGGTTCCTTTG	AGGGACGTATTCCATAACCATGT

β-actin	CGAGTCGCGTCCACCC	CATCCATGGCGAACTGGTG

List of primers used for qRT-PCR.

ESM Table 3

Antibody	Species	Vendor	Catalog number	Dilution/conc	RRID
anti-MFN1	mouse	Abcam	ab126575	1 in 500	RRID:AB_11141234
anti-MFN2	mouse	Abcam	ab56889	1 in 500	RRID:AB_2142629
anti-GAPDH	goat	Cell signalling	#2118s	1 in 10 000	RRID:AB_561053
anti-HRP	goat	Abcam	ab205719	1 in 5 000	RRID:AB_2755049
β*Mfn1/2* dKO IHC					
anti-Insulin	guinea pig	Agilent	#A0564	1 in 500	RRID:AB_10013624
anti-glucagon	mouse	Sigma-Aldrich	G2654	1 in 1 000	RRID:AB_259852
Alexa Fluor 488	goat	Thermo Fisher	#A-11073	1 in 1 000	RRID:AB_2534117
Alexa Fluor 568	goat	Thermo Fisher	#A-11004	1 in 1 000	RRID:AB_2534072
Pdx1CreER IHC					
anti-Insulin	guinea pig	Agilent	#A0564,	1 in 2 000	RRID:AB_10013624
anti-glucagon	rabbit	Abcam	ab92517	1 in 300	RRID:AB_10561971
anti-somatostatin	rabbit	Abcam	ab111912	1 in 1 000	RRID:AB_10903864
Alexa Fluor 488	donkey	Jackson Immuno	#711-545-152	1 in 1 000	RRID:AB_2313584
Alexa Fluor 568	donkey	Jackson Immuno	#706-165-148	1 in 1 000	RRID:AB_2340460

List of antibodies used in immunohistochemistry (IHC) experiments.

ESM Table 4

Condition	Ctrl Average	±SEM	dKO Average	±SEM
3G	225.130794	31.9313528	137.3442788	16.5058023
10G	350.937357	99.2151864	238.6717601	47.844241
17G	1007.68015	144.488618	302.4013885	79.2604199
EX4	1019.23968	204.149417	820.6378323	21.4037722
GLP1	982.176667	3.3427251	833.1233333	55.4545809
GIP	927.603	3.5275689	732.67	20.5050002
FSK	864.981483	8.97886477	783.514548	31.6922934
IBMX	866.672401	23.8144433	711.4497483	15.3320754
KCl	657.561878	107.611853	284.9369204	51.8648557
3G+30mM KCl	238.214722	103.220044	196.2304897	8.12945181
17G+30mM KCl	920.67843	30.819347	907.6114857	5.17694852
10G+H89	513.305815	157.535336	808.3442542	15.0070073
IBMX/FSK	1312.07246	152.327607	1161.305076	13.6682706
IBMX/FSK/H89	1641.45142	83.8140161	1314.467588	173.287437
10G+activ	918.086618	52.9726612	870.8674045	53.8147534
10G+activ+H89	892.469171	48.2800591	1534.612807	90.3019959

Total insulin content measured per GSIS condition (ng/10 islets).

ESM Table 5

Metabolites	Abbreviations	control mean	dKO mean	log_2 (fold change)	Student t-test (p value)
AADA	Aminoadipic acid	1909.1	699.12	-1.4493	0.1347
a(R)-OHB/a(S)-OHB	Alpha-hydroxybutyric acid	2000.2	2105.2	0.0738	0.9064
ADMA/SDMA	(A)symmetric dimethylarginine	151.88	152.32	0.0042	0.9968
Ala	Alanine	50606	35866	-0.4967	0.3161
β-OHB	β-hydroxybutyric acid	3990.9	5578.9	0.4833	0.4692
CA	Cholic acid	1181.3	4177.4	1.8222	0.1482
CDCA	Chenodeoxycholic acid	327.1	348.92	0.0931	0.2608
Cit	Citrulline	6926.6	6273.8	-0.1428	0.5838
DCA	Deoxycholic acid	216.51	252.52	0.222	0.266
GBB	Gamma-butyrobetaine	801.64	760.72	-0.0756	0.6991
GCA	Glycocholic acid	547.92	655.65	0.259	0.0166
Gln	Glutamine	97592	93082	-0.0683	0.7184
Glu	Glutamic acid	21063	17968	-0.2293	0.5822
Gly	Glycine	20756	16462	-0.3344	0.1185
GUDCA	Glycoursodeoxycholic acid	492.84	492.78	-0.0002	0.8557
HCit	Homocitrulline	991.28	979.06	-0.0179	0.3277
Ile	Isoleucine	14195	19491	0.4575	0.0196
IndS	Indoxyl sulfate	8683.7	6507.5	-0.4162	0.119
Kynu	Kynurenine	714.87	729.99	0.0302	0.4022
Leu	Leucine	17020	21708	0.351	0.029
N-MNA	N-methylnicotineamide	547.54	547.58	1E-04	0.3752
Phe	Phenylalanine	11509	11749	0.0298	0.8802
Taurine	Taurine	128076	100512	-0.3496	0.4514
TCA	Taurocholic acid	30302	110668	1.8687	0.0522
TDCA/TCDCA	Tauro(cheno)deoxycholic acid	723.01	1904.5	1.3973	0.0056
Trp	Tryptophan	8152.9	8051.9	-0.018	0.9343
TUDCA	Tauroursodeoxycholic acid	548.74	640.49	0.223	0.3052
Tyr	Tyrosine	12364	12391	0.0031	0.9929
UDCA	Ursodeoxycholic aicd	418.55	437.05	0.0624	0.2671

Metabolite differences found in plasma samples of control vs dKO mice according to metabolic class and both fold-change and t-test criteria.

Supplemental Figure legends

Supplemental Fig.1 Boxplots showing differences between HFHS (yellow) and RC (green) diet in 6 mouse strains over time for *Mfn1* (A) and *Mfn2* (B) genes. The bottom and top of the boxes represent the first and third quartiles, with the horizontal line representing the median. The upper whiskers represent the third quartile plus 1.5x IQR (interquartile range); the lower whiskers represent the first quartile minus 1.5x IQR. Outlier points beyond this range are indicated above or below the whiskers. Statistically significant comparisons following false discovery rate (FDR) correction (FDR <= 0.05) are indicated by a double asterisk. Marginally significant comparisons (raw p value <= 0.05) are indicated by a single asterisk.

Supplemental Fig.2 Pdx1CreER activation has no detectable effect on glycaemia both *in vivo* and *in vitro* and on key beta-cell gene expression and islet morphology. (A) Glucose tolerance measured by IPGTT (2 g/kg body weight) in WT and Pdx1CreER mice (*n*=6 mice per genotype) at 8 weeks of age. (B) Insulin secretion measured during serial incubations in batches in 3 or 20 mmol/l glucose (*n*=6 mice per genotype in three independent experiments) at 8 weeks of age. (C) (a,b) MafA (red) and insulin (green) expression levels in WT and Pdx1CreER islets. (c,d) Typical distribution of beta- (insulin, red), alpha- (glucagon, green), and delta-cells (Somatostatin, SS, green) in 8-week old islet sections (*n*= 50 islets, 3 male mice per genotype). Note that both alpha and delta cells were unidentifiable as these were stained in green. Scale bar: 20 μm. Data are presented as mean±SD. Data assessed by two-way ANOVA test and Sidak's multiple comparisons test.

Supplemental Fig.3 Body weight loss, insulin resistance and increased β-ketone production is observed in β*Mfn1/2* dKO mice. (A) qRT-PCR quantification of *Mfn1, Mfn2* expression in tissues extracted from control and dKO animals relative to *β-actin* (*n*=3-5 mice per genotype in two independent experiments). (B) Measured body weight in control and β*Mfn1/2* dKO mice (*n*=3-6 mice per genotype) at 7-22 weeks of age. (C) Glucose tolerance measured by IPGTT (1 g/kg body weight) in 20-week-old mice in β*Mfn1/2* dKO and control mice (*n*=8 mice per genotype, in 2 independent experiments). (D) Challenging β*Mfn1/2* dKO mice with a 0.75 U/kg body weight insulin injection as compared with control mice at 14 weeks of age (*n*=6 mice per genotype).

Data normalised to baseline (%). (E) Plasma insulin levels during IPGTT of 3g/kg of glucose in dKO and control mice (*n*=5 mice per genotype) (F) Proinsulin to insulin ratio measured in *n*=5 mice per genotype. (G) Glucose and (H) β-ketone bodies measured before or after an overnight (16h) fasting in 14-week control and dKO mice. (I) Plasma insulin levels were quantified under fed and fasted conditions in 14-week dKO and control mice (*n*=6 mice per genotype). Data are presented as mean±SD. *p<0.05; **p<0.01; ***p<0.001; ****p<0.0001 as indicated, or at the time points indicated analysed by unpaired two-tailed Student's t-test and Mann–Whitney correction or two-way ANOVA test and Sidak's multiple comparisons test. Experiments were performed in 14 or 20-week-old male mice as stated accordingly.

Supplemental Fig.4 β*Mfn1/2* dKO mice show impaired glucose tolerance and insulin secretion at 14 and 20 weeks of age following an IP injection of glucose versus an OG. (A) Glucose tolerance measured by IPGTT (using 1g/kg body weight) in β*Mfn1/2* dKO and control mice at 14 weeks of age. (B) Plasma insulin levels during IPGTT in dKO and control mice. (C) Glucose tolerance measured by IPGTT (using 1g/kg body weight) in β*Mfn1/2* dKO and control mice at 20 weeks of age. (D) Plasma insulin levels during IPGTT in dKO and control mice (*n*=5-6 mice per genotype). (E) Glucose tolerance measured by OGTT (using 1g/kg body weight) in β*Mfn1/2* dKO and control mice at 14 weeks of age. (F) Plasma insulin levels during IPGTT in dKO and control mice. (G) Glucose tolerance measured by OGTT (using 1g/kg body weight) in β*Mfn1/2* dKO and control mice at 20 weeks of age. (H) Plasma insulin levels during IPGTT in dKO and control mice (*n*=5-6 mice per genotype). Data are presented as mean±SEM. *p<0.05 as indicated, analysed by two-way ANOVA test and Sidak's multiple comparisons test.

Supplemental Fig.5 Mitochondrial ultrastructure, glycaemia and beta cell mass are not altered 2 weeks post tamoxifen administration in β*Mfn1/2* dKO mice. (A) Confocal images of the mitochondrial network of dissociated beta cells stained with Mitotracker green; scale bars: 5 μm. (B) Mitochondrial morphology analysis on deconvolved confocal images of dissociated beta cells. A macro was developed to quantify the number of mitochondria per cell and measure the elongation, perimeter, circularity (0: elongated; 1: circular mitochondria), density and surface area of the

organelles in control and dKO animals (*n*=20-50 cells; *n*=3 mice per genotype). (C) Blood glycaemia measured in fed mice before or 2 weeks post-tamoxifen injection in control and dKO mice (*n*=7 mice per genotype). (D) Glucose tolerance measured by IPGTT (3 g/kg body weight) in 10-week-old β*Mfn1/2* dKO and control mice (*n*=7 mice per genotype). (E) Plasma insulin levels were quantified under fasted conditions in 10-week dKO and control mice (*n*=7 mice per genotype). (F) The beta cell and alpha cell surface (G) measured within the whole pancreatic area in control and dKO mice were determined, as well as the beta/alpha cell ratio in (H), (*n*=67-76 islets, 3 mice per genotype; experiment performed in duplicate). (I) The relative mitochondrial DNA copy number was measured by determining the ratio of the mtDNA-encoded gene *mt-Nd1* to the nuclear gene *Ndufv1* (*n*=3 mice per genotype). Data are presented as mean±SD. *p<0.05, **p<0.01 as indicated, analysed by unpaired two-tailed Student's t-test and Mann–Whitney correction or two-way ANOVA test and Sidak's multiple comparisons test. Experiments were performed in 10-week-old male mice.

Suppl. Fig.6 Heatmap of differential gene expression between β*Mfn1/2* dKO and control islet mRNA. Changes in key beta or alpha cell genes, disallowed genes, mitochondrial, ER stress or mito/autophagy genes were assessed by qRT-PCR in control and dKO islets according to the colour coded median values from 0 to 1, white to dark blue respectively (*n*=3-4 mice per genotype; experiment performed in duplicate). Expression values for each gene were normalised to β-*actin*. *p<0.05; **p<0.01, assessed by two-way ANOVA test and Sidak's multiple comparisons test. Experiments were performed in 14-week-old male mice.

Supplemental Fig.7 Impact of *Mfn1/2* deletion on intercellular connectivity. (A) Representative cartesian maps of islets with colour coded lines connecting cells according to the strength of Pearson analysis (colour coded *r* values from 0 to 1, blue to red respectively) under 3mmol/L (3G), 17mmol/L (17G) glucose or 20mmol/L KCl; scale bars: 40 μm.(B) Representative heatmaps depicting connectivity strength (*r*) of all cell pairs according to the colour coded *r* values from 0 to 1, blue to yellow respectively.(C) Percentage of correlated cell pairs at 3G, 17G or KCl (*n*=17-26 islets, 4 mice per genotype).(D) *r* values between beta cells in response to glucose or KCl (*n*=4 mice per genotype).(E) qRT-PCR quantification of *Cx36* expression relative to β-

actin (*n*=3–4 mice per genotype in two independent experiments). Data are presented as mean±SD. *p<0.05, assessed by unpaired two-tailed Student's t-test and Mann–Whitney correction or two-way ANOVA test and Sidak's multiple comparisons test. Analysis and experiments were performed on data collected from 14-week-old male mice.

Supplemental Fig.8 Impaired insulin secretion observed in Clec16a$^{\Delta panc}$ islets can be rescued by GLP-1R agonists *in vitro.* (A) Insulin secretion measured in control (Pdx1-Cre) and Clec16a$^{\Delta panc}$ mice in 3 mmol/l glucose (3G), 17 mmol/l glucose (17G), or 10 nmol/l exendin-4 (ex4) (*n*=4 mice per genotype). (B) Glucose tolerance measured by IPGTT (1.5 g/kg body weight) in 8-week-old male Pdx1-Cre and Clec16a$^{\Delta panc}$ mice or OGTT (1.5 g/kg body weight) in 9–10-week-old animals. (C) The corresponding AUC is shown in (B) (*n*=4-5 mice per genotype). (*p<0.05,**p<0.01, control OGTT vs Clec16a$^{\Delta panc}$; #p<0.05, ##p<0.01, control IPGTT vs Clec16a$^{\Delta panc}$). Data are presented as mean±SD and assessed by two-way ANOVA test and Sidak's multiple comparisons test.

Supplemental Fig.9 Insulin granule density is increased in β*Mfn1/2* dKO beta cells. (A) Confocal images of NPY-Venus fluorescence in dissociated fixed pancreatic beta cells isolated from control and dKO mice. Scale bar: 10 μm.(B) Effect of KCl on exocytosis as reported with NPY-Venus in pancreatic beta cells. Traces represent mean normalised fluorescence intensity over time (F/F_{min}). (C) Confocal images of ZIMIR fluorescence imaging in dissociated pancreatic beta cells isolated from control and dKO mice. Scale bar: 10 μm.(D) Representative time courses of ZIMIR signal fold change above baseline (F/F_{min}) upon KCl-stimulated insulin/Zn^{2+} release and (E) fold change of peaks in dissociated control and dKO cells. (*n*=19 cells from 3 control mice; *n*=12 cells from 3 β*Mfn1/2* dKO mice). Data are presented as mean±SD. *p<0.05,**p<0.01; assessed by unpaired two-tailed Student's t-test and Mann–Whitney correction or two-way ANOVA test and Sidak's multiple comparisons test. Experiments were performed in 14-week-old male mice.

Supplemental Fig.10 Volcano plots showing alterations in metabolites and lipids from plasma samples of control and β*Mfn1/2* dKO mice. (A) Volcano plot summarising both fold-change and t-test criteria for all metabolites. Results are

summarised in a scatter-plot of the negative $\log_{10}$-transformed p values from the t-test plotted against the $\log_2$ fold change. Negative values indicate downregulated metabolites in dKO mice, while positive values reflect upregulated metabolites. Metabolites with statistically significant differential levels according to the t-test lie above a horizontal threshold line (red dots). Metabolites with large fold-change values lie far from the vertical threshold line at $\log_2$ fold change = 0, indicating whether the metabolite is up or downregulated. The list of analysed metabolites with their abbreviations is presented in ESM table 5. (B) Lipids that were found downregulated in dKO mice with statistically significant differential levels according to the t-test are presented above a horizontal threshold line. Plasma samples were isolated from *n*=3 animals per genotype. The most significantly downregulated lipids are annotated. SM, sphingomyelins; CER, ceramide; CE, cholesterol esters; DG, di(acyl/alkyl)glycerols; FA, fatty acids; TG, tri(acyl/alkyl)glycerols; LPC, lysophosphatidylcholines; PC, phosphatidylcholines;LPE,lysophosphatidylethanolamines;PE,phosphatidylethanola mines; PG, phosphatidylglycerols; PI, phosphatidylinositols; PS, phosphatidyserines. Experiments were performed in 14-week-old male mice.

Supplemental Fig.11 Impact of Mfn1/2 deletion on glucose and incretin stimulated-insulin secretion in beta cells. (A) In control animals, glucose is taken up by beta cells through GLUT2 and metabolised by mitochondria (elongated structure) through the citrate (TCA) cycle, leading to an increased mitochondrial proton motive force (hyperpolarised $\Delta\psi_m$), accelerated ATP synthesis and O_2 consumption rate (OCR). Consequently, the cytoplasmic ATP:ADP ratio rises, which causes closure of KATP channels, depolarisation of plasma membrane potential (ψm), opening of VDCCs and influx of cytosolic Ca^{2+}. Elevated $[Ca^{2+}]_{cyt}$ triggers a number of ATP-dependent processes including insulin secretion and improved beta-beta cell communication through connexin 36 (Cx36). (B) Following *Mfn1/2* deletion (β*Mfn1/2* dKO), highly fragmented mitochondria were associated with reduced mitochondrial Ca^{2+} ($[Ca^{2+}]_m$) accumulation, leading to a less polarised $\Delta\psi_m$, weaker OCR, lower mtDNA copy number and decreased ATP synthesis. This is expected to result in weaker ψm depolarisation, cytosolic Ca^{2+} influx and beta-beta cell connectivity due to lower expression of Cx36. Despite observing a higher number of docked insulin granules on the plasma membrane, insulin secretion was highly suppressed in these animals. This was also associated with increased beta cell death and reduced beta

cell mass. (C) In response to incretins, insulin secretion is potentiated through the activation of GLP1-R and cAMP signalling involving PKA- and EPAC-dependent pathways. Elevated $[Ca^{2+}]_{cyt}$ triggers a number of ATP-dependent processes including insulin secretion and Ca^{2+} mobilisation into the endoplasmic reticulum (ER).(D) In β*Mfn1/2* dKO cells, activation of the GLP1-R is linked with a potentiation of the EPAC pathway (inhibited by PKA), an increased ER Ca^{2+} uptake and improved beta-beta cell communication. Red and bold arrows represent enhanced pathways; dashed arrows represent impaired pathways. This figure was produced using illustrations from Servier Medical Art, http://smart.servier.com/

ESM Videos

ESM Video 1

Fluorescence imaging of cytosolic Ca^{2+} oscillations using Cal-520 in control (left) and β*Mfn1/2* dKO (right) whole islets in response to 3G, 3 mmol/l glucose, 17 mmol/l glucose (17G; with or without diazoxide [diaz]) or 20 mmol/l KCl with diaz. Scale bars: 50µm.

ESM Video 2

Fluorescence imaging of mitochondrial Ca^{2+} oscillations using R-GECO in control (left) and β*Mfn1/2* dKO (right) whole islets in response to 3G, 3 mmol/l glucose, 17 mmol/l glucose (17G; with or without diazoxide [diaz]) or 20 mmol/l KCl with diaz. Scale bars: 50µm.

ESM Video 3

Changes in $[Ca^{2+}]_{ER}$ were measured by fluorescence imaging of cytosolic Ca^{2+} oscillations using Cal-520 in control (left) and β*Mfn1/2* dKO (right) whole islets in response to 3G, 3 mmol/l glucose, 17 mmol/l glucose (17G; with or without diazoxide [diaz] or Acethylcholine [Ach]) or 20 mmol/l KCl with diaz. Scale bars: 50µm.

ESM Video 4

Fluorescence imaging of cytosolic Ca^{2+} oscillations using Cal-520 in control (left) and β*Mfn1/2* dKO (right) whole islets in response to 3G, 3 mmol/l glucose, 10 mmol/l glucose (10G; with or without Exendin-4 [ex4]) or 20 mmol/l KCl. Scale bars: 50µm.

DB21-0800.R2

Mitofusins *Mfn1* and *Mfn2* are required to preserve glucose- but not incretin-stimulated beta cell connectivity and insulin secretion

Eleni Georgiadou[1], Charanya Muralidharan[2], Michelle Martinez[2], Pauline Chabosseau[1], Elina Akalestou[1], Alejandra Tomas[1], Fiona Yong Su Wern[3], Theodoros Stylianides[4], Asger Wretlind[5], Cristina Legido-Quigley[5,6], Ben Jones[7], Livia Lopez Noriega[1], Yanwen Xu[8], Guoqiang Gu[8], Nour Alsabeeh[9], Céline Cruciani-Guglielmacci[10], Christophe Magnan[10], Mark Ibberson[11], Isabelle Leclerc[1], Yusuf Ali[3], Scott A. Soleimanpour[12,13] Amelia K. Linnemann[2], Tristan A. Rodriguez[14] and Guy A. Rutter[1,3,15*].

[1]Section of Cell Biology and Functional Genomics, Division of Diabetes, Endocrinology and Metabolism, Department of Medicine, Imperial College London, London, W12 0NN, UK
[2]Center for Diabetes and Metabolic Diseases, Indiana University School of Medicine, Indianapolis, IN, 46202, USA
[3]Lee Kong Chian School of Medicine, Nanyang Technological University, 637553, Singapore
[4]Loughborough University, Centre of Innovative and Collaborative Construction Engineering, Leicestershire, LE11 3TU, UK
[5]Systems Medicin, Steno Diabetes Center Copenhagen, 2820, Denmark
[6] Institute of Pharmaceutical Science, Kings College London, London, SE1 9NH, UK
[7] Section of Endocrinology and Investigative Medicine, Imperial College London, W12 0NN,UK
[8]Department of Cell and Developmental Biology, Program of Developmental Biology, and Vanderbilt Center for Stem Cell Biology. Vanderbilt University, School of Medicine, Nashville, TN, 37232, USA.
[9]Kuwait University, Department of Physiology, Health Sciences Center, 13110, Kuwait
[10]Université de Paris, BFA, UMR 8251, CNRS, Regulation of Glycemia by Central Nervous System, Paris, 75205, France
[11]Vital-IT Group, SIB Swiss Institute of Bioinformatics, Lausanne, CH-1015, Switzerland
[12]Division of Metabolism, Endocrinology & Diabetes and Department of Internal Medicine, University of Michigan Medical School, Ann Arbor, MI 48105, USA
[13]VA Ann Arbor Healthcare System, Ann Arbor, MI 48105, USA
[14]National Heart and Lung Institute, Imperial Centre for Translational and Experimental Medicine, Imperial College London, London, W12 0NN, UK
[15] Centre of research of CHUM, University of Montreal, Quebec, H2X 0A9, Canada

*Address correspondence to Professor Guy A. Rutter, g.rutter@imperial.ac.uk, +44 20 759 43340

Word count: 4445

Tweet: Deletion of Mitofusins 1 and 2 in beta cells of adult mice causes dramatic mitochondrial fragmentation and disrupts Ca^{2+} dynamics, insulin release and glucose homeostasis in vivo. Strikingly, these deficiencies are corrected by incretin hormones through an EPAC-dependent mechanism. Study led by @guy_rutter and @EleniGe0. **Figure**: (Suppl. Fig. 11).

Abstract

Mitochondrial glucose metabolism is essential for stimulated insulin release from pancreatic beta cells. Whether mitofusin gene expression, and hence mitochondrial network integrity, is important for glucose or incretin signalling has not previously been explored. Here, we generated mice with beta cell-selective, adult-restricted deletion of the mitofusin genes *Mfn1* and *Mfn2* (β*Mfn1/2* dKO). β*Mfn1/2* dKO mice displayed elevated fed and fasted glycaemia and a >five-fold decrease in plasma insulin. Mitochondrial length, glucose-induced polarisation, ATP synthesis, cytosolic and mitochondrial Ca^{2+} increases were all reduced in dKO islets. In contrast, oral glucose tolerance was more modestly affected in β*Mfn1/2* dKO mice and GLP-1 or GIP receptor agonists largely corrected defective GSIS through enhanced EPAC-dependent signalling. Correspondingly, cAMP increases in the cytosol, as measured with an Epac-camps based sensor, were exaggerated in dKO mice. Mitochondrial fusion and fission cycles are thus essential in the beta cell to maintain normal glucose, but not incretin, sensing. These findings broaden our understanding of the roles of mitofusins in beta cells, the potential contributions of altered mitochondrial dynamics to diabetes development and the impact of incretins on this process.

Keywords: Ca^{2+} dynamics; exendin-4; glucose-stimulated insulin secretion; incretins; intercellular connectivity; mitochondrial dysfunction; mitofusins; pancreatic beta cell; Type 2 diabetes.

List of abbreviations

$[Ca^{2+}]_{cyt}$: Cytoplasmic Ca^{2+} concentration

$[Ca^{2+}]_{mito}$: Mitochondrial free Ca^{2+} concentration

AA: Antimycin A

Ach: Acetylcholine

cAMP: adenosine 3',5'-cyclic monophosphate

Clec16a$^{\Delta panc}$: Pancreatic islet specific Clec16a knock-out

Diaz: Diazoxide

dKO: double knock-out

Ex4: Exendin-4

FCCP: Carbonyl cyanide-4-phenylhydrazone

GIP: Glucose-dependent insulinotropic peptide

GLP-1: Glucagon-like peptide-1

GSIS: Glucose-stimulated insulin secretion

IMM: Inner mitochondria membrane

IPGTT: Intraperitoneal glucose tolerance test

OGTT: Oral gavage and glucose tolerance test

Oligo: Oligomycin

OMM: Outer mitochondrial membrane

r: Pearson correlation coefficient

Rot: Rotenone

TMRE: Tetramethylrhodamine ethyl ester

T2D: Type 2 diabetes

β*Mfn1/2* dKO: beta cell specific Mitofusin 1 and 2 double knock-out

$\Delta\psi_m$: Mitochondrial membrane potential

Introduction

Mitochondria are often referred to as the powerhouses or “chief executive organelles” of the cell, using fuels to provide most of the energy required to sustain normal function [1]. Mitochondrial oxidative metabolism plays a pivotal role in the response of pancreatic beta cells to stimulation by glucose and other nutrients [2]. Thus, as blood glucose increases, enhanced glycolytic flux and oxidative metabolism lead to an increase in ATP synthesis, initiating a cascade of events which involve the closure of ATP-sensitive K^+ (K_{ATP}) channels [3], plasma membrane depolarisation and the influx of Ca^{2+} via voltage-dependent Ca^{2+} channels (VDCC). The latter, along with other, less well defined “amplifying” signals [4], drive the biphasic release of insulin [2]. Gut-derived incretin hormones including glucagon-like peptide-1 (GLP-1) and glucose-dependent insulinotropic peptide (GIP) [5] further potentiate secretion by binding to class-B G-protein coupled receptors (GPCRs) to generate adenosine 3',5'-cyclic monophosphate (cAMP) and other intracellular signals [5].

Under normal physiological conditions, mitochondria undergo fusion and fission cycles which are essential for quality control and adaptation to energetic demands [6]. Thus, highly inter-connected mitochondrial networks allow communication and interchange of contents between mitochondrial compartments, as well as with other organelles such as the endoplasmic reticulum (ER) [7]. These networks exist interchangeably with more fragmented structures, displaying more “classical” mitochondrial morphology [8]. Mitochondrial fission is also necessary for “quality control” and the elimination of damaged mitochondria by mitophagy [9].

Whilst the mitofusins MFN1 and MFN2, homologues of the *D. melanogaster* fuzzy onions (*fzo*) and mitofusin (*dmfn*) gene products [10], are GTPases that mediate fusion

of the outer mitochondrial membrane (OMM), optic atrophy protein 1 (OPA1) controls that of the inner mitochondrial membrane (IMM). Dynamin related protein 1 (DRP1) is responsible for mitochondrial fission [11]. Other regulators include FIS1, mitochondrial fission factor (MFF) and MiD49/51 [12].

Earlier studies [13-18] have shown that perturbations in mitochondrial structure in beta cells have marked effects on GSIS. Surprisingly, whether the canonical and evolutionarily-conserved machinery involved in mitochondrial fusion, i.e the mitofusins, control mitochondrial structure in beta cells has not been explored yet. Furthermore, none of the earlier studies have investigated the actions of mitochondrial structure destruction in adult mice. Finally, whether and to what extent they impact secretion stimulated by other agents including incretins is less clear. This question is important given that changes in mitochondrial oxidative metabolism [19] and structure contribute to type 2 diabetes (T2D).

Here, we first explored the potential contribution of mitofusins to the effects of diabetic conditions. We next determined whether deletion of *Mfn1* and *Mfn2* in beta cells in adult mice may impact insulin secretion. Lastly, we aimed to determine whether incretins may rescue or bypass any observed perturbations. We show that mitofusin ablation exerts profound effects on insulin release, glucose homeostasis and Ca^{2+} dynamics. Remarkably, the deficiencies in insulin secretion are largely corrected by incretin hormones. This suggests a possible approach to ameliorating the consequences of mitochondrial fragmentation with these agonists in some forms of diabetes.

Research Design and Methods

Study approval C57BL/6J mice were housed in individually ventilated cages in a pathogen-free facility at 22ºC with a 10-14 h light-dark cycle and were fed *ad libitum* with a standard mouse chow diet (Research Diets, New Brunswick, NJ, USA). All *in vivo* procedures were approved by the UK Home Office, according to the Animals (Scientific Procedures) Act 1986 with local ethical committee approval under personal project license (PPL) number PA03F7F07 to I.L.

Generation of beta cell selective *Mfn1/Mfn2* knockout (β*Mfn1/2* dKO), *Clec16a* null and Pdx1CreER mice C57BL/6J male mice bearing *Mfn1* (Mfn1^{tm2Dcc}; JAX stock #026401) and *Mfn2* (B6.129(Cg)-Mfn2^{tm3Dcc}/J; JAX stock #026525; The Jackson Laboratory, Bar Harbor, ME,USA) alleles [20] with *lox*P sites flanking exons 4 and 6 were purchased from the Jackson laboratory and crossed to C57BL/6J transgenic animals carrying an inducible *Cre* recombinase under *Pdx1* promoter control (Pdx1-Cre^{ERT2}) [21]. Mice bearing floxed *Mfn* alleles but lacking *Cre* recombinase were used as littermate controls in this study. Mice were genotyped following protocols described by the Jackson laboratory for each of these strains (See ESM Table 1). Recombination was achieved by daily tamoxifen (10mg/mouse [diluted in corn oil; Sigma-Aldrich, Dorset, UK]) i.p. injections for five days at 7-8 weeks of age in both control and β*Mfn1/2* dKO (dKO) groups.

Animals with floxed *Clec16a* alleles were bred to mice carrying the Pdx1-Cre transgene (*Clec16a*$^{\Delta panc}$) as previously described [22]. Pdx1-Cre alone mice were used as littermate controls. Pdx1CreER mice were generated as previously described [21].

RNA extraction and quantitative reverse transcription PCR For measurements of mRNA levels, pancreatic islets from control and β*Mfn1/2* dKO mice were isolated by collagenase digestion [23]. Total RNA from islets (50-100) was extracted and reverse transcribed as previously described [24] (see ESM Table 2 for primer details).

Tissue DNA extraction and measurement of mtDNA copy number Total islet DNA was isolated using Puregene Cell and Tissue Kit (Qiagen, Manchester, UK) and was amplified (100ng) using NADH dehydrogenase I primers [25], also known as complex I (*mt9/mt11)* for mtDNA and *Ndufv1* for nuclear DNA.

SDS-PAGE and western blotting Islets were collected and lysed (20 µg) as previously described [24]. The antibodies used are summarised in ESM Table 3.

Intraperitoneal (i.p.) or oral gavage (OG) of glucose followed by insulin, proinsulin or ketone levels measurement and insulin tolerance test (TT) *in vivo* IPGTTs, IPIITTs, OGTTs and plasma insulin measurements were performed as previously described [24]. Plasma proinsulin levels were measured in fasted (16h) animals using a rat/mouse proinsulin ELISA kit (Mercodia). Plasma β-ketones were measured from fed or fasted (16h) mice using an Area 2K device (GlucoMen, Berkshire, UK).

***In vitro* insulin secretion** Islets were isolated from mice and incubated for 1 h in Krebs-Ringer bicarbonate buffer containing 3 mmol/l glucose as previously described [24].

Single-cell fluorescence imaging Dissociated islets were incubated with 100nM Mitotracker green (Thermo Fisher Scientific) in Krebs-Ringer bicarbonate buffer containing 11 mmol/l glucose for 30 min. Mitotracker green was then washed with Krebs buffer with 11 mmol/l glucose before fluorescence imaging. Experiments with tetramethylrhodamine ethyl ester (TMRE) were performed as previously described [24]. Clusters of dissociated islets were transduced for 48h with an adenovirus encoding the low-Ca^{2+}-affinity sensor D4 addressed to the ER, Ad-RIP-D4ER (MOI: 100), as described in [26]. Bleaching was corrected as described in [27].Clusters of dissociated islets were transduced for 24h with an adenovirus encoding Epac1-camps, as described in [28].

Mitochondrial shape analysis For each stack, one image at the top, middle and bottom of the islet was analysed. After background subtraction, the following parameters were measured for each cell: number of particles, perimeter, circularity, elongation (1/circularity), density and surface area of each particle [29].

Whole-islet fluorescence imaging Cytosolic, mitochondrial Ca^{2+} imaging, and ATP:ADP changes in whole islets were performed as previously described [24].

TIRF fluorescence imaging Experiments using the membrane-located zinc sensor ZIMIR (50 μmol/l) [30] or the fluorescent genetically-encoded and vesicle-located green marker NPY-Venus were performed as previously described [31].

Pancreas immunohistochemistry Isolated pancreata were fixed and imaged as described in [24]. The antibodies used are summarised in ESM Table 3. For

examination of apoptosis, TUNEL assay was performed using a DeadEnd Fluorometric TUNEL system kit and DNase I treatment (Promega, Madison, Wisconsin, USA) according to the manufacturer's instructions.

Metabolomics/lipidomics Metabolites were quantified using targeted ultra-high-performance liquid-chromatography coupled triple quadrupole mass spectrometry (UHPLC-QqQ-MS/MS) as described earlier [32]. Lipidomic sample preparation followed the Folch procedure with minor adjustments. Significance was tested by Student's two-tailed t-test using GraphPad Prism 8 software.

Measurement of oxygen consumption rate XF96 assays (Seahorse Bioscience, Agilent, Santa Clara, CA, USA) using mouse islets (~10 per well) were performed as described in [33]. Parameters were analysed as in [34].

Electron microscopy (EM) For conventional EM, islets were fixed and imaged as described in [35].

Connectivity analysis

Pearson (*r*)-based connectivity and correlation analyses Correlation analyses in an imaged islet were performed as previously described [36].

RNA-Seq data analysis Processing and differential expression analysis of RNA-Seq data from islets isolated from high fat high sugar (HFHS, D12331, Research Diets) and regular chow (RC) fed mice (C57Bl/6J, DBA/2J, BALB/cJ, A/J, AKR/J, 129S2/SvPas) was performed as previously described [37] using the *Limma* package

in R and p-values were adjusted for multiple comparisons using the Benjamini Hochberg procedure [38].

Statistics Data are expressed as mean ± SD unless otherwise stated. Significance was tested by Student's two-tailed t-test and Mann–Whitney correction or two-way ANOVA with Sidak's multiple comparison test for comparison of more than two groups, using GraphPad Prism 9 software (San Diego, CA, USA). $p < 0.05$ was considered significant. Experiments were not randomised or blinded.

Data and Resource Availability The datasets generated and/or analysed during the current study are available from the corresponding author upon reasonable request. No applicable resources were generated or analysed during the current study.

Results

Changes in *Mfn1* and *Mfn2* expression in mouse strains maintained on regular chow (RC) or high fat high sugar (HFHS) diet. To determine whether the expression of *Mfn1* or *Mfn2* might be affected under conditions of hyperglycaemia mimicking T2D in humans, we interrogated data from a previous report [37] in which RNA sequencing was performed on six mouse strains. BALB/cJ mice showed “antiparallel” changes in *Mfn1* and *Mfn2* expression in response to maintenance on high fat high sugar (HFHS) diet for 10 days, and similar changes were obtained in DBA/2J mice at 30 and 90 days (Suppl.Fig.**1A-B**).

Generation of a conditional β*Mfn1/2* dKO mouse line. Efficient deletion of *Mfn1* and *Mfn2* in the beta cell was achieved in adult mice using the Pdx1-Cre^{ERT2} transgene and tamoxifen injection at 7-8 weeks. Possession of this transgene (which does not contain the human growth hormone (hGH) cDNA [21]) alone had no effect on glycaemic phenotype or cellular composition of pancreatic islets (Suppl. Fig.**2A-C**). Deletion of mitofusin genes was confirmed by qRT-PCR (Fig.**1A**) and Western (immuno-) blotting (Fig.**1B**) analysis, ~7 weeks post-tamoxifen injection. Relative to *β-actin*, expression of the *Mfn1* and *Mfn2* transcripts in isolated islets from dKO mice decreased by ~83 and 86% accordingly vs control islets (Fig.**1A**), consistent with selective deletion in the beta cell compartment [39]. No differences were detected in the expression of other mitochondrial fission and fusion mediator genes such as *Opa1*, *Drp1* and *Fis1* in islets (Fig.**1A**) or in *Mfn1* and *Mfn2* in other relevant tissues (Suppl.Fig.**3A**). dKO mice were significantly lighter than control animals after 20-21 weeks (Suppl.Fig.**3B**).

β*Mfn1/2* dKO mice are glucose intolerant with impaired GSIS *in vivo.* Glucose tolerance was impaired in dKO mice compared to control littermates at 14 weeks (Fig.**1C-D**) and this difference was further exaggerated at 20 weeks (Suppl. Fig.**3C**). At 14 weeks, β*Mfn1/2* dKO mice (with a 27 mmol/l glycaemia at 15 min.; Fig.**1E-F**) showed a dramatically lower insulin excursion upon glucose challenge vs control animals (Fig.**1G-H**). Following an oral gavage, glucose tolerance was more modestly affected in dKO mice (Fig.**1I-J**) while plasma insulin levels in these animals (with a glycaemia of 27 mmol/l at 15min.) were indistinguishable from control animals (Fig.**1K-L**; 0 vs 15min. in dKO). Insulin tolerance was unaltered in β*Mfn1/2* dKO vs control mice (Suppl.Fig.**3D**) while proinsulin conversion was impaired (Suppl.Fig.**3E-F**). dKO mice displayed significantly elevated plasma glucose (Suppl.Fig.**3G**) under both fed and fasted conditions and β-ketones (ketone bodies) were also elevated in fasted vs control animals (Suppl.Fig.**3H**), whereas plasma insulin levels were lower (Suppl.Fig.**3I**). Apparent insulin secretion was also impaired after IP injection with a lower glucose in 14- and 20-week-old dKO vs control mice (Suppl. Fig.**4A-D**). In contrast, plasma insulin levels were not statistically different between control and dKO animals following an OGTT at either age (Suppl. Fig.**4E-H**), though a trend towards lower insulin excursion was evident in dKO mice.

Deletion of *Mfn1/2* alters mitochondrial morphology in beta cells. While the mitochondrial network was highly fragmented in dKO cells (Fig.**2A;** and inset), the number of mitochondria per cell or density were not altered (Fig.**2B**). Mitochondrial elongation, perimeter and surface area were also significantly decreased in β*Mfn1/2* dKO cells, while circularity was increased (Fig.**2B**). Transmission electron microscopy (TEM) confirmed these changes (Fig.**2C**). Cristae structure and organisation were also

altered in β*Mfn1/2* dKO cells with a single crista often running the length of a mitochondrial section. Finally, dKO islets displayed a ~75% reduction in mtDNA (Fig.**2D**).

***Mitofusin* deletion leads to modest changes in beta cell mass.** Pancreatic beta cell mass decreased by 33% whereas alpha-cell mass was not affected in dKO mice (Fig.**3A-C**). Beta cell-alpha cell ratio was decreased by 53% (Fig.**3D**) in line with an increase in TUNEL-positive beta cells in dKO vs control animals (Fig.**3E-F**)

Mitochondrial fragmentation, beta cell mass deterioration and hyperglycaemia emerge in dKO mice two weeks post tamoxifen administration. We next sought to exclude the possibility that mitochondrial fragmentation may simply be the consequence of the observed hyperglycaemia. Two distinct groups of organelles (both elongated and circular) were apparent in β*Mfn1/2* dKO cells (Suppl. Fig. **5A-B**) two weeks post tamoxifen treatment. Neither fed nor fasted glycaemia or plasma insulin levels following glucose challenge were different between groups (Suppl. Fig. **5C-E**). A trend towards lower beta cell mass and mtDNA was detected in dKO animals (Suppl. Fig. **5F-I**).

Beta cell identity is modestly altered in β*Mfn1/2* dKO islets. Whilst *Ins2*, *Ucn3* and *Glut2* (*Slc2a2*) were significantly downregulated, *Trpm5* was upregulated in dKO islets (Suppl.Fig.**6**). No changes in alpha- or beta cell disallowed genes [40] were detected. In contrast, genes involved in mitochondrial function such as *Smdt1* and *Vdac3* were upregulated in dKO beta cells (Suppl.Fig.**6**). Lastly, genes involved in ER stress and

mito/autophagy were also affected, with *Chop (Ddit3)* and *p62* being upregulated and *Lc3* and *Cathepsin L* downregulated.

Mitofusins are essential to maintain normal glucose-stimulated Ca^{2+} dynamics, mitochondrial membrane potential and ATP levels. Increased cytosolic Ca^{2+} is a key trigger of insulin exocytosis in response to high glucose [2]. dKO mouse islets exhibited a significantly smaller glucose-induced $[Ca^{2+}]_{cyt}$ rise *vs* control islets (Fig.**4A-C**). When the K_{ATP} channel opener diazoxide and a depolarising K^+ concentration were then deployed together to bypass the regulation of these channels by glucose, cytosolic Ca^{2+} increases were not significantly impaired in dKO compared to control animals (Fig.**4B-C**). A substantial reduction in mitochondrial free Ca^{2+} concentration ($[Ca^{2+}]_{mito}$) in response to 17 mmol/l glucose [24] was also observed in dKO islets (Fig.**4D-F**). Of note, subsequent hyperpolarisation of the plasma membrane with diazoxide caused the expected lowering of mitochondrial $[Ca^{2+}]_{mito}$ in control islets (reflecting the decrease in $[Ca^{2+}]_{cyt}$;**Fig.4E-F**), but was almost without effect on dKO islets.

Glucose-induced increases in $\Delta\psi_m$ were also sharply reduced in dKO vs control mouse islets (Fig.**4G-H**). Addition of 2-[2-[4-(trifluoromethoxy)phenyl]hydrazinylidene]-propanedinitrile (FCCP) resulted in a similar collapse in apparent $\Delta\psi_m$ in islets from both genotypes (Fig.**4G**). Cytosolic Ca^{2+} oscillations and synchronous $\Delta\psi_m$ depolarisation were also largely abolished in response to glucose in dKO cells when measured by intravital imaging *in vivo* [41]. Finally, to assess whether deletion of *Mfn1* and *Mfn2* may impact glucose-induced increases in mitochondrial ATP synthesis we performed real-time fluorescence imaging using Perceval (Fig.**4I-J**). While control

islets responded with a time-dependent rise in the ATP:ADP ratio in response to a step increase in glucose from 3 mmol/l to 17 mmol/l, β*Mfn1/2* dKO beta cells failed to mount any response (Fig.**4J**).

Beta cell-beta cell connectivity is impaired by *Mfn1/2* ablation. Intercellular connectivity is required in the islet for a full insulin secretory response to glucose [42]. To assess this, individual Ca^{2+} traces recorded from Cal-520-loaded beta-cells in mouse islets (Fig.**4A-B**) were subjected to correlation (Pearson *r*) analysis to map cell-cell connectivity (Suppl.Fig.**7A**). Following perfusion at 17 mmol/l glucose, β*Mfn1/2* dKO beta cells tended to display an inferior, though not significantly different, coordinated activity than control cells, as assessed by counting the number of coordinated cell pairs (Suppl.Fig.**7C**; 0.94 vs 0.90 for control vs dKO, respectively). By contrast, beta cells displayed highly coordinated Ca^{2+} responses upon addition of 20 mmol/l KCl in dKO islets. Similarly, analysis of correlation strength in the same islets revealed significant differences in response to 17 mmol/l glucose between genotypes. In fact, dKO islets had weaker mean beta-beta cell coordinated activity (Suppl. Fig.**7B, D**; $p<0.05$; 0.88 vs 0.77 for control vs dKO, respectively), indicating that mitofusins affect the strength of connection rather than the number of coordinated beta cell pairs. A tending towards lower expression of the gap junction gene *Cx36/Gjd2* was observed in dKO islets (Suppl.Fig.**7E**). Beta cell "hub" and "leader" distributions [43] were also impaired in the dKO group (not shown, see [41]).

Unaltered ER Ca^{2+} mobilisation but decreased mitochondrial O_2 consumption and mtDNA depletion in β*Mfn1/2* dKO islets. No differences in cytosolic Ca^{2+} responses between genotypes were observed after agonism at the Gq-coupled

metabotropic acetylcholine (Ach) receptor [44, 45] (Fig.**5A-C**). In contrast, measurements of O_2 consumption revealed that basal, proton leak and maximal respiratory capacities were significantly impaired in dKO islets (Fig.**5D-E**).

Impaired GSIS *in vitro* and beta cell connectivity can be rescued by incretins in β*Mfn1/2* dKO mouse islets. While GSIS was markedly impaired in dKO islets (Fig.**6A**; Suppl. Table 4), incretins (GLP-1 or GIP), or the GLP1R agonist exendin-4, at a submaximal concentration of 10 mmol/l glucose, led to a significant potentiation in GSIS in both groups. Consequently, insulin secretion in response to 10 mmol/l glucose was no longer different between control and β*Mfn1/2* dKO islets after incretin addition (Fig.**6A-B**). Moreover, under these conditions, forced increases in intracellular cAMP imposed by the addition of forskolin (FSK) or 3-isobutyl-1-methylxanthine (IBMX), which activate adenylate cyclase (AC) and inhibit phosphodiesterase (PDE) respectively, eliminated differences in GSIS between the genotypes (Fig.**6B**). No differences in insulin secretion were observed between control and dKO islets after depolarisation with KCl.

We next explored whether the incretin-mediated improvements in insulin secretion in response to incretins were the result of altered $[Ca^{2+}]_{cyt}$ dynamics. Islets from isolated dKO mice displayed a delayed increase in $[Ca^{2+}]_{cyt}$ in response to 10 mmol/l glucose compared to control islets (Fig.**6C-D**). Addition of exendin-4 led to the emergence of oscillatory activity in both groups and under these conditions, differences between genotypes, as seen in Fig.**4B**, were no longer evident (Fig.**6C**). Measured at 10mmol/l glucose, control and dKO islets displayed increases in ER Ca^{2+} in response to exendin-4 (Fig.**6E-F**) while the response exaggerated in the latter group. Neither group

displayed significant changes in ATP:ADP ratio in response to exendin-4 (Fig.**6G-H**). Analysis of OCR revealed no significant differences between genotypes at 10mmol/l glucose in the presence or absence of exendin-4 or FSK (Fig.**6I**).

Moreover, mitofusin deletion may lead to a partial activation of "amplification" pathways of GSIS [46] at 3 mmol/l glucose since insulin secretion was enhanced in dKO islets after depolarisation of the plasma membrane with KCl in the presence of diazoxide (Fig. **6J**). Conversely, no differences between islet genotypes were observed at 17 mmol/l glucose (Fig.**6J**).

Whilst glucose-induced beta cell-beta cell connectivity, as assessed by monitoring Ca^{2+} dynamics (Fig.**6C**), was markedly impaired in dKO islets (Fig. **7A** and Suppl. Fig.**7**), these differences were largely abolished in the presence of exendin-4 (Fig. **8B-D**).

Insulin secretion is rescued by incretins through an EPAC-dependent activation. To explore the actions of mitochondrial disruption on incretin signalling, we next used a pharmacological approach. Glucose-stimulated insulin secretion was more strongly enhanced in dKO vs control islets by IBMX, FSK or the protein kinase A (PKA) inhibitor H89 alone (Fig.**8A**; Suppl. Table 4). Selective activation of EPAC also tended to lead to a larger increase in insulin secretion in dKO than control islets, and this difference became significant when PKA was inhibited with H89 (Fig.**8B**).

Glucose-dependent increases in cytosolic cAMP, assessed using the Epac-camps sensor, were also markedly amplified in dKO vs control cells (Fig.**8C-D**). This

difference persisted in the presence of IBMX and FSK, added separately or alone (Fig.**8C,E**). No changes in the expression of *Epac*, *Adcy* or *Prkar* (PKA) subunits were apparent between control and dKO islets (Fig.**8F**).

Defective glucose-stimulated insulin secretion is rescued by GLP-1R agonism in *Clec16a* null mice. To determine whether incretins may reverse defective insulin secretion in an alternative model of mitochondrial dysfunction, we examined mice lacking the mitophagy regulator *Clec16a* selectively in the pancreatic islet (*Clec16a*$^{\Delta panc}$) [22]. Glucose-stimulated insulin secretion was sharply inhibited in null vs Pdx1-Cre control mice, and these differences between genotype were largely corrected in by the addition of exendin-4 (Suppl. Fig.**8A**). Correspondingly, whereas the difference between *Clec16a*$^{\Delta panc}$ and control mice was significant for IPGTTs there was no such (significant) difference for the OGTTs at 15mins, in line with the findings above for β*Mfn1/2* dKO mice (Suppl. Fig.**8B-C**).

Defective secretion of a preserved pool of morphologically-docked granules in β*Mfn1/2* dKO mouse beta cells. To determine whether the markedly weaker stimulation of insulin secretion in dKO islets may reflect failed recruitment of secretory granules into a readily releasable or morphologically-docked pool beneath the plasma membrane, we next deployed total internal reflection fluorescence (TIRF) microscopy in dissociated beta cells. By over-expressing NPY-Venus, the number of insulin granules was significantly higher in close proximity with the plasma membrane in dKO cells after treatment with 20 mmol/l KCl (Suppl.Fig.**9A-B).** However, when we then used ZIMIR [30] in response to depolarisation as a surrogate for insulin secretion, release events were fewer in number and smaller in dKO (Suppl.Fig.**9C-E**).

Altered plasma metabolomic and lipidomic profiles in β*Mfn1/2* dKO mice. We applied an -omics approach to study metabolite and lipid changes in peripheral plasma samples from control and dKO mice (Suppl.Fig.**10**). Of 29 metabolites, the levels of five metabolic species (shown in red) were significantly altered in β*Mfn1/2* dKO animals (Suppl.Fig.**10A**). In the lipidomics analysis, the majority of lipid classes displayed a remarkably homogeneous downward trend in dKO samples (Suppl.Fig.**10B**).

Discussion

The key goal of the present study was to determine the role of mitofusins in controlling mitochondrial dynamics and hence glucose- and incretin-stimulated insulin secretion in the beta cell. Our strategy involved deleting both mitofusin isoforms since the expression of *Mfn1* and *Mfn2* is similar in the beta cell [47], suggestive of partial functional redundancy [48]. Our measurements of *Mfn1* and *Mfn2* expression in mouse models of T2D nonetheless revealed changes in the expression of these genes which may contribute to the disease.

Importantly, we show that *Mfn1* and *Mfn2* are critical regulators of the mitochondrial network in beta cells and consequently of insulin secretion *in vitro* and *in vivo* (Suppl.Fig.**11A-B**); see also [41]). These findings are in line with earlier studies, albeit involving the deletion of genes other than the mitofusins [13-18]. Additionally, we show that changes in *Mfn1* and *Mfn2* expression occur in models of diabetes and hence, their forced changes, as achieved in our study, may have relevance for the patho-etiology of beta cell failure in T2D and metabolic changes consistent with insulin deficiency. These include higher levels of bile acids as previously described in rodent models of T1D and T2D and in humans [49, 50], elevated leucine and isoleucine, as observed in human T1D [51], and an altered triglyceride profile [52]. Finally, these metabolomic/lipidomic data provide further support for the expected actions of mitofusin deletion via altered beta cell function, with changes that are somewhat more in line with metabolomic changes in human T1D (and models thereof) than T2D [53]. Indeed, dKO mice gain less weight than controls as they show the classic symptoms of diabetes mellitus [54, 55]. This is likely to be the result of metabolic dyshomeostasis in the face of lowered circulating insulin levels, leading to impaired fat storage, loss of

liver and muscle glycogen and eventually loss of muscle mass i.e. the cardinal symptoms of T1D and of advanced insulin-requiring T2D in humans.

Of note, none of the earlier reports investigating the effects of mitochondrial disruption in the beta cell explored the effects on incretin-stimulated secretion. Suggesting a differential effect on glucose- *vs* incretin-stimulated secretion we show here, firstly, that insulin secretion and glucose excursion were less markedly affected by mitofusin knockout during OGTTs, where an incretin effect is preserved [56], than during IPGTTs. Correspondingly, insulin secretion stimulated by incretins was largely preserved in dKO cells, in contrast to the ablation of glucose-stimulated secretion (Suppl. Fig. **11C-D**). Strikingly, mitofusin deletion also enhanced incretin-stimulated cytosolic cAMP increases. That this effect was preserved in the face of PDE inhibition (IBMX) and AC activation was surprising, but may reflect an increase in total AC activity or distribution in dKO cells.

While PKA suppression is considered to be either neutral or inhibitory towards GSIS in WT beta cells [57-59], our data show a rather striking increase in insulin secretion in the presence of H89 in islets from mice of either genotype. Whilst unexpected, and in contrast with those of others that support a role for PKA downstream of cAMP in the beta cell, Bryan and colleagues provide some evidence for the stimulation of GSIS by H89 under certain conditions [57]. Nevertheless, several studies have stressed the importance of both PKA-dependent and -independent effects of increased $[cAMP]_i$ on GSIS from islets [60]. Thus, PKA-independent exocytosis occurs through interactions between Epac-2/cAMP- guanine-nucleotide-exchange factor II [61, 62], Rab3A and Rim2 (proteins involved in vesicle trafficking [57, 63, 64] and fusion) [65]. On the other

hand, GLUT2, Kir6.2, and SUR1 and α-SNAP (a vesicle-associated protein), have been reported to be phosphorylated by PKA [58]. Here, we show that the effect of mitofusin deletion on GSIS is preserved when PKA is inhibited by H89, and even potentiated by EPAC-activation (Suppl. Fig. **11C-D)**. These changes appear to be exerted at the post transcriptional level, since we observed no changes in levels of mRNAs encoding the relevant beta cell isoforms of *Epac*. Whether there are changes in the level or the corresponding proteins including EPAC, their subcellular localisation or interaction with upstream regulators or downstream effectors, remains to be explored. Finally, the latter findings could indicate that an intact mitochondrial reticulum restricts signalling by EPAC through a mechanism that is inhibited by PKA. Future studies, using additional or alternative PKA inhibitors [66], will be needed to explore these possibilities.

Possibly contributing to these differences in the effects on responses to glucose vs incretin, exendin-4 treatment led to greater Ca^{2+} accumulation in the ER in dKO cells. By enhancing Ca^{2+} cycling across the ER membrane this could conceivably drive larger local increases in cytosolic Ca^{2+} which, in turn, may influence plasma membrane potential, trigger Ca^{2+} influx via VDCCs and hence, stimulate insulin release [67].

We also demonstrate that preserved mitochondrial ultra-structure is critical for normal beta cell-beta cell connectivity, itself required for normal insulin secretion [41, 68]. The mechanisms underlying impaired connectivity in the absence of mitofusins are unclear but may involve altered *Cx36/Gjd2* expression, phosphorylation or activity, impacting gap junctions [42].

In summary, we show that acute treatment with incretins, commonly used as treatments for T2D and obesity [56], largely reverses the deficiencies in insulin secretion which follow mitochondrial disruption. Future studies will be needed to address the relevance of these findings to human beta cells and to the action of incretins in clinical settings.

Acknowledgements

We thank Stephen M. Rothery from the Facility for Imaging by Light Microscopy (FILM) at Imperial College London for support with confocal and widefield microscopy image recording and analysis. We thank Professor Julia Gorelik and Sasha Judina (Imperial College) for providing the Epac1-camps sensor. We also thank Aida Di Gregorio from the National Heart and Lung Institute (Imperial College) for genotyping the mice.

Author contributions

EG performed experiments and analysed data. EG supported the completion of confocal and widefield microscopy and analysis. ATC performed the EM sample processing and data analysis. CM, MM and AKL were responsible for the *in vivo* intravital Ca^{2+} imaging in mice presented in the bioRxiv paper. PC contributed to the analysis and manipulation of the *in vivo* intravital Ca^{2+} measurements as well as the preparation and imaging of TIRF samples. TS contributed to the generation of the MATLAB script used for connectivity analysis. FYSW and YA generated and performed Monte Carlo-based signal binarization. BJ assisted with the cAMP assays. EA and LLN performed the oral gavage in live animals. YX and GG performed studies with Pdx1CreER mice. NA assisted with Seahorse experiment protocols. CLQ and AW contributed to the metabolomics analysis. CCG, CM and MI were responsible for the RNAseq data analysis. SAS performed studies with Clec16a mice. TAR was involved in the design of the floxed *Mfn* alleles. TAR and IL were responsible for the maintenance of mouse colonies and final approval of the version to be published. GAR (University of Montreal, Imperial College) designed the study and wrote the manuscript with EG (Imperial College) with input and final approval of the version to be published from all authors. GAR is the guarantor of this work and, as such, had full access to all

the data in the study and takes responsibility for the integrity of the data and the accuracy of the data analysis.

Funding

GAR was supported by a Wellcome Trust Senior Investigator Award (098424AIA) and Investigator Award (212625/Z/18/Z), MRC Programme grants (MR/R022259/1, MR/J0003042/1, MR/L020149/1), an Experimental Challenge Grant (DIVA, MR/L02036X/1), an MRC grant (MR/N00275X/1), and a Diabetes UK grant (BDA/11/0004210, BDA/15/0005275, BDA16/0005485). IL was supported by a Diabetes UK project grant (16/0005485). This project has received funding from the Innovative Medicines Initiative 2 Joint Undertaking, under grant agreement no. 115881 (RHAPSODY). This Joint Undertaking receives support from the European Union's Horizon 2020 research and innovation programme and EFPIA. This work is supported by the Swiss State Secretariat for Education, Research and Innovation (SERI), under contract no. 16.0097. AT was supported by MRC project grant MR/R010676/1. Intravital imaging was performed using resources and/or funding provided by National Institutes of Health grants R03 DK115990 (to AKL), Human Islet Research Network UC4 DK104162 (to AKL; RRID:SCR_014393). BJ acknowledges support from the Academy of Medical Sciences, Society for Endocrinology, The British Society for Neuroendocrinology, the European Federation for the Study of Diabetes, an EPSRC capital award and the MRC (MR/R010676/1). SAS was supported by the JDRF (CDA-2016-189, SRA-2018-539, COE-2019-861), the NIH (R01 DK108921, U01 DK127747), and the US Department of Veterans Affairs (I01 BX004444).

Conflict of interest

Authors' relationships and activities GAR has received grant funding and consultancy fees from Les Laboratoires Servier and Sun Pharmaceuticals. The remaining authors declare that there are no relationships or activities that might bias, or be perceived to bias, their work.

Guarantor Statement

GAR is the guarantor of this work and, as such, had full access to all the data in the study and takes responsibility for the integrity of the data and the accuracy of the data analysis.

Prior Presentation Information

This study has been previously presented as an oral or poster presentation at ADA 2021, Australasian Diabetes Congress 2021, ADA 2020, Diabetes UK 2019, Gordon Research conferences 2019, Rhapsody Consortium, EASD 2018.

References

1. Anderson, A.J., et al., Mitochondria-hubs for regulating cellular biochemistry: emerging concepts and networks. Open biology, 2019. 9(8): p. 190126-190126.
2. Rutter, G.A., et al., Pancreatic β-cell identity, glucose sensing and the control of insulin secretion. Biochem J, 2015. 466(2): p. 203-18.
3. Rorsman, P. and F.M. Ashcroft, Pancreatic β-Cell Electrical Activity and Insulin Secretion: Of Mice and Men. Physiol Rev, 2018. 98(1): p. 117-214.
4. Henquin, J.C., Triggering and amplifying pathways of regulation of insulin secretion by glucose. Diabetes, 2000. 49(11): p. 1751-60.
5. Jones, B., et al., Control of insulin secretion by GLP-1. Peptides, 2018. 100: p. 75-84.
6. Yang, D., et al., Mitochondrial Dynamics: A Key Role in Neurodegeneration and a Potential Target for Neurodegenerative Disease. Frontiers in Neuroscience, 2021. 15(359).
7. Rutter, G.A. and R. Rizzuto, Regulation of mitochondrial metabolism by ER Ca2+ release: an intimate connection. Trends in Biochemical Sciences, 2000. 25(5): p. 215-221.
8. Westermann, B., Bioenergetic role of mitochondrial fusion and fission. Biochim Biophys Acta, 2012. 1817(10): p. 1833-8.
9. Ma, K., et al., Mitophagy, Mitochondrial Homeostasis, and Cell Fate. Front Cell Dev Biol, 2020. 8: p. 467.
10. Filadi, R., et al., On the role of Mitofusin 2 in endoplasmic reticulum-mitochondria tethering. Proc Natl Acad Sci U S A, 2017. 114(12): p. E2266-e2267.
11. Rovira-Llopis, S., et al., Mitochondrial dynamics in type 2 diabetes: Pathophysiological implications. Redox Biol, 2017. 11: p. 637-645.
12. Serasinghe, M.N. and J.E. Chipuk, Mitochondrial Fission in Human Diseases. Handb Exp Pharmacol, 2017. 240: p. 159-188.
13. Reinhardt, F., et al., Drp1 guarding of the mitochondrial network is important for glucose-stimulated insulin secretion in pancreatic beta cells. Biochem Biophys Res Commun, 2016. 474(4): p. 646-651.
14. Hennings, T.G., et al., In Vivo Deletion of beta-Cell Drp1 Impairs Insulin Secretion Without Affecting Islet Oxygen Consumption. Endocrinology, 2018. 159(9): p. 3245-3256.
15. Supale, S., et al., Loss of prohibitin induces mitochondrial damages altering β-cell function and survival and is responsible for gradual diabetes development. Diabetes, 2013. 62(10): p. 3488-3499.
16. Stiles, L. and O.S. Shirihai, Mitochondrial dynamics and morphology in beta-cells. Best Pract Res Clin Endocrinol Metab, 2012. 26(6): p. 725-38.
17. Zhang, Z., et al., The dynamin-related GTPase Opa1 is required for glucose-stimulated ATP production in pancreatic beta cells. Mol Biol Cell, 2011. 22(13): p. 2235-45.
18. Men, X., et al., Dynamin-related protein 1 mediates high glucose induced pancreatic beta cell apoptosis. The International Journal of Biochemistry & Cell Biology, 2009. 41(4): p. 879-890.
19. Del Guerra, S., et al., Functional and Molecular Defects of Pancreatic Islets in Human Type 2 Diabetes. Diabetes, 2005. 54(3): p. 727-735.
20. Chen, H., J.M. McCaffery, and D.C. Chan, Mitochondrial fusion protects against neurodegeneration in the cerebellum. Cell, 2007. 130(3): p. 548-62.

21. Gu, G., J. Dubauskaite, and D.A. Melton, Direct evidence for the pancreatic lineage: NGN3+ cells are islet progenitors and are distinct from duct progenitors. Development, 2002. 129(10): p. 2447-57.
22. Soleimanpour, S.A., et al., The diabetes susceptibility gene Clec16a regulates mitophagy. Cell, 2014. 157(7): p. 1577-1590.
23. Ravier, M.A. and G.A. Rutter, Isolation and culture of mouse pancreatic islets for ex vivo imaging studies with trappable or recombinant fluorescent probes. Methods Mol Biol, 2010. 633: p. 171-84.
24. Georgiadou, E., et al., The pore-forming subunit MCU of the mitochondrial Ca2+ uniporter is required for normal glucose-stimulated insulin secretion in vitro and in vivo in mice. Diabetologia, 2020. 63(7): p. 1368-1381.
25. Kolesar, J.E., et al., Two-dimensional intact mitochondrial DNA agarose electrophoresis reveals the structural complexity of the mammalian mitochondrial genome. Nucleic Acids Res, 2013. 41(4): p. e58.
26. Ravier, M.A., et al., Mechanisms of control of the free Ca2+ concentration in the endoplasmic reticulum of mouse pancreatic β-cells: interplay with cell metabolism and [Ca2+]c and role of SERCA2b and SERCA3. Diabetes, 2011. 60(10): p. 2533-45.
27. Varadi, A. and G.A. Rutter, Dynamic imaging of endoplasmic reticulum Ca2+ concentration in insulin-secreting MIN6 Cells using recombinant targeted cameleons: roles of sarco(endo)plasmic reticulum Ca2+-ATPase (SERCA)-2 and ryanodine receptors. Diabetes, 2002. 51 Suppl 1: p. S190-201.
28. Nikolaev, V.O., et al., Novel Single Chain cAMP Sensors for Receptor-induced Signal Propagation. Journal of Biological Chemistry, 2004. 279(36): p. 37215-37218.
29. Wiemerslage, L. and D. Lee, Quantification of mitochondrial morphology in neurites of dopaminergic neurons using multiple parameters. J Neurosci Methods, 2016. 262: p. 56-65.
30. Li, D., et al., Imaging dynamic insulin release using a fluorescent zinc indicator for monitoring induced exocytotic release (ZIMIR). Proc Natl Acad Sci U S A, 2011. 108(52): p. 21063-8.
31. Tsuboi, T. and G.A. Rutter, Multiple forms of "kiss-and-run" exocytosis revealed by evanescent wave microscopy. Curr Biol, 2003. 13(7): p. 563-7.
32. Ahonen, L., et al., Targeted Clinical Metabolite Profiling Platform for the Stratification of Diabetic Patients. Metabolites, 2019. 9(9): p. 184.
33. Taddeo, E.P., et al., Mitochondrial Proton Leak Regulated by Cyclophilin D Elevates Insulin Secretion in Islets at Nonstimulatory Glucose Levels. Diabetes, 2020. 69(2): p. 131-145.
34. Brand, M.D. and D.G. Nicholls, Assessing mitochondrial dysfunction in cells. The Biochemical journal, 2011. 435(2): p. 297-312.
35. Carrat, G.R., et al., The type 2 diabetes gene product STARD10 is a phosphoinositide-binding protein that controls insulin secretory granule biogenesis. Molecular Metabolism, 2020. 40: p. 101015.
36. Akalestou, E., et al., Intravital imaging of islet Ca2+ dynamics reveals enhanced β cell connectivity after bariatric surgery in mice. Nature Communications, 2021. 12(1): p. 5165.
37. Cruciani-Guglielmacci, C., et al., Molecular phenotyping of multiple mouse strains under metabolic challenge uncovers a role for Elovl2 in glucose-induced insulin secretion. Molecular Metabolism, 2017. 6(4): p. 340-351.

38. Benjamini, Y. and Y. Hochberg, Controlling the false discovery rate: a practical and powerful approach to multiple testing. Journal of the Royal Statistical Society Series B, 1995. 57: p. 289–300.
39. Elayat, A.A., M.M. el-Naggar, and M. Tahir, An immunocytochemical and morphometric study of the rat pancreatic islets. J Anat, 1995. 186 (Pt 3)(Pt 3): p. 629-37.
40. Pullen, T.J., M.O. Huising, and G.A. Rutter, Analysis of Purified Pancreatic Islet Beta and Alpha Cell Transcriptomes Reveals 11β-Hydroxysteroid Dehydrogenase (Hsd11b1) as a Novel Disallowed Gene. Frontiers in Genetics, 2017. 8(41).
41. Georgiadou, E., et al., Mitofusins Mfn1 and Mfn2 are required to preserve glucose-but not incretin-stimulated beta cell connectivity and insulin secretion. bioRxiv, 2021: p. 2020.04.22.055384.
42. Rutter GA, et al., Metabolic and functional specialisations of the pancreatic beta cell: gene disallowance, mitochondrial metabolism and intercellular connectivity. Diabetologia under review, 2020.
43. Johnston, N.R., et al., Beta Cell Hubs Dictate Pancreatic Islet Responses to Glucose. Cell Metab, 2016. 24(3): p. 389-401.
44. Gautam, D., et al., A critical role for beta cell M3 muscarinic acetylcholine receptors in regulating insulin release and blood glucose homeostasis in vivo. Cell Metab, 2006. 3(6): p. 449-61.
45. Gautam, D., et al., Beneficial metabolic effects caused by persistent activation of beta-cell M3 muscarinic acetylcholine receptors in transgenic mice. Endocrinology, 2010. 151(11): p. 5185-94.
46. Gembal, M., P. Gilon, and J.C. Henquin, Evidence that glucose can control insulin release independently from its action on ATP-sensitive K+ channels in mouse B cells. The Journal of Clinical Investigation, 1992. 89(4): p. 1288-1295.
47. Benner, C., et al., The transcriptional landscape of mouse beta cells compared to human beta cells reveals notable species differences in long non-coding RNA and protein-coding gene expression. BMC Genomics, 2014. 15(1): p. 620.
48. Sidarala, V., et al., Mitofusins 1 and 2 collaborate to fuel pancreatic beta cell insulin release via regulation of both mitochondrial structure and DNA content. bioRxiv, 2021: p. 2021.01.10.426151.
49. Andersén, E., G. Karlaganis, and J. Sjövall, Altered bile acid profiles in duodenal bile and urine in diabetic subjects. Eur J Clin Invest, 1988. 18(2): p. 166-72.
50. Uchida, K., S. Makino, and T. Akiyoshi, Altered Bile Acid Metabolism in Nonobese, Spontaneously Diabetic (NOD) Mice. Diabetes, 1985. 34(1): p. 79-83.
51. Sailer, M., et al., Increased plasma citrulline in mice marks diet-induced obesity and may predict the development of the metabolic syndrome. PLoS One, 2013. 8(5): p. e63950.
52. Lamichhane, S., et al., Dynamics of Plasma Lipidome in Progression to Islet Autoimmunity and Type 1 Diabetes - Type 1 Diabetes Prediction and Prevention Study (DIPP). Scientific reports, 2018. 8(1): p. 10635-10635.
53. George, A.M., A.G. Jacob, and L. Fogelfeld, Lean diabetes mellitus: An emerging entity in the era of obesity. World journal of diabetes, 2015. 6(4): p. 613-620.

54. Mitchell, R.K., et al., The transcription factor Pax6 is required for pancreatic β cell identity, glucose-regulated ATP synthesis and Ca2+ dynamics in adult mice. Journal of Biological Chemistry, 2017.
55. Martinez-Sanchez, A., M.-S. Nguyen-Tu, and G.A. Rutter, DICER Inactivation Identifies Pancreatic β-Cell "Disallowed" Genes Targeted by MicroRNAs. Molecular endocrinology (Baltimore, Md.), 2015. 29(7): p. 1067-1079.
56. Nauck, M.A., et al., GLP-1 receptor agonists in the treatment of type 2 diabetes - state-of-the-art. Mol Metab, 2020: p. 101102.
57. Nakazaki, M., et al., cAMP-Activated Protein Kinase-Independent Potentiation of Insulin Secretion by cAMP Is Impaired in SUR1 Null Islets. Diabetes, 2002. 51(12): p. 3440-3449.
58. Kashima, Y., et al., Critical Role of cAMP-GEFII·Rim2 Complex in Incretin-potentiated Insulin Secretion*. Journal of Biological Chemistry, 2001. 276(49): p. 46046-46053.
59. Chepurny, O.G., et al., PKA-dependent potentiation of glucose-stimulated insulin secretion by Epac activator 8-pCPT-2'-O-Me-cAMP-AM in human islets of Langerhans. Am J Physiol Endocrinol Metab, 2010. 298(3): p. E622-33.
60. Renström, E., L. Eliasson, and P. Rorsman, Protein kinase A-dependent and -independent stimulation of exocytosis by cAMP in mouse pancreatic B-cells. The Journal of physiology, 1997. 502 (Pt 1)(Pt 1): p. 105-118.
61. de Rooij, J., et al., Epac is a Rap1 guanine-nucleotide-exchange factor directly activated by cyclic AMP. Nature, 1998. 396(6710): p. 474-7.
62. Kawasaki, H., et al., A family of cAMP-binding proteins that directly activate Rap1. Science, 1998. 282(5397): p. 2275-9.
63. Ozaki, N., et al., cAMP-GEFII is a direct target of cAMP in regulated exocytosis. Nat Cell Biol, 2000. 2(11): p. 805-11.
64. Kashima, Y., et al., Critical role of cAMP-GEFII--Rim2 complex in incretin-potentiated insulin secretion. J Biol Chem, 2001. 276(49): p. 46046-53.
65. Wang, Y., et al., Glucagon-like peptide-1 can reverse the age-related decline in glucose tolerance in rats. J Clin Invest, 1997. 99(12): p. 2883-9.
66. Lochner, A. and J.A. Moolman, The many faces of H89: a review. Cardiovasc Drug Rev, 2006. 24(3-4): p. 261-74.
67. Gilon, P., et al., Uptake and release of Ca2+ by the endoplasmic reticulum contribute to the oscillations of the cytosolic Ca2+ concentration triggered by Ca2+ influx in the electrically excitable pancreatic B-cell. J Biol Chem, 1999. 274(29): p. 20197-205.
68. Salem, V., et al., Leader β-cells coordinate Ca2+ dynamics across pancreatic islets in vivo. Nature Metabolism, 2019. 1(6): p. 615-629.

Figure legends

Fig.1 Generation of a conditional β*Mfn1/2* dKO mouse line which displays a highly impaired glucose tolerance *in vivo*. (A) qRT-PCR quantification of *Mfn1, Mfn2, Drp1, Opa1* and *Fis1* expression in control and dKO islets relative to *β-actin* (*n*=3-5 mice per genotype in two independent experiments).(B) Western blot analysis demonstrating efficient MFN1 (84 kDa) and MFN2 (86 kDa) deletion relative to GAPDH (36 kDa) in isolated islets (*n*=3-4 mice per genotype in three independent experiments).(C) Glucose tolerance was measured in dKO mice and littermate controls by IPGTT (1 g/kg body weight).(D) Corresponding AUC from (C) (*n*=8 mice per genotype,in 2 independent experiments). (E) Glucose tolerance measured by IPGTT (using 3 g/kg body weight) and (F) the corresponding AUC were assessed in β*Mfn1/2* dKO and control mice (*n*=8 mice per genotype in two independent experiments). (G) Plasma insulin levels during IPGTT in dKO and control mice (*n*=11-12 mice per genotype in three independent experiments) and (H) the corresponding AUC. (I) Glucose tolerance post-oral gavage (3 g/kg body weight) was measured in *n*=8 animals per genotype in two independent experiments. Glucose baseline values between control and dKO mice were significantly different (*p<0.05). Increases in glucose from baseline in control animals were ****p<0.0001, ***p<0.001 and **p<0.01 and ****p<0.0001 in dKO animals from 15 to 60mins accordingly. The corresponding AUC is shown in (J). (K) Plasma insulin levels during OGTT in dKO and control mice (*n*=8 mice per genotype in two independent experiments) and (L) the corresponding AUC. (Blue, *control* mice; red, *dKO* mice. Data are presented as mean±SD in A and mean±SEM in B-L. *p<0.05; **p<0.01; ***p<0.001; ****p<0.0001 as indicated, or *control* vs *dKO* mice at the time points as indicated in (K), analysed by unpaired two-tailed Student's t-test and Mann–Whitney correction or two-way ANOVA test and Sidak's multiple comparisons test. All experiments were performed in 14-week-old male mice.

Fig.2 Mitochondrial ultrastructure is altered following *Mfn1/2* deletion. (A) Confocal images of the mitochondrial network of dissociated beta cells stained with Mitotracker green; scale bar: 5 μm. Lower right panels: magnification of selected areas. (B) Mitochondrial morphology analysis on deconvolved confocal images of dissociated beta cells. A macro was developed to quantify the number of mitochondria

per cell and measure the elongation, perimeter, circularity (0: elongated; 1: circular mitochondria), density and surface area of the organelles in control and dKO animals (*n*=40-54 cells; *n*=3 mice per genotype). (C) Electron micrographs of mitochondria indicated with black arrows in islets isolated from control and dKO mice; scale bars: 1μm. Right panel: magnification of selected areas showing the cristae structure (black arrow heads); scale bar: 0.5 μm. Schematic representation of enlarged mitochondria. (D) The relative mitochondrial DNA copy number was measured by determining the ratio of the mtDNA-encoded gene *mt-Nd1* to the nuclear gene *Ndufv1* (*n*=3 mice per genotype). Data are presented as mean±SEM in A-C and mean±SD in D. *p<0.05, ***p<0.001, ****p<0.0001 as indicated, analysed by unpaired two-tailed Student's t-test and Mann–Whitney correction. Experiments were performed in 14-week-old male mice.

Fig.3 Absence of *Mfn1/2* in beta cells leads to decreased beta cell mass and increased beta cell apoptosis.(A) Representative pancreatic sections immunostained with glucagon (red) and insulin (green); scale bars: 50μm.(B) The beta cell and alpha cell surface (C) measured within the whole pancreatic area in control and dKO mice were determined, as well as the beta/alpha cell ratio in (D), (*n*=79-86 islets, 4 mice per genotype; experiment performed in triplicate).(E) Representative confocal images of islets with TUNEL positive (green) apoptotic beta cells (ROI) and insulin (red). Magnification of selected area displaying each fluorescent channel; scale bar: 5μm. DNase I treated sections were used as a positive control in the TUNEL assay. Scale bars: 20μm.(F) Quantification of the percentage of islets containing TUNEL positive cells (*n*=114-133 islets, 4 mice per genotype; experiment performed in triplicate). Data are presented as mean±SD. *p<0.05, assessed by unpaired two-tailed Student's t-test and Mann–Whitney correction. Experiments were performed in 14-week-old male mice.

Fig.4 *Mfn1/2* deletion from pancreatic beta cells impairs cytosolic and mitochondrial Ca^{2+} uptake and changes mitochondrial potential and ATP synthesis *in vitro*. (A) Each snapshot of isolated control (i–iv) and dKO-derived (v–viii) islets was taken during the time points indicated by the respective arrows in (B). Scale bar: 50 μm. See also ESM Video 1. (B) $[Ca^{2+}]_{cyt}$ traces in response to 3G, 3

mmol/l glucose, 17 mmol/l glucose (17G; with or without 100μmol/l diazoxide [diaz]) or 20 mmol/l KCl with diaz were assessed following Cal-520 uptake in whole islets. Traces represent mean normalised fluorescence intensity over time (F/F_{min}).(C) The corresponding AUC is also presented (*n*=17-26 islets, 4 mice per genotype); 17G AUC measured between 245 s and 1045 s, 17G+diaz AUC measured between 1200 s and 1320 s, and KCl+diaz AUC measured between 1424 s and 1500 s. For each genotype different baselines (ctrl diaz/KCl: 0.95, dKO diaz/KCl: 0.8 were taken into consideration to measure AUCs.(D) Each snapshot of isolated control (i–iv) and dKO-derived (v–viii) islets was taken during the time points indicated by the respective arrows in (E). Scale bar: 50 μm. See also ESM Video 2. (E) $[Ca^{2+}]_{mito}$ changes in response to 17G (with or without diazoxide [diaz]) and 20 mmol/l KCl were assessed in islets following R-GECO infection. Traces represent mean normalised fluorescence intensity over time (F/F_{min}) where F_{min} is the mean fluorescence recorded during imaging under 3 mmol/l glucose.(F) The corresponding AUC is also shown (*n*=20-23 islets, 3 mice per genotype; 17G AUC measured between 270 s and 1100 s, 17G+diaz AUC measured between 1101 s and 1365 s and KCl AUC measured between 1366 s and1500 s).(G) Dissociated beta cells were loaded with TMRE to measure changes in $\Delta\psi_m$, and perifused with 3 mmol/l glucose (3G), 17G or FCCP as indicated. Traces represent normalised fluorescence intensity over time (F/Fmin).(H) AUC was measured between 700–730 s (under 17G exposure) from the data shown in (G) (*n*=146-254 cells,3-6 mice per genotype).(I) Changes in the cytoplasmic ATP:ADP ratio ([ATP:ADP]) in response to 17 mmol/l glucose (17G) was examined in whole islets using the ATP sensor Perceval.(J) AUC values corresponding to (I) were measured between 418–1400 s (under 17G exposure) (data points from *n*=22-23 islets, 3-6 mice per genotype). Data are presented as mean±SD. *p<0.05, **p<0.01, assessed by unpaired two-tailed Student's t-test and Mann–Whitney correction or two-way ANOVA test and Sidak's multiple comparisons test. Experiments were performed in 14-week-old male mice.

Fig.5 O_2 consumption and mtDNA are deleteriously affected when *Mfn1/2* are abolished in beta cells, while $[Ca^{2+}]_{ER}$ mobilisation remains unchanged. (A) Each snapshot of isolated control (i–v) and dKO-derived (vi–x) islets was taken during the time points indicated by the respective arrows in (B). Scale bar: 50 μm. See also ESM Video 3. (B) Changes in $[Ca^{2+}]_{ER}$ were measured in whole islets incubated with Cal-

520 and perifused with 17 mmol/l glucose (17G; with or without diazoxide [diaz]), 17G with 100μmol/l acetylcholine (Ach) and diaz, or 20 mmol/l KCl with diaz (C) AUC values corresponding to (B) were measured (17G AUC measured between 260 s and 740 s, 17G+diaz AUC measured between 846 s and 1020 s, 17G+diaz+Ach AUC measured between 1021 s and 1300 s and KCl AUC measured between 1301 s and 1500 s) (n=29-31 islets, 3 mice per genotype). (D) Representative oxygen consumption rate (OCR) traces of islets (~10 per well) were acutely exposed to 20 mmol/l glucose (final concentration), 5μM Oligomycin A (Oligo), 1μM FCCP, and 5μM Rotenone with Antimycin A (AA) (performed in *n*=7 mice, in two independent experiments).(E) Mitochondrial metabolic parameters were extracted from the OCR traces shown in (D). Data are presented as mean±SD in A-C and mean±SEM in D-E. *p<0.05,**p<0.01 assessed by unpaired two-tailed Student's t-test and Mann–Whitney correction or two-way ANOVA test and Sidak's multiple comparisons test. Experiments were performed in 14-week-old male mice.

Fig.6 Impaired insulin secretion can be rescued by GLP-1R agonists *in vitro* by increasing cytosolic Ca^{2+} oscillation frequency. (A) (A) Insulin secretion measured during serial incubations in batches in 3 mmol/l glucose (3G), 10 mmol/l glucose (10G), 17 mmol/l glucose (17G), 10G supplemented with 100 nmol/l exendin-4 (ex4), GLP-1, GIP, 10 μmol/l FSK, 100 μmol/l IBMX or 3G with 20 mmol/l KCl (*n*=3-7 mice per genotype in two independent experiments); (control: 3G vs ex4; p<0.05 and dKO: 3G vs ex4; p<0.0001, or 3G vs GLP-1; p<0.001, or 3G vs GIP; p<0.001). (B) Glucose tolerance measured by IP co-injection of 1g/kg glucose and 3nmol/kg ex4 were assessed in β*Mfn1/2* dKO and control mice (*n*=4-5 mice per genotype, dotted lines). (C) $[Ca^{2+}]_{cyt}$ changes in response to 3G, 3 mmol/l glucose, 10 mmol/l glucose (10G; with or without exendin-4 [ex4]) or 20 mmol/l KCl were assessed following Cal-520 uptake in whole islets. Traces represent mean normalised fluorescence intensity over time (F/F_{min}). See also ESM video 4. Dashed ROIs represent fluorescent segments of extended time scales. Both control and dKO traces reveal faster oscillatory frequencies in response to exendin-4. (D) The corresponding AUC is also presented (*n*=19-20 islets, 3 mice per genotype; 10G AUC measured between 200 s and 660 s, 10G+ex4 AUC measured between 800 s and 950 s), and KCl AUC measured between 1200 s and 1500 s); AUC 10G: control vs dKO; p=0.09; AUC control: 10G vs ex4;

p<0.05; AUC dKO: 10G vs ex4; p<0.001; ex4 vs KCl; p<0.05).(E) Dissociated beta cells were transfected with D4ER to measure changes in $[Ca^{2+}]_{ER}$, and perifused with 10 mmol/l glucose (10G), 10G+ex4 or thapsigargin (10G+thapsi) as indicated. Traces represent corrected ratio values post-linear fitting over time. (F) AUC was measured between 350–900 s (under 10G+ex4) and 900-1300 s (10G+thapsi) from the data shown in (E) (*n*=44-46 cells,4-5 mice per genotype). (G) Changes in cytoplasmic ATP:ADP ratio ([ATP:ADP]) in response to 10G or 10G with 100nmol/l ex4 was examined in whole islets.(H) AUC values corresponding to (G) were measured between 185-720s (under 10G exposure) or 721-1200s (under 10G with ex4) (data points from *n*=3 mice per genotype). (I) Average OCR values of islets (~10 per well) that were exposed to 3mmol/l or 10mmol/l glucose (final concentration), 10mmol/l glucose supplemented with ex4, FSK, Oligomycin A (Oligo), FCCP, and Rotenone with Antimycin A (AA) (*n*=3 mice per genotype; experiment performed in duplicate). (J) Insulin secretion measured during serial incubations in batches in 3 or 17 mmol/l glucose supplemented with 100μmol/l diazoxide and 30mmol/l KCl, (*n*=3 mice per genotype in two independent experiments). Data are presented as mean±SD. *p<0.05;**p<0.01, ****p<0.0001 assessed by two-way ANOVA test and Sidak's multiple comparisons test. Experiments were performed in 14-week-old male mice.

Fig.7 The GLP1-R agonist, exendin-4, improves intercellular connectivity in βMfn1/2 dKO β-cells. (A) Representative cartesian maps of control and dKO islets with colour coded lines connecting cells according to the strength of Pearson analysis (colour coded *r* values from 0 to 1, blue to red respectively) under 10mmol/L (10G), 10mmol/L with 100nmol/l exendin-4 (10G+ex4) glucose or 20mmol/L KCl; scale bars: 40 μm.(B) Representative heatmaps depicting connectivity strength (*r*) of all cell pairs according to the colour coded *r* values from 0 to 1, blue to yellow respectively.(C) Percentage of connected cell pairs at 10G, 10G+ex4 or KCl (*n*=19-20 islets, 3 mice per genotype).(D) *r* values between β-cells in response to glucose, exendin-4 or KCl (*n*=3 mice per genotype).Data are presented as mean±SD. *p<0.05,**p<0.01, ***p<0.001 assessed by two-way ANOVA test and Sidak's multiple comparisons test. Experiments were performed in 14-week-old male mice.

Fig.8 Insulin secretion is rescued through an EPAC-dependent activation in dKO islets. (A) Insulin secretion measured during serial incubations in batches in 3 mmol/l glucose (3G), 10 mmol/l glucose (10G), or 10 mmol/l glucose supplemented with 10µmol/l H89, 10 µmol/l FSK with 100 µmol/l IBMX or H89 (*n*=3 mice per genotype, in two independent experiments). (B) Insulin secretion measured during serial incubations in batches in 10 mmol/l glucose (10G), or 10 mmol/l glucose supplemented with 6µmol/l EPAC-activator, or EPAC-activator with 10µmol/l H89 (*n*=3 mice per genotype, in two independent experiments). (C) Representative Epac1-camps FRET traces in response to 3 or 10 mmol/l glucose, or 10 mmol/l glucose supplemented with 100nmol/l exendin-4 (10G+ex4), or 10 µmol/l FSK with 100 µmol/l IBMX in dissociated beta cells. (D) Fluorescence ratio peak values corresponding to (C) were measured between 200-250s (under 10G), 620-720s (under 10G with ex4) or 1110-1160s (under 10G with IBMX and FSK), (*n*=3-4 mice per genotype, 15-35 cells in two independent experiments). (E) Representative Epac1-camps FRET traces in response to 10 mmol/l glucose, 10 mmol/l glucose supplemented with 100nmol/l exendin-4 (10G+ex4), 10 µmol/l FSK (dark blue or purple traces) or 100 µmol/l IBMX (light blue or pink traces) in dissociated beta cells (*n*=3 mice per genotype,15-45 cells). (F) qRT-PCR quantification of *Epac, Adcy* and *Prka* genes expression in control and dKO islets relative to *β-actin* (*n*=3 mice per genotype in two independent experiments). Data are presented as mean±SD. *p<0.05,**p<0.01, ***p<0.001 assessed by two-way ANOVA test and Sidak's multiple comparisons test. Experiments were performed in 14-week-old male mice.